LEVEL II

(12)

RADC-TR-80-122
In-House Report
March 1980

A MODEL FOR HIGH FREQUENCY RADAR AURORAL CLUTTER

Terence J. Elkins

DTIC
ELECTE
S OCT 31 1980 D
E

APPROVED FOR PUBLIC RELEASE; DISTRIBUTION UNLIMITED

ROME AIR DEVELOPMENT CENTER
Air Force Systems Command
Griffiss Air Force Base, New York 13441

80 10 27 084

This report has been reviewed by the RADC Public Affairs Office (PA) and is releasable to the National Technical Information Service (NTIS). At NTIS it will be releasable to the general public, including foreign nations.

RADC-TR-80-122 has been reviewed and is approved for publication.

APPROVED: Edward A. Lewis
EDWARD A. LEWIS, Chief
Propagation Branch

APPROVED: Allan C. Schell
ALLAN C. SCHELL, Chief
Electromagnetic Sciences Division

FOR THE COMMANDER: John P. Huss
JOHN P. HUSS
Acting Chief, Plans Office

If your address has changed or if you wish to be removed from the RADC mailing list, or if the addressee is no longer employed by your organization, please notify RADC (EEP) Hanscom AFB MA 01731. This will assist us in maintaining a current mailing list.

Do not return this copy. Retain or destroy.

Unclassified

SECURITY CLASSIFICATION OF THIS PAGE (When Data Entered)

REPORT DOCUMENTATION PAGE		READ INSTRUCTIONS BEFORE COMPLETING FORM
(14) RADC-TR-80-122	2. GOVT ACCESSION NO. AD-A091 049	3. RECIPIENT'S CATALOG NUMBER
4. TITLE (and Subtitle) (6) A MODEL FOR HIGH FREQUENCY RADAR AURORAL CLUTTER		5. TYPE OF REPORT & PERIOD COVERED In-House
		6. PERFORMING ORG. REPORT NUMBER
(10) Terence J. Elkins		8. CONTRACT OR GRANT NUMBER(s)
9. PERFORMING ORGANIZATION NAME AND ADDRESS Deputy for Electronic Technology (RADC/EEP) Hanscom AFB Massachusetts 01731		10. PROGRAM ELEMENT PROJECT, TASK AREA & WORK UNIT NUMBERS 61102F (16) 2305J201 (17) J2
11. CONTROLLING OFFICE NAME AND ADDRESS Deputy for Electronic Technology (RADC/EEP) Hanscom AFB Massachusetts 01731		(11) March 1980
		13. NUMBER OF PAGES 112
14. MONITORING AGENCY NAME & ADDRESS(if different from Controlling Office) (12) 111		15. SECURITY CLASS. (of this report) Unclassified
		15a. DECLASSIFICATION DOWNGRADING SCHEDULE

16. DISTRIBUTION STATEMENT (of this Report)

Approved for public release; distribution unlimited.

17. DISTRIBUTION STATEMENT (of the abstract entered in Block 20, if different from Report)

18. SUPPLEMENTARY NOTES

19. KEY WORDS (Continue on reverse side if necessary and identify by block number)

OTH radar
Auroral modelling
Ionospheric modelling

20. ABSTRACT (Continue on reverse side if necessary and identify by block number)

A model is developed to permit estimation of the effects of irregularities in the auroral ionosphere in producing clutter experienced by Over-The Horizon radars operating at high geomagnetic latitudes. The model is based on various sources of data, including auroral radar (HF, VHF, UHF), vertical incidence ionosondes, satellite particle detectors, and optical sensors (ground-based and satellite-borne). The model addresses both the amplitude and Doppler components of auroral radar clutter and also the effect of ionospheric refraction that is extremely important at high frequencies.

DD FORM 1 JAN 73 1473

Unclassified

SECURITY CLASSIFICATION OF THIS PAGE (When Data Entered)

309050

20. (Cont)

Consideration is given to the question of predictability of the effects of auroral clutter on HF radar systems. An important component of the model is the incorporation of data from the Polar Fox II experiment conducted for the purpose of evaluating auroral clutter effects on OTH radars.

Contents

1.	THE RADIO AURORA	7
1.1	Introduction	7
1.2	Ionospheric Irregularities and Clutter	9
1.3	Magnetosphere-Ionosphere Interaction	10
1.4	Coordinate Systems	10
1.5	The Auroral Oval	12
1.6	Regular Ionospheric Features at High Latitudes	14
2.	RADIO PROPAGATION CONSIDERATIONS	17
2.1	Ionospheric Models	17
2.2	Numerical Ray-tracing	17
2.3	Absorption	18
2.4	Magnetic Field Model	19
3.	IONOSPHERIC IRREGULARITY MORPHOLOGY	22
3.1	E-region Irregularities	22
3.2	F-region Irregularities	23
3.3	Plasma Motion	26
3.4	Summary of Auroral Radar Experiments	28
3.5	Altitude of the Radio Aurora	31
4.	AURORAL CLUTTER MODEL	32
4.1	E-region Probability of Occurrence	32
4.2	F-region Probability of Occurrence	40
4.3	Scatter Volume and Volume Reflectivity	43
4.4	Aspect Sensitivity of Auroral Clutter	60
4.5	Auroral Clutter Amplitude	61
4.6	Estimation of Minimum Range for Slant-F	67

5. DOPPLER SHIFT MODEL 70
- 5.1 E-region Velocity Model 71
- 5.2 F-region Velocity Model 72
- 5.3 Doppler Shift Computations 74
- 5.4 Doppler Spread 77

6. PREDICTABILITY OF AURORAL CLUTTER 81
- 6.1 Statistical Considerations 82
- 6.2 Interplanetary Parameters 83
- 6.3 Satellite Imagery 85
- 6.4 Ground Based Magnetometers 85
- 6.5 Back Scatter Sounder in Polar Cap 86

REFERENCES 87

APPENDIX A: F-region Irregularities 93

APPENDIX B: Doppler Geometry 95

APPENDIX C: Backscatter Volume 99

APPENDIX D: F-region Volumetric Cross-section 105

APPENDIX E: Simple Doppler Shift Models 107

APPENDIX F: Auroral E-Layer Effect 111

Illustrations

1. Schematic View of the Earth's Magnetosphere Showing Regions of Plasma Storage 11
2. Equatorial Cross Section of Magnetosphere Showing Plasma Convection Pattern 11
3. Map of Northern Polar Regions Showing Location of the Auroral Oval at 12 UT for Average Geomagnetic Activity 13
4. Schematic Representation of the F-layer Ionospheric Trough and Plasma Ring, in Corrected Geomagnetic Coordinates, Relative to the Auroral Oval 15
5. Contours of Vertical Auroral Absorption at 30 MHz (Hartz and Montbriand) 20
6. Comparison Between Jenson-Cain Multipole Geomagnetic Field Model and Dipole Model, Showing Angle Between Horizon Ray From a Site at (61° N; 0° E) and Geomagnetic Field Vector as a Function of Azimuth 21
7. A Model of F-layer Plasma Drift, Including Effect of Earth Rotation (after Heppner, 1977) 27

8. (a-f) Contours of Probability of E-region Irregularity in CGS at 12 UT for Summer, Equinox and Winter and for $K_p = 2$ and 4 34

9. Probability of E-region Irregularity as Function of Range and Azimuth for Site at 61° CGL; June, $K_p = 2$, UT = 00 40

10. Same as Figure 8, Except for F-region 44

11. Probability of F-region Irregularity as Function of CGL for July at Magnetic Midnight and Midday ($K_p = 2$; UT = 12) 50

12. Same as Figure 11, Except for 03 and 06 MLT 50

13. Same as Figure 9, Except for F-Region 51

14. Illustrating Intersection of a Radar Pulse With a Thin Auroral Layer 52

15. Scatter Volume in the Presence of Ionospheric Refraction 53

16. Probability Distribution of "Pseudo" Volumetric Backscatter Cross-section, Measured at 8 MHz by the Polar Fox II Radar for Nighttime Hours in October 1972, (Ring and Richard, 1978) 55

17. Same as Figure 16, Except at 12 MHz 55

18. Same as Figure 16, Except at 15 MHz 56

19. Same as Figure 16, Except Interpolated to 10 MHz 56

20. Diurnal Variation of f_oE_s for October 1972 for Fort Churchill (CH), Goose Bay (GB), Ottawa (OT), and St. Johns (SJ) 58

21. Range-azimuth Variation of Geomagnetic Aspect Angle at 110 km Altitude for Line-of-sight Propagation From Site at 61° CGL, Using Jensen-Cain Model of the Geomagnetic Field 65

22. Range-elevation Angle Dependence for Clutter at Altitudes of 110 km and 300 km (line-of-sight propagation) 66

22a. Minimum Virtual Slant Range for F-region Clutter as a Function of Frequency, Normalized to Critical Frequency of a Spherical Stratified Layer 70

23. E-region Plasma Drift Velocity in CGS, Computed From Model 71

24. Computation of Radial Component of Plasma Velocity for Site at S, When Velocity Components (V_E, V_N) are Specified in Geomagnetic Coordinates 75

25. Contours of E-region Doppler Shift Computed for Site at (44.5° N, 67.5° W) at 0730 UT 76

26. Same as Figure 25, Except for F-region Clutter 76

27. Universal Time Dependence of E-region Doppler Shift at 10 MHz, for Azimuths 0 and -60 degrees, From Site at 61° CGL at Constant Range of 600 km 78

28. Same as Figure 27, Except for F-region 79

29. Azimuthal Dependence of E-region Doppler Shift at 10 MHz, for Universal Times 00 and 03, From Site at 61° CGL Constant 600 km Range 80

Illustrations

30. Same as Figure 29, Except for F-region 80

31. DMSP Photograph of Northern Europe Showing Moderately Active Aurora 86

B1. Geometry for Doppler Shift Calculations in Spherical Coordinate System 96

C1. Definition of Scatter Volume for Refracted Ionospheric Propagation 100

C2. Ray Trajectory in the F-region, Showing the Variation of Geomagnetic Aspect Angle With Range 101

C3. Variation Along Ray Trajectory of Altitude and Rate-of-Change of Geomagnetic Aspect Angle With Group Path and Take-off Elevation Angle at the Radar 102

C4. Variation Along Ray Trajectory of Group Path With Elevation Angle of Take-off, Showing the Range of Elevation Angles, at 1000 km Radar Range, Defined by the Radar Pulse 103

E1. Simplified Models for Doppler Calculations: Straight Line Motion (upper diagram); Curved Velocity Trajectory Along Circle of Constant Geomagnetic Latitude (lower diagram) 108

E2. Doppler Shift Calculated on Basis of Curved Trajectory Model in Figure E1, as a Function of Magnetic Azimuth 109

F1. Contours of Calculated Geomagnetic Orthogonality at Altitude 110 km Using an Ionospheric Model Containing an Auroral E-layer 112

Tables

1. E-Region Plasma Velocities in CGS 72

2. F-Region Plasma Velocities at $\Phi = 80°$ 74

3. Duration of Magnetically Disturbed Periods 83

A Model for High Frequency Radar Auroral Clutter

1. THE RADIO AURORA

1.1 Introduction

The so called "radio-aurora" or "radar-aurora" is a phenomenon closely related to the visible aurora, but differing from the latter in several important respects. The visible aurora is caused by optical emissions stimulated by collisional excitation of atmospheric atoms by energetic charged particles of magnetospheric origin. The radio aurora, on the other hand, is the result of radio wave scattering from inhomogeneities in the ionospheric plasma. It happens that the general region of the visible aurora is also one of intense small scale ionospheric irregularities, so that there are similarities in the spatial and temporal characteristics exhibited by the visible and radio auroras. However, since these phenomena are generated by different physical processes, it may reasonably be expected that they would exhibit some different properties.

The morphology of the visible aurora has been extensively studied, since the necessary optical techniques have been available for over a century. It has become well accepted that the visible aurora is confined to a narrow region (a "ring" or "belt") surrounding the geomagnetic poles. With the relatively recent advent of sensitive photometers and satellite optical scanners, a hitherto unsuspected optical component of the aurora was discovered which is below the intensity level for normal

---

(Received for publication 4 April 1980)

optical or photographic viewing. This diffuse, sub-visual aurora occupies a greater region of space than the bright visible aurora, and appears to be more stable in time. Since the charged particle precipitation responsible for the visible and sub-visual aurora is strongly affected by the geomagnetic field, these phenomena are best ordered in a system of coordinates based on the structure of the earth's magnetic field. Various geomagnetic coordinate systems have been proposed and used to order charged particle precipitation observations. The one currently most used is that of Hakura,[1] known as the "corrected geomagnetic" coordinate system (CGS), which is discussed in Section 1.4.

The radio aurora is also better ordered in the CGS than in the conventional geographic coordinate system, but it does not exhibit precisely the same properties, in this system, as does the visible aurora. The ionospheric inhomogeneities responsible for radio wave scattering are caused by plasma instabilities which are driven by ionospheric currents. These currents in turn flow in response to impressed electric fields of magnetospheric origin, and their intensity and space-time distribution reflect both the properties of these impressed electric fields and of the conductivity of the ionosphere. The conductivity depends, among other things, on the degree of ionization of the atmosphere, and to the extent that this ionization is caused by particle precipitation, this, too, is best ordered in the CGS. However, solar ultra-violet radiation also ionizes the atmosphere to an extent dependent on the elevation angle of the sun, so there is a component of ionospheric conductivity which is ordered in the standard geographic coordinate system. This complexity is partly responsible for the different properties of visible and radio auroras. Intense ionospheric currents do not necessarily flow in the same region of the ionosphere as that in which intense particle precipitation occurs. Thus, although information relating to charged particle precipitation and optical emissions is available in profusion, care needs to be exercised in using this data to deduce properties of the radio aurora.

In this section, the relationship between small scale ionospheric irregularities and radio auroral clutter is briefly reviewed. A review of magnetosphere-ionosphere interaction follows, aimed at placing the subject of the high latitude ionosphere in proper geophysical perspective. The various coordinate systems employed in modelling the high latitude ionosphere, auroral phenomena, and radar clutter are discussed and the concept of the "auroral oval" is reviewed. Finally there is a discussion of the regular or predictable features of the high latitude ionosphere. The model of auroral radar clutter, which will subsequently be developed, is based on the above concepts.

---

[1] Hakura, Y. (1965) Tables and maps of geomagnetic coordinates corrected by the higher order spherical harmonic terms, Rept. Ionosph. Space Res. (Japan), **19**:121.

1.2 Ionospheric Irregularities and Clutter

Radar clutter, induced by the aurora, is simply the result of radio wave backscatter from ionospheric irregularities in the vicinity of the aurora. These irregularities are strongly anisotropic in form, due to the anisotropy of the ionospheric plasma conductivity brought about by the presence of the geomagnetic field. The irregularities may be visualized as thin plasma cylinders, whose axes are aligned with the local geomagnetic field direction, and present in a continuum of scale sizes. Due to the high degree of anisotropy in the shape of the irregularities, their radio backscatter cross section is highly directional, that is, it is a strong function of the angle of incidence of the radio propagation vector on the geomagnetic field direction.

The two prerequisites for the occurrence of auroral clutter are:

(1) A region, in the ionosphere, of small scale irregularities must be illuminated by the radar,

(2) The radio propagation vector must be approximately orthogonal to the geomagnetic field vector in the region of ionospheric irregularities.

Since the spatial and temporal distributions of ionospheric irregularities are moderately well known, the incidence of auroral clutter (and techniques for minimizing it) reduce largely to a study of the factors influencing the magnetic aspect angle. These factors are primarily the radio frequency and the ambient ionospheric structure, which together determine the amount of refraction which the radar beam experiences.

Were it not for the large refraction which the ionosphere imposes on HF radio waves, the regions of near-orthogonal magnetic aspect angle would be very small, as they are in the case of UHF line-of-sight propagation. Even if the HF radar possessed a narrow ("pencil") antenna beam, the assessment of effects of auroral clutter and the means of its mitigation would not present major problems. However, the fact that the radar beam is usually very wide in the elevation plane adds considerable complexity to the problem since the ionospheric refraction then permits the orthogonality criterion to be met over a very large range extent. In fact, when the possibility of multiple ionospheric hops is considered, the range extent over which the orthogonality criterion can be satisfied becomes virtually unlimited. This does not imply that the amplitude of the observed auroral clutter will be uniform in range; several factors, principally radio wave absorption, contribute to pronounced variations of clutter amplitude with range. In particular, in the case of multiple hop propagation, there may be a large amplitude difference between clutter signals observed via one and two or more hops, especially in daytime when the absorption in the lower ionosphere is strongest.

1.3 Magnetospheric-Ionosphere Interaction

An understanding of the special features of the high-latitude ionosphere requires an appreciation of the relationship between ionospheric and magnetospheric properties. The earth's magnetic environment (loosely termed the "magnetosphere") is in many ways, analogous to a plasma bottle in laboratory magneto-plasma physics. Figure 1 shows a schematic representation of the magnetosphere. The solar wind—a stream of charged particles, primarily electrons and protons, emanating from the sun—impinges on the earth's magnetic field. A complex interaction takes place in which a standing shock wave is formed at a geocentric distance of about 15 earth radii (R_e), and the magnetic field lines behind the shock are swept back to form a "tail" in anti-solar direction. The region immediately behind the shock contains hot plasma, moving at a velocity less than the local speed of sound; this plasma has a narrow region (cleft) of direct access to the dayside of the ionosphere, between the first swept-back field line and the last "unbroken" field line. At the center of the tail region there exists a narrow sheet of plasma which is in constant convective motion and in which some spatial energy differentiation is maintained. This "plasma-sheet" is also directly connected to the high-latitude ionosphere, on the nightside of the earth and its plasma is subject to acceleration by sporadic electric fields which are induced across the tail, in the East-West direction, by the solar wind. Figure 2 shows an equatorial cross section of the magnetosphere in which the plasma convection pattern is illustrated. In both Figures 1 and 2, a region known as the "plasmasphere" is depicted, extending to a geocentric distance of about 4 R_e. The plasmasphere boundary is the surface separating plasma which is co-rotating with the earth from that which is being convected under the influence of the solar wind. For many purposes the demarcation between the high-latitude ionosphere and mid-latitude ionosphere may be defined as the intersection in the ionosphere of the magnetic field lines which bound the plasmasphere.

1.4 Coordinate Systems

A complicating factor in studying the high-latitude ionosphere and, specifically in modelling, it is the fact that major parameters are ordered in two different coordinate systems. In computing the combined effects of these parameters it is always necessary to keep track of their position in each system. In particular, when computing radar-related quantities such as clutter intensity and Doppler shift of the radar signal, it is of course necessary to consider a system of coordinates, defined by range and azimuth, centered on the radar. The temperate zone ionosphere is largely ordered in the conventional geodetic system of coordinates, defined by geographic latitude and longitude, and local time. This follows from the fact that solar illumination is the dominant contributing factor to its production and consequently solar zenith angle is the single most important variable. Conventional coordinate transformation techniques are appropriate for conversion between the standard geographic coordinates and a geodetic system centered on the radar. The high-latitude ionosphere, however, possesses an important component ordered in another coordinate system related to the structure of the geomagnetic field; this is not a spherically symmetric system and consequently the techniques for transformation to and from the geodetic system are complicated.

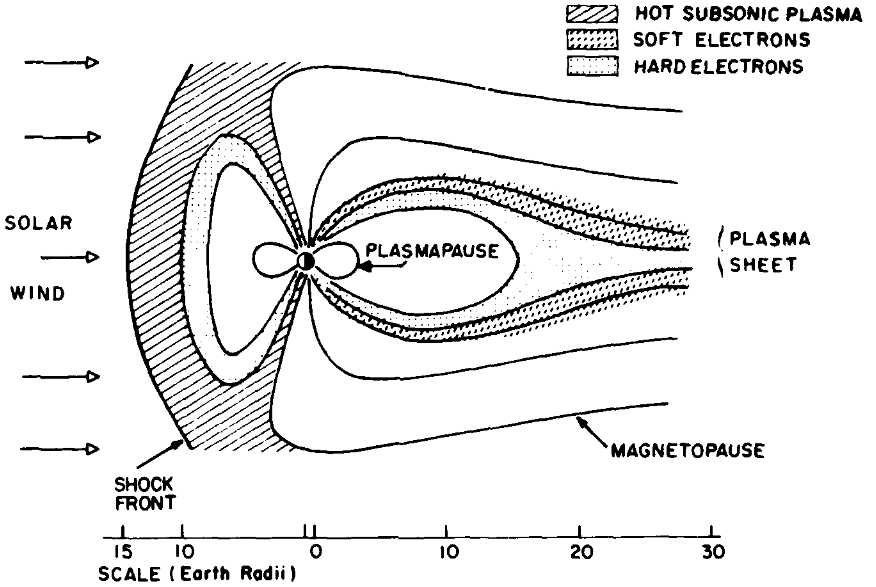

Figure 1. Schematic View of the Earth's Magnetosphere Showing Regions of Plasma Storage

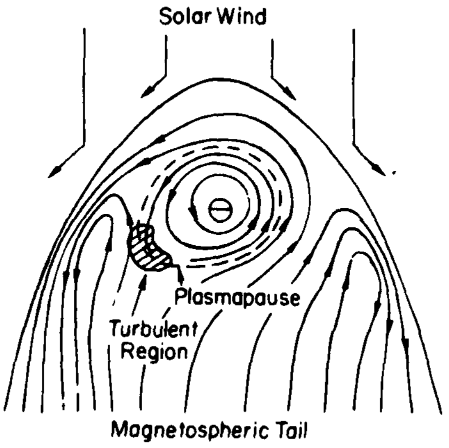

Figure 2. Equatorial Cross Section of Magnetosphere Showing Plasma Convection Pattern

While it was well-known, at an early date, that high-latitude ionospheric properties, especially the aurora, were best organized and represented in geomagnetic coordinates, substantial discrepancies and anomalies were observed when the earth's magnetic field was approximated by a dipole. A gradual understanding of the importance of higher order terms in the spherical harmonic representation of the true earth's magnetic field culminated in the formulation of the "corrected geomagnetic (CG) coordinate system"—abbreviated in this work as CGS. The charged particles which generate auroral and ionospheric effects are strongly influenced by magnetic field structure at large distances from the earth; this results in a magnetic latitudinal dependence of particle precipitation, together with a temporal variation introduced by the earth's rotation. The coordinate system best adapted to ordering charged particle precipitation data (as well as other related effects) is defined by corrected geomagnetic latitudes (CGL) and corrected geomagnetic time (CGT). For some approximate purposes, a reasonable degree of accuracy is obtained by substituting local (solar) time for corrected geomagnetic time.

The transformation between the geographic coordinate system and the CGS is accomplished by a numerical mapping procedure, based on the work of Gustaffson.[2]

1.5 The Auroral Oval

A major advance was achieved in understanding the morphology of the high-latitude ionosphere with the discovery of the auroral oval. Prior to this discovery, it had been known that auroral activity was confined to a fairly narrow range of latitudes, centered on the geomagnetic pole, but no clear concept existed of the coupling of spatial and temporal aspects of auroral occurrence. The aurora is now known to be caused by the injection of energetic charged particles into the earth's atmosphere, and its spatial extent is determined by the projection on the ionosphere of the magnetospheric regions of plasma having direct access to the ionosphere (see Figures 1 and 2). Since the earth's rotation introduces a time variability factor, it is necessary to consider the auroral region as having both latitudinal and temporal dependences. The auroral oval is depicted in Figure 3, showing its inner and outer boundaries as heavy lines, in CGS coordinates at 12 UT, for a moderate level of geomagnetic activity (Q = 3). It is important to note that the auroral oval concept is a statistical one, deduced originally from photographic data and describing the visible aurora. Subsequent work has shown that, with minor modifications, the auroral oval is a valid representation of some other effects, in particular ionospheric structure, and that the concept has some validity on an instantaneous basis as well as a statistical one. The auroral oval is a valuable device for ordering

---

[2] Gustafsson, G. (1970) A revised corrected geomagnetic coordinate system, Arkiv f. Geofysik, 5(No. 40):595.

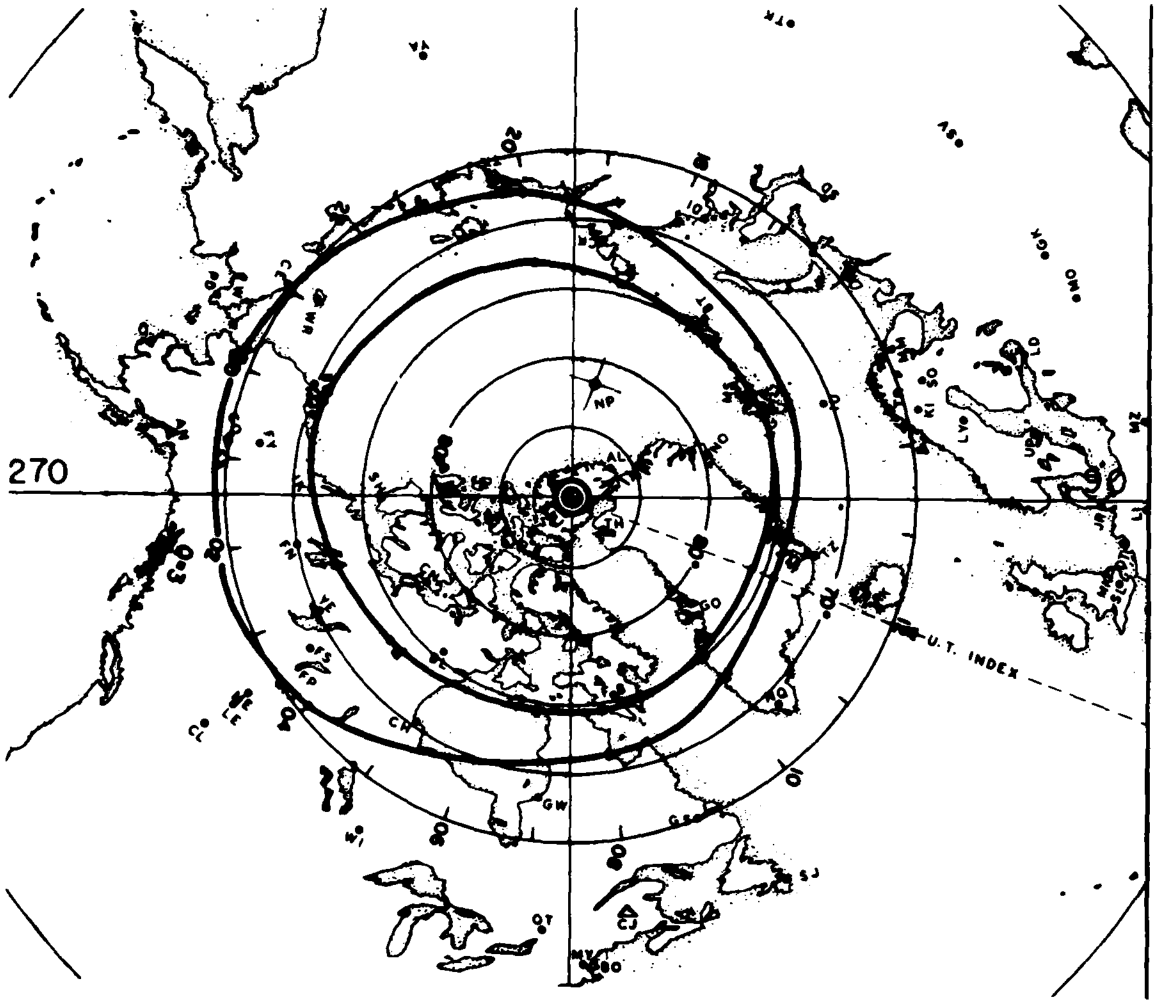

Figure 3. Map of Northern Polar Regions Showing Location of the Auroral Oval at 12 UT for Average Geomagnetic Activity. Locations of vertical incidence ionosondes during the IGY are indicated

and describing high latitude ionospheric phenomena, but certain limitations must be borne in mind. Aside from the fact that the auroral oval is a descriptor of a certain type of optical emissions (bright, spatially discrete, and limited in spectral width), Eather[3] has pointed out that the concept ignores variations in intensity of particle precipitation with time. Such variations around the oval are important in assessing the impact of auroral clutter on a backscatter radar system.

1.6 Regular Ionospheric Features at High Latitudes

Regular features of the high-latitude ionosphere may be defined as those which conform to the morphological model illustrated in Figures 1, 2, and 3. The effects of the magnetosphere-ionosphere coupling are superimposed on the well known direct solar ionization of the atmosphere which is manifested globally. The latter, of course, is best represented in the standard geographic coordinate system (geographic latitude and solar time); this leads to complications since the superposition of the two controlling influences must be made with due regard to the relevant coordinate systems. It is also necessary to consider the special nature of the direct solar ionizing influence at high latitudes, where the sun can be above or below the horizon for long periods, in summer and winter respectively. The principal effects of this feature are:

(a) The diurnal and seasonal variations of ionospheric properties are strongly coupled,

(b) In winter, in the absence of direct solar ultra violet (UV) radiation, the particle-related effects tend to predominate,

(c) In summer, the polar ionosphere is dominated by solar UV ionization.

While the roles of direct solar illumination and charged particle precipitation are at least intuitively apparent, other physical factors are also at work in influencing the structure of the quiet polar ionosphere. Perhaps the most significant of these factors are the chemical composition of the upper atmosphere and the coupling between the neutral and ionized atmospheric constituents. The chemical composition of the high atmosphere in the polar region is dominated by an upwards diffusive flow, known as the "polar wind," which results in a great reduction of the lighter atmospheric constituents (hydrogen and helium) relative to the corresponding composition at mid-latitudes. The net result is a general reduction of electron density over the polar cap, together with an increase in the effective plasma scale height, especially at high altitudes. The viscous-like coupling between movements of neutral and ionized atmospheric constituents gives rise to ionospheric effects induced by neutral winds which can be a significant factor in the long winter nighttime when ionization production is low.

---

[3] Eather, R.H. (1973) The auroral oval - A reevaluation, *Rev. Geophys. Space Phys.* **11**:155.

Plasma scale height is a parameter, having dimensions of length, which characterizes the exponential decay with height of plasma density.

1.6.1 THE IONOSPHERIC TROUGH

A notable feature of the high-latitude ionosphere is the ionospheric trough, which is a region of strongly depressed electron density, occurring at F-region altitudes, primarily on the night-side of the earth. The trough is aligned approximately with a circle at a constant geomagnetic latitude of about 60°. The equatorial edge of the trough coincides approximately with the locus of the plasmapause, and the electron density there increases gradually from the deepest point (~ 60° CGL) to the mid-latitude value. The polar edge of the trough is much steeper than the equatorial edge and coincides with the equatorial edge of the auroral oval. The local time dependence of the electron density in the trough region shows a minimum at about 0300, and onset and disappearance at variable time, corresponding respectively to sunrise and sunset at the trough latitude. Thus the trough can be represented schematically in the CG coordinate system as shown in Figure 4.

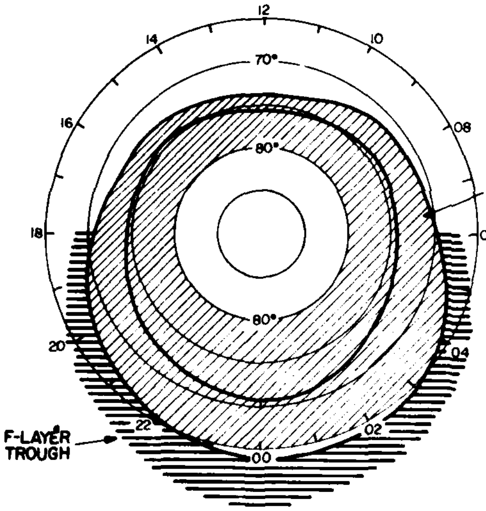

Figure 4. Schematic Representation of the F-layer Ionospheric Trough and Plasma Ring, in Corrected Geomagnetic Coordinates, Relative to the Auroral Oval

The ionospheric trough is a highly variable feature which appears to be very prevalent in the topside ionosphere but is also frequently present at the F-peak and below. Spiro et al[4] have presented a convincing argument explaining the trough as the result of the complex magnetospheric convective flow near the plasmapause. Ionospheric plasma in this region is influenced by the earth's rotation and by the cross-tail electric field in such a way that a region of flow stagnation exists on the

---

[4] Spiro, R.W., Heelis, R.A., and Hanson, W.B. (1978) Ion convection and the formation of the mid-latitude ionization trough, J. Geophys. Res. **83**:4255.

night side of the earth. In the absence of ionization sources, normal F-region recombination acting over a long period results in strong reduction in the degree of ionization, giving rise to a trough-shaped plasma depression. The trough is observed most frequently in winter and in the early morning, and its intensity and location are fairly closely correlated with the level of geomagnetic activity. Thus, the latitude (CGL) of the trough electron density minimum moves equatorwards by 1.8 - 2.0 degrees per unit increase in K_p (the planetary magnetic index).

1.6.2 AURORAL E-LAYER

In the vicinity of the auroral oval there appears a relatively regular, thick layer of ionization at E-region altitudes, produced by a steady flux of charged particles in the kilo-electron volt (keV) energy range. The maximum plasma frequency in this "auroral-E"layer is typically 1.5 - 2.5 MHz. On the day-side of the earth, the auroral-E contribution augments the solar UV-produced E-layer.

1.6.3 AURORAL SPORADIC-LAYER

Highly variable fluxes of charged particles (electrons and protons) produce auroral sproadic-E, which is mainly confined to the auroral oval region. Plasma instabilities induced by the intense "auroral electrojet" current system give rise to additional small scale structure in the E-region within and immediately adjacent to the auroral oval. Auroral sporadic-E is capable of scattering incident radio waves at very high frequencies (well into the VHF range) and create serious multipath problems on radio links in the auroral region.

1.6.4 F-REGION IRREGULARITIES

The F-region in the auroral nighttime ionosphere very often displays substantially lower electron densities than the E-region, and is virtually always irregular in nature. On the day-side of the auroral oval, a special situation is observed virtually permanently; a region of several degrees latitudinal extent containing irregular F-region ionization of relatively high intensity is observed, which is the result of direct access of solar wind plasma into the ionosphere through the magnetospheric cleft. The zone surrounding the magnetic pole in which low energy particle precipitation produces excess irregular ionization is sometimes referred to as the "plasma ring", depicted schematically in Figure 4. The region interior to the plasma ring, in the immediate vicinity of the magnetic pole, is one of depleted electron density, especially during the long winter night; this region is sometimes referred to as the "polar cavity."

2. RADIO PROPAGATION CONSIDERATIONS

An essential element in computing the incidence and intensity of auroral clutter on a HF radar is the computation of the radio ray trajectories in the ionosphere. This involves the construction of a suitable numerical model for the ionosphere, appropriate to the geophysical conditions of interest, and subsequent numerical ray tracing through this model. In order to compute the intensity of auroral backscatter, a model for the ionospheric irregularity cross section is necessary, and an estimate of the absorption of the radio waves in the ionosphere must be made. Because of the aspect sensitivity of auroral backscatter, a suitable global model for the geomagnetic aspect angle must be computed at all points along the ray trajectory.

2.1 Ionospheric Models

The model of the ionosphere, chosen in this study to represent the high-latitude ionosphere, is one developed at Rome Air Development Center and its predecessor organization—AFCRL. This model is described by Rush et al[5] and Miller and Gibbs.[6] The dominant component of any ionospheric model intended for ray tracing, is the f_oF_2 model. In the RADC model, this component is essentially that of the ITS-78 model[7] with empirical modifications to incorporate magnetic activity dependence and the ionospheric trough in the CGS. The model provides a three-dimensional median numerical ionospheric specification as a function of:

(1) Sunspot number (SSN),
(2) Planetary magnetic index (K_p),
(3) Universal Time (UT),
(4) Season (that is, month),
(5) Latitude and longitude.

2.2 Numerical Ray-Tracing

Ray tracing is the technique of computing the trajectories of radio waves through a modelled ionosphere by solution of the so-called Haselgrove equations.[8] This is accomplished numerically by use of a computer program originally developed by Jones[9] and later modified extensively at Rome Air Development Center.[10, 11] Among the modifications made are the inclusion of sporadic-E, the input of arbitrary ionospheric specifications, the calculation of deviative absorption and a variety of output options. For the purposes of the present study, the modification of prime interest is the incorporation of an accurate geomagnetic field model, and the continuous computation, along the ray trajectory, of the angle between the propagation vector and the geomagnetic field vector (magnetic aspect angle). The geomagnetic field model will be described in Section 2.5.

(Due to the large number of references cited above, they will not be listed here. See References, page 87.)

The ray tracing program permits computation of the ray trajectory over an arbitrary number of hops for a given azimuth and elevation angle from any chosen location. In the present study, the maximum number of hops was taken as two, and rays were computed in an azimuthal range of -60° to +60°, and for elevations of 1° to 21°.

2.3 Absorption

The calculation of ionospheric absorption in the polar regions is complicated by the presence of two different absorption components:

(1) "Normal" D-region absorption, which is primarily a function of the intensity of the solar ionizing radiation (Lyman-alpha) and is therefore, dependent on the solar zenith angle,

(2) "Auroral" absorption, caused by ionization of the lower ionosphere by energetic charged particle precipitation.

The "normal" component of absorption is relatively deterministic and exhibits a large seasonal component which "seasonal anomaly" is apparently due to seasonal changes in the molecular composition of the lower ionosphere, and is also latitude-dependent. A model for the normal D-region absorption[12] has been accepted as an international standard by the CCIR, and is used for computation in this study. A computer program, based on the Bradley-George[12] algorithm, was incorporated into the ray trajectory calculations.

The auroral component of absorption is more complicated, being essentially a random process but possessing certain deterministic features. Among the many workers who have studied auroral absorption, Hartz et al[13] and Hargreaves and Cowley[14] have published quantitative data suitable for computational purposes. More recently Foppiano[15] has published a numerical method of predicted auroral absorption of HF skywaves. Elkins[16] has summarized the quantitative features of auroral absorption events in a manner suitable for computation for a typical case. Auroral absorption occurs during so-called "auroral sub-storms," and is confined to a belt of latitude approximately 5° - 10° in extent, located slightly equatorwards

---

[12] Bradley, P.L., and George, P.A. (1974) A new method of predicting the ionospheric absorption of high frequency waves at oblique incidence, Telecomm. J. **41**:307.

[13] Hartz, T.R., Montbriand, L.E., and Vogan, E.L. (1963) A study of auroral absorption at 30 Mc/s, Can J. Phys. **41**:581.

[14] Hargreaves, J.K., and Cowley, F.C. (1967) Studies of auroral radio absorption events at three magnetic latitudes - II. Differences between conjugate regions, Planet. Space Sci. **15**:1571.

[15] Foppiano, A. (1975) CCIR, IWP 611, Docs. 3 and 10.

[16] Elkins, T.J. (1972) A Model of Auroral Substorm Absorption, AFCRL-TR-72-0413, AD A749859.

of the auroral oval. Auroral sub-storms occur sporadically and with varying intensity. It is reasonable to represent auroral absorption as a statistical random variable, recognizing that its effects are superimposed on the "normal" absorption component. When no auroral substorm is in progress, the residual absorption present is that predicted by the Bradley-George model.[12]

In the present study, auroral absorption will be represented by its median value, derived as a function of geomagnetic latitude and time from the references cited in the previous paragraph. Since auroral absorption is ordered in the corrected geomagnetic coordinate system, an additional complexity is introduced in including it, since the normal D-region absorption is primarily a function of geographic latitude and time. Figure 5 shows, in the CGS, the percentage of time that one way, vertical incidence absorption at 30 MHz exceeds one dB.[13] The contours are labelled in percent. Note that maximum auroral absorption occurs between 08 and 09 CGT and at 65° CGL. In order to use this data in computing oblique incidence HF clutter absorption, median values for the statistical distributions of absorption values need to be derived, and appropriate scaling needs to be applied for frequency and obliquity of propagation.

2.4 Magnetic Field Model

Several models exist, with varying degrees of complexity, to represent the structure of the geomagnetic field in those dimensions. For an application such as the present one, in which it is necessary to locate the "orthogonality point" to an accuracy considerably better than 100 km, the simplest model (that of an eccentric dipole) is much too inaccurate. The two models which were considered for this study were the International Geomagnetic Reference Field - IGRF[17, 18] and the "Jensen-Cain" model.[19] These are both higher order spherical harmonic expansions of the geomagnetic potential; the IGRF is an 8th order expansion and the Jensen-Cain model is a 6th order expansion. Other expansions have been proposed[20] having even a greater number of spherical harmonic terms but the improved accuracy, if any, inherent in their use does not warrant the additional computational complexity.

---

[17] IAGA Commission 2, Working Group 4 (1969) International geomagnetic reference field, 1965. 0, J. Geophys. Res. 74:4407.

[18] Mead, G. D. (1970) International geomagnetic reference field 1965. 0 in dipole coordinates, J. Geophys. Res. 75:4372.

[19] Jensen, D. C., and Cain, J. C. (1962) An interim geomagnetic field (abstract), J. Geophys. Res. 67:3568.

[20] Cain, J. C., and Sweeney, R. E. (1970) Magnetic field mapping of the inner magnetosphere, J. Geophys. Res. 75:4360.

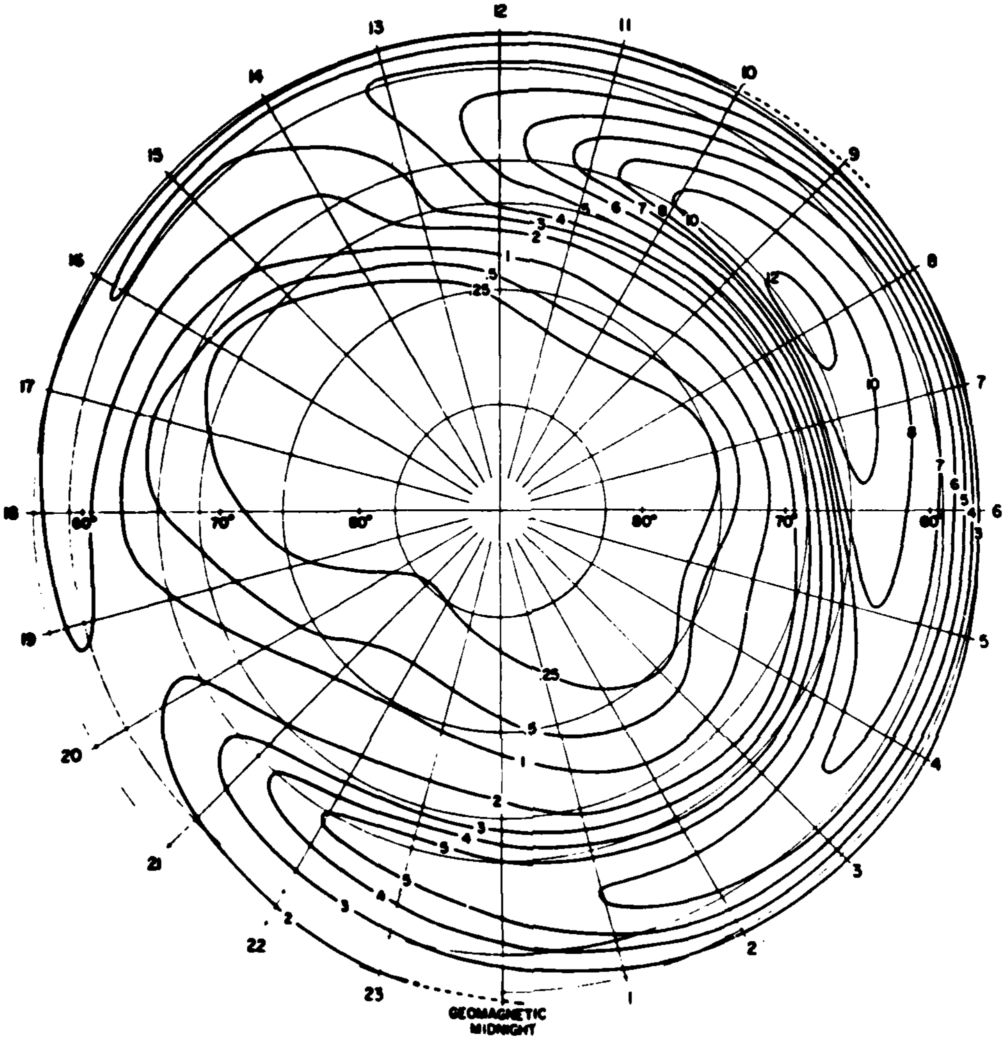

Figure 5. Contours of Vertical Auroral Absorption at 30 MHz (Hartz and Montbriand). Numbers represent percentage of time absorption exceeds 1 dB

In order to compare the IGRF and Jensen-Cain models for the auroral backscatter application, a series of ray tracings was performed using an actial ionospheric model, and computing the geomagnetic aspect angle (ψ) for both magnetic field models. When the results were averaged over a range interval from the radar of 200-1100 km, a root-mean-square difference in the computed values of ψ for both models was found to be 0.05 degrees. This value is sufficiently small so that no further effort was judged necessary in establishing which of the two models is the more accurate for this application. Because of its greater simplicity and for other reasons of convenience, the Jensen-Cain model was chosen to represent the geomagnetic field in this study.

As a matter of interest, a comparison was made between the Jensen-Cain model and the eccentric dipole model. The angle ψ was computed at a radar location (61° latitude, 0° longitude) for zero elevation take-off angle, as a function of azimuth. Figure 6 shows the results of this comparison. Typical values of several degrees for the discrepancy in ψ are apparent. The difference in computed magnetic inclinations at the radar is 2.3° and the difference in computed declinations is 13°. It is, therefore, clear that the eccentric dipole model is inadequate for the present application.

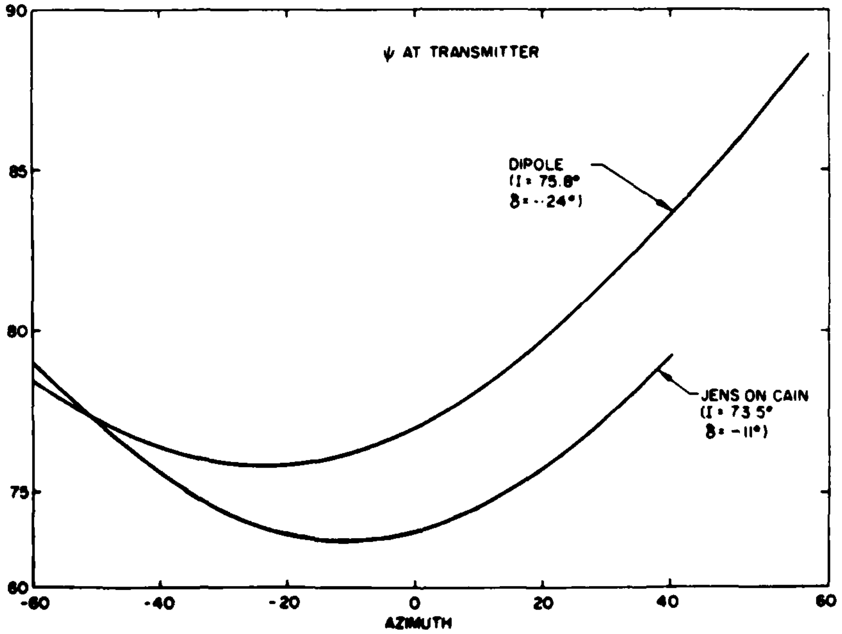

Figure 6. Comparison Between Jensen-Cain Multipole Geomagnetic Field Model and Dipole Model, Showing Angle Between Horizon Ray From a Site at (61° N; 0° E) and Geomagnetic Field Vector as a Function of Azimuth. Magnetic inclination and declination for the site are shown for each model

3. IONOSPHERIC IRREGULARITY MORPHOLOGY

A reliable predictive model for auroral radar clutter must, of necessity, take into account the spatial, temporal, seasonal, and magnetic activity dependences of ionospheric irregularity occurrence. Unfortunately, these have not been sufficiently well studied by the backscatter radar technique to permit construction of a model based on data of the most relevant kind—namely HF backscatter. On the other hand, the study of ionospheric irregularities has always been a prominent part of ionospheric radio physics and an extensive data base exists, accumulated over many years by a variety of techniques. The most comprehensive component of this data base is that collected by the world-wide network of vertical incidence ionospheric sounders. Figure 3 shows a map of the northern hemisphere, with the auroral oval superimposed and with the locations of high latitude vertical incidence sounding stations marked. It can be seen that this network has achieved reasonably well distributed coverage of the high latitudes. A similar, but sparser network has operated in the southern high latitudes and some of this data has been incorporated into the model as well as the northern data.

3.1 E-region Irregularities

Small scale irregularities in the E-region give rise to the phenomenon of sporadic-E reflections, observed in routine vertical incidence sounding of the ionosphere. The most useful study of sporadic-E morphology is that of Besprozvannaya and Shchuka[21] who developed percentage occurrence statistics in the CGS. Specifically, these authors presented the percentage of time that the maximum frequency of high-latitude sporadic-E reflections exceeded 3 MHz, as a function of geomagnetic latitude, geomagnetic time, season, magnetic activity, and sunspot number. In retrospect, the choice of such a low maximum frequency as 3 MHz was somewhat unfortunate since a "saturation" effect of occurrence values close to 100 percent is often in evidence. Despite this minor shortcoming, the model for E-region auroral clutter is based on the above-mentioned study. Implicit in this procedure is the assumption that the same ionospheric irregularities give rise to both vertical incidence sporadic-E and oblique incidence HF auroral clutter. This assumption is regarded as valid in view of the similar frequency ranges involved in observing both phenomena. It would be more in question if the model were intended to characterize VHF or UHF auroral clutter, since the irregularity scale size regimes in question would then be different by several orders of

---

[21] Besprozvannaya, A.S., and Shchuka, T.I. (1971) *Geomag. and Aeron.* 6:878; and (1972) Space-time distribution of E_s formations associated with visible auroral forms, *Geomag. and Aeron.* 12:401.

magnitude; since quite different plasma instability processes might be dominant at low and high wave numbers, the assumption of such a direct relationship between sporadic-E and UHF backscatter clutter is questionable.

The model for E-region auroral clutter incidence exhibits the following general properties:

(1) A strong tendency for geomagnetic latitude control,

(2) A strong midnight maximum, in winter especially, which is assumed to be predominantly direct-E. This maximum occurs within the auroral oval boundaries.

(3) Strong maxima in occurrence at lower latitudes (~60°) at 04 and 19 MLT. These maxima are assumed to correspond to diffuse radar returns,

(4) A pronounced minimum in occurrence frequency at 65° CGL,

(5) A pronounced dependence of occurrence frequency on magnetic activity,

(6) A virtual independence of occurrence frequency on sunspot number, after the solar cycle dependence of geomagnetic activity has been removed,

(7) A tendency for low latitude (~60°) occurrence frequencies to be greater in summer than in winter.

Many of the features exhibited by the sporadic-E-based models have also been observed in backscatter experiments. Among the studies of diurnal variations are those of Unwin,[22] Presnell et al,[23] Hellgren and Meos,[24] Brooks,[25] Czechowsky et al,[26] and Sprenger and Glode.[27] Several of these studies confirm some aspects of the latitudinal distribution although the requirements for magnetic aspect angle are usually too restrictive to permit reliable extraction of latitudinal dependence in a UHF radar.

3.2 F-region Irregularities

Small scale irregularity of the F-region polar ionosphere is a very common phenomenon—in fact, considering that the F-region may be defined as extending from an altitude of ~170 km to one of ~1000 km, small scale irregularities in this region may be regarded as a permanent feature of the high-latitude ionosphere. Aarons,[28] using the satellite scintillation technique, reports that the F-region ionosphere across the polar cap (within the equatorial boundary of the auroral oval, approximately) is permanently filled with irregularities. From the viewpoint of HF backscatter, this observation is not as relevant as for satellite communications,

---

(Due to the large number of references cited above, they will not be listed here. See References, page 87.)

for example, since only irregularities on the underside of the F-layer, below the F-peak, would normally affect an HF system. The model adopted, in this report, for F-region irregularity will be based on observations of the bottomside ionosphere, by vertical incidence sounders. A HF radar sees F-region irregularities as "slant-F" clutter, named for its characteristic appearance on oblique-incidence ionograms.

Slant-F clutter-producing irregularities can be assumed to fill the radar beam completely; these are the same irregularities which produce spread-F on vertical incidence ionosondes. That this is so was demonstrated by Bates,[29] among others. If the F-region irregularities in question extend over the radar location and down range, slant-F is seen continuously in range at all frequencies which do not penetrate the ionosphere. The intensity of slant-F clutter is proportional to the illuminated volume (V_s) within the irregularity region, and to the volumetric cross section of the irregularities. At high geomagnetic latitudes, where the magnetic field lines are nearly vertical, a simple rule of thumb is that slant-F clutter occurs at about half the range of ground clutter as seen by the sky-wave (for the same take-off angle).

3.2.1 MORPHOLOGY OF SLANT-F

Since slant-F and spread-F are produced by the same ionospheric irregularities, it is possible to deduce the spatial and temporal properties of slant-F from those of spread-F. Spread-F has been extensively studied on a global basis.[30-33] In general, the following properties may be assigned to high latitude spread-F:

(1) Latitudinal dependence: Controlled principally by geomagnetic latitude, with the probability of spread-F occurrence increasing towards high latitudes,

(2) Temporal dependence: A maximum in probability of occurrence is found in the auroral F-region at around 02-04 magnetic local time (MLT). A second maximum was reported by several authors to be permanently located over Northeastern Canada, but it is probable that this is associated with the day-side auroral oval zone of low energy particle precipitation (see Appendix A),

---

29. Bates, H.F. (1971) J. Atmos. Terr. Phys. 33:111.

30. Shimazaki, T. (1959) The occurrence of spread-F and the geomagnetic field, J. Rad. Res. Labs, (Japan) 7:437.

31. Penndorf, R.B. (1960) Research Concerning Forecasting Anomalous Propagation at High Latitudes, AFCRL-TR-60-1162.

32. Tao, K. (1965) World-wide maps of the occurrence percentage of spread-F in years of high and low sunspot numbers, J. Radio Res. Labs, (Japan) 12:317.

33. Singleton, D.G. (1960) The geomorphology of spread-F, J. Geophys. Res. 65:3615.

(3) Seasonal dependence: Maximum probability of spread-F occurrence occurs in winter, with the minimum in summer. This is most likely a solar illumination phenomenon, since it seems that high-latitude spread-F is sharply reduced by the stabilizing influence of ionizing solar radiation. During the long winter night, spread-F is a virtually permanent feature of the high-latitude ionosphere. In day-time, spread-F is normally only seen in the vicinity of the day-side auroral zone (projection of the magnetospheric cleft).

(4) Magnetic activity dependence: At high latitudes, there is a pronounced tendency for the occurrence of spread-F to increase with increasing magnetic activity.[30] This tendency is more apparent at the equinoxes than at the solstices, when a less pronounced correlation with magnetic activity is observed. The equatorward boundary of the spread-F region moves to lower latitudes with increasing geomagnetic activity.[34]

3.2.2 OBSERVATIONS OF SLANT-F

The slant-F phenomenon has been studied by a number of authors.[35, 36, 37] All of these authors note the solar zenith angle control of the occurrence frequency of slant-F. Baggaley, working at Sheffield, England, has presented the most thorough analysis of this aspect of slant-F. He showed that the onset of slant-F is most likely to occur when the solar zenith angle is between 90-110°. From Figures 11 and 12 of Peterson et al[36] a similar conclusion may be drawn, assuming that the echo regions observed by them were about 1000 km to the north. Baggaley notes that the mean duration of slant-F events is 1.5 hr, whereas Peterson et al indicate that many events persist throughout the night, until sunrise in the ionosphere. The difference between these two observations is that Baggaley's were made at sunspot minimum at a northerly latitude, while those of Peterson et al were made at a higher sunspot number and at a more southerly latitude. After sunset, the 17 MHz transmitted beam of Baggaley penetrated the ionosphere as the latter's critical frequency diminished, whereas the ionosphere to the north of Stanford,

---

[34] Davis, R. M. (1973) Dependence of High Latitude Spread-F Occurrence on Solar and Magnetic Activity, U.S. Dept. of Commerce, OT Rept. 73-23.

[35] Baggaley, W. J. (1970) Backscatter observations of F-region field-aligned irregularities during the I.Q.S.Y., J. Geophys. Res. **75**:152.

[36] Peterson, A. M., Villard, O. G., Leadabrand, R. L., and Gallagher, P. B. (1955) Regularly-observable aspect - sensitive radio reflections from ionization aligned with the earth's magnetic field and located within the ionospheric layers at middle latitudes, J. Geophys. Res. **60**:497.

[37] Weaver, P. F. (1965) Backscatter echoes from field-aligned irregularities in the F-region, J. Geophys. Res. **70**:5425.

where the observations of Peterson et al were made, was sufficiently strong to reflect their 17.3 MHz transmissions throughout most nights.

All three authors mentioned above, note that the F-region slant echoes display a range dependence exhibiting an abrupt onset at a short range which may vary considerably. This observation is also related to ionospheric penetration, with the abrupt inner boundary of the echo region corresponding to one half of the classical "skip distance" for ground to ground propagation. All three authors note the aspect sensitivity of the echoes, but the observations of Baggaley are especially interesting because they permit a quantitative estimate to be made of this aspect sensitivity. Baggaley, in his Figure 7, gives the dependence of echo activity on magnetic aspect angle, based on the azimuthal variation of the minimum echo range. He shows the echo strength dropping below noise level (presumably) at 10 degrees off-orthogonality, and the maximum number of echoes at 5 degrees. By relating these results to the probability distribution of F-region echoes recorded in the Polar Fox II experiment,[38] taking into account the different sensitivities of the two equipments, a figure of about 10 dB/degree off perpendicularity is reached.

Baggaley shows that radial velocity of F-region scatterers may lie between 0 and 150 msec, with a mean value of 65 m/sec. This observation made in the United Kingdom, is relevant for a magnetic latitude of about 63°, at night.

3.3 Plasma Motion

The Doppler shift experienced by a radar signal backscattered from ionospheric irregularities is a result of the motion of the plasma in which these irregularities are embedded, together with any component of motion of the irregularities relative to the plasma. The motion of ionospheric plasma in the earth's polar regions is predominantly due to the electrodynamic effects induced by the magnetospheric electric potential distribution. This takes the form of a linear gradient of electric potential in the east-west direction across the earth's magnetospheric tail (see Section 1.3). Figure 2 illustrates the convection pattern induced by this electric field in the equatorial plane of the magnetosphere. The convection pattern in the ionosphere may be visualized by mapping the magnetospheric convection pattern down into the ionosphere along the geomagnetic field lines. Maeda[39] has constructed a model for the E- and F-region plasma drifts, based on a realistic representation of the cross-tail electric field and the electrical conductivity of the ionosphere. Maeda's numerical estimates of ionospheric plasma velocities are in general agreement with many measured values.

---

38. Millman, G. H. (1975) An Evaluation of HF Ionospheric Backscatter Echoes, G. E. Company Rept. R75EMH19.

39. Maeda, H. (1977) Neutral winds and ion drifts in the polar ionosphere caused by convection electric fields - 2, J. Atmos. Terr. Phys. **39**:849.

The basic pattern of ionospheric plasma drift is a "two-cell" pattern[40] in which counter-rotating flows around the periphery of the auroral oval close in an anti-sunward direction across the polar cap. Figure 7 contains an additional plasma drift component due to co-rotation of the earth's atmosphere with the solid earth (see Section 1.3) and is thus the pattern which would be observed from a non-rotating frame of reference, for example, a satellite. This co-rotational component is relatively small compared to the cross-tail magnetospheric electric field component. This pattern has been substantiated and confirmed by a variety of satellite and ground-based measurements. Heelis et al[41] using the Atmospheric Explorer-C satellite at an altitude of 250 km, measured plasma velocities in the region of the dayside cleft and reported velocities in excess of 1 km/sec, exhibiting a reversal near the noon meridian, which is characteristic of the two-cell pattern. Tsunoda et al[42] used data from a ground-based backscatter sounder in the polar cap and confirmed the two-cell pattern by noting the azimuthal pattern of slant-E echoes. Similar inferences can be drawn from the studies of polar cap sporadic-E by Taieb[43] and from measurements of polar cap auroral backscatter made during the Polar Cap III experiment. A useful review of measurements of plasma drift velocities at high latitudes is contained in the works of Doupnik et al,[44] and Doupnik.[45]

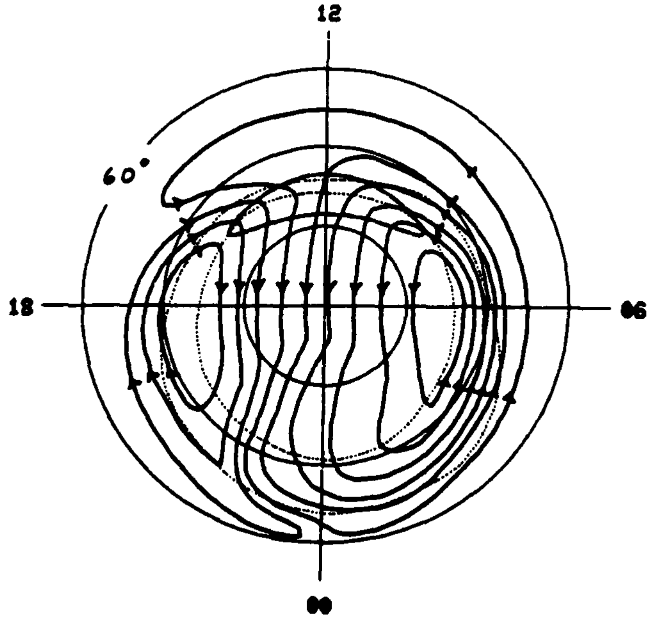

Figure 7. A Model of F-layer Plasma Drift, Including Effect of Earth Rotation (after Heppner, 1977). The drift speed is proportional to the density of flow lines, being about 0.5 km/sec near the pole. The coordinate system is the CGS. The auroral oval (Q = 3) is shown dotted and the region of magnetiospheric cleft precipitation near noon is shown dashed

---

(Due to the large number of references cited above, they will not be listed here. See References, page 87.)

The velocity pattern for E-region plasma differs significantly from the F-region pattern. Due to the very low F-region collision rates, the Hall conductivity of the F-region is negligibly small, whereas in the E-region it is very high. Thus the motion of plasma in the F-region is in the direction of the imposed electric field, whereas in the E-region, there is a large component orthogonal to the electric field. The analysis of Maeda[39] has taken into account these and other factors and will be used as the basis of the model to be developed for radar Doppler shifts in Section 5.

3.4 Summary of Auroral Radar Experiments

A wealth of experimental evidence has been collected over a span of three decades on the subject of the radio aurora. In spite of this large data base, many aspects of this complex phenomenon remain obscure. Unwin[46] published a general survey of the morphology of radar aurora including its diurnal and seasonal variations, noting that E-region radio aurora manifests itself in two distinctly different forms—diffuse and discrete. Unwin and Baggaley[47] have published an updated review of the E-region radio aurora, and a great many authors have reported experimental studies performed with a variety of instruments. An exhaustive survey of this work would be far too lengthy to be included in this section, and only major findings will be discussed. In particular, since primary interest in this work is in connection with HF radio aurora, special attention will be given to observations made at HF and low VHF.

Diffuse aurora exhibits little structure in both spatial and Doppler domains, and is found to exhibit a close relationship to the eastward auroral electrojet, occurring equatorward of the statistical auroral oval in the late afternoon and evening. Discrete radio aurora is found predominantly in the hours around midnight and shortly after, and exhibits sharply defined structure in space and velocity. Discrete aurora is associated with the so-called "break-up" phase of the visual aurora. While discrete auroral returns are rare in the late afternoon and evening, diffuse returns are observed at all times, though in combination with discrete returns after midnight. Greenwald et al[48] have demonstrated convincingly that the diffuse auroral backscatter is collocated with auroral currents. The observations of Unwin[46] demonstrate that the currents associated with the aurora at CGL ~60° are

---

46. Unwin, R.S. (1966) The morphology of VHF radio aurora at sunspot maximum II. The behavior of different echo types, J. Atmos. Terr. Phys. 28:1183.

47. Unwin, R.S., and Baggaley, W.J. (1972) Ann. Geophys. 28:111.

48. Greenwald, R.A., Eckland, W.L., and Balsley, B.B. (1975) Radar observations of auroral electrojet currents, J. Geophys. Res. 80:3635.

frequently intense enough to produce strong radio aurora at that latitude. Many other experiments,[49,50,51] also have demonstrated appreciable radar backscatter from sub-auroral latitudes.

The diurnal variation of auroral backscatter exhibits two maxima, corresponding to the diffuse and discrete echo types. Summarizing the results of many experiments, too numerous to cite individually, the evening maximum of diffuse aurora occurs between 16 and 19 CGT, and the "midnight" maximum of discrete echoes occurs between 23 CGT and 02 CGT. The intensity of auroral backscatter also exhibits periodicities on a long time scale (seasonal and solar cycle). The seasonal variation exhibits maxima at the equinoxes, with a minimum in summer and a still deeper minimum in winter. In terms of probability of occurrence, the equinoctial maxima are roughly twice as great as the winter minimum. The solar cycle dependence shows a positive correlation between radio auroral activity and sunspot number, with the former lagging the latter by 1-2 years. These seasonal and solar cycle periodicities are consistent with the generation of auroral irregularities by ionospheric currents, being very similar to the corresponding long term periodicities in magnetic activity index (see Section 6). In fact, as many authors have demonstrated, auroral radar intensity is strongly correlated with geomagnetic activity. Unger et al[52] obtained better correlation between auroral radar activity and a composite "solar-planetary" index (the product of K_p and sunspot number) than with either index separately.

The observations noted thus far were made at VHF and UHF and relate to the E-region, since geometric constraints make F-region irregularities inaccessible to line-of-sight radars. In order to observe ionospheric backscatter from the F-region, observations at HF are necessary, utilizing ionospheric refraction to achieve magnetic orthogonality at the required altitudes. The most comprehensive HF auroral radar experiment yet performed was the Polar Fox II experiment[53] in Northern Maine. The results of this experiment will be used extensively in developing the clutter model in this report. F-region backscatter was found by Polar Fox II to be virtually always present, during nighttime at some range. Another thorough

---

[49] Flood, W.A. (1960) VHF auroral backscatter measurements, J. Geophys. Res. 65:2261.

[50] Gartlein, C.W., Sprague, G., and Waag, R.C. (1960) 41 Mc/s IGY auroral radar at Ithaca, New York, J. Geophys. Res. 65:2255.

[51] Watkins, C.D. (1961) Auroral radio-echoes and magnetic disturbance, J. Atmos. Terr. Phys. 20:131.

[52] Unger, J.H.W., Hardin, R.H., and Horan, H.H. (1973) Joint Radar Propagation Study, Bell Telephone Labs, October 1.

[53] Edwards, L.C., Katz, A.H., Patton, D.E., and Campbell, J.W. (1973) Polar Fox II - Experimental Phase, Vol. II, Executive Summary RADC-TR-73-203.

study of HF auroral backscatter was conducted at Ava, New York,[54] at CGL = 56°. The maximum occurrence of auroral associated F-region backscatter was found to occur between 20 MLT and 08 MLT in both winter and summer. The probability of F-region backscatter, at 03 MLT at the ionospheric intersection point (~67° CGL) was over 90 percent. A high power backscatter experiment conducted in the south of England produced similar results. The probability of F-region backscatter in this experiment was over 80 percent, and the amplitude of the returns from the auroral region exceeded that from the temperate latitude ionosphere by 30-50 dB. The F-region backscatter was found to have a sharp leading edge and a gradual trailing edge, and the apparent scatter cross section, in the range 8-10 MHz was found to increase with decreasing frequency. In one particular instance, the sharp leading edge of F-backscatter was observed at 700 km, when the operating frequency was 10.1 MHz and the F-region critical frequency was 3 MHz. An analysis performed in Section 4.6 will show that this observation is consistent with refracted propagation through an irregular F-region. The amplitude of F-region clutter was found to be strongly correlated with magnetic activity.

Other experiments performed at HF include those of Hower et al[55], Weaver,[37] Swenson,[56] Brooks,[25] Baggaley,[35] Peterson et al,[36] Malik and Aarons,[57] Czeckowsky et al,[26] and Sprenger and Glode.[27] In general these experiments all show F-region auroral related backscatter to be a highly common phenomenon, especially at night and increasing in intensity with increasing geomagnetic activity. Another important fact which these experiments revealed is that the characteristics of the ionospheric propagation path between radar and irregularities are a factor of major importance in determining the probability of F-region backscatter.

Recently, Oksman et al[58] have conducted a comparison between VHF auroral measurements and HF backscatter observations. They have shown that the backscatter cross section of the radio aurora follows a wavelength cubed low in this frequency range. These workers found that F-region radio aurora often occurred on the same magnetic L-shells as E-region radio aurora and often occurred in two different geomagnetic latitude regions—one associated with the auroral oval and a

---

54. Katz, A.H. (1971) HF Auroral Backscatter Study, AVCO Rept. AVSD-0378-71-RR.
55. Hower, G.L., Ranz, D.M., and Allison, C.L. (1966) Comparison of HF radar echoes and high latitude spread-F measurements, J. Geophys. Res. 71:3215.
56. Swenson, E.M. (1972) Aspect-sensitive reflections from ionization irregularities in the F-region, J. Atmos. Terr. Phys. 34:1469.
57. Malik, C., and Aarons, J. (1964) A study of auroral echoes at 19.4 megacycles per second, J. Geophys. Res. 69:2731.
58. Oksman, J., Moller, H.G., and Greenwald, R. (1979) Comparisons between strong HF backscatter and VHF radar aurora, Radio Sci. 14:1121.

second with the poleward wall of the ionospheric trough. This second group of trough-related echoes appears only at sunspot minimum and is absent at sunspot maximum.

Many workers have studied the Doppler characteristics of the radio aurora over many years. A controversy exists over whether or not auroral plasma irregularities travel at the local ion-acoustic velocity, or at the electron drift velocity or at some combination of these two. Measurements at UHF[59] tend to support the first of these alternatives, but measurements at lower frequencies (for example, at 50 MHz)[60] tend to support the second alternative. A recent paper by Greenwald et al[61] has discussed this "velocity question". In developing the velocity/Doppler model in this report, it will be assumed that the apparent velocity of auroral scatterers, in the HF range, is that of the electron drift velocity.

3.5 Altitude of the Radio Aurora

Many studies have established that the E-region radio aurora is confined to a narrow range of altitudes, centered at about 110 km. For example, Unwin[22] deduced a height of 110.9 ± 3.1 km, with a vertical thickness of the radio scattering layer of ~5 km. Abel and Newell[59] reported an altitude of ~110 km with thickness of 10-15 km. Barber et al[62] reported an altitude of 110 ± 1 km with a thickness of a few kilometers. Unger et al[52] report an altitude of 110-120 km with a thickness of 6-8 km. The altitude of F-region radio scatterers in the auroral region is, on the other hand, much less well-defined. Irregularities almost certainly exist throughout the entire altitude range of the F-region, from about 180-200 km and upwards. The intensity of these F-region irregularities is roughly proportional to the ambient electron density, so that the most intense irregularities may be expected near the peak of the F-layer (typically 250-350 km).

In this report, the altitude of the E-region radio aurora will be taken as 110 km. The average vertical thickness of the scattering layer will be taken as ± 5 km between -10 dB points, that is, between altitudes at which the backscatter volumetric cross section is 10 dB lower than its value at 110 km. Where it is necessary to

---

59. Abel, W.J., and Newell, R.E. (1969) Measurements of the afternoon radio aurora at 1295 MHz, J. Geophys. Res. 74:231.
60. Greenwald, R.A., and Eckland, W.L. (1975) A new look at radar auroral motions, J. Geophys. Res. 80:3642.
61. Greenwald, R.A., Weiss, W., Neilsen, E., and Thomson, N.R. (1978) STARE: A new radar auroral backscatter experiment in northern Scandinavia, Radio Sci. 13:1201.
62. Barber, D., Sutcliffe, H.K., and Watkins, C.D. (1962) Some radar observations of meteors and aura at 300 and 500 Mc/s using a large radio telescope - II. Observations of the aurora borealis, J. Atmos. Terr. Phys. 24:599.

assume an altitude for F-region auroral scatterers, this will be taken as any altitude above 180 km. At night, the peak F-region volumetric backscatter cross section will be assumed to occur at 300 km.

4. AURORAL CLUTTER MODEL

As a first step towards a model predicting the magnitude of auroral backscatter, the morphological data discussed in Section 3 has been used to construct a model for the distribution, in space and time, of the probability of irregularity occurrence. This model will subsequently be translated into a model for the auroral backscatter magnitude.

4.1 E-Region Probability of Occurrence

The space-time distribution of the probability that fE_s exceeds 3 MHz, deduced by Besprozvannaya and Shchuka,[21] referred to in Section 3.1, is used as the basis for the quantitative model for E-region irregularity occurrence. These authors reported that auroral sporadic-E appeared to be confined to two ring-shaped maxima encircling the geomagnetic pole, separated by a minimum at about 65° geomagnetic latitude. If the probability that $fE_s \geq 3$ MHz is represented by the product of a function of geomagnetic latitude and one of geomagnetic time, it may be written as

$$p_1(E) = p_1(\Phi) \cdot p_1(T)$$

for the high latitude ring, and

$$p_2(E) = p_2(\Phi) \cdot p_2(T)$$

for the low latitude ring where

$$p_1(\Phi) = \exp \frac{(\Phi - A)^2}{9}$$

and

$$A = 72 - 1.5\,(K_p - 2) + 2 \cos \frac{\pi}{12}(T - 18)$$

$$p_1(T) = 0.5 + 0.3 \cos \frac{\pi}{12}(T - 1)$$

$$p_2(\Phi) = \exp - \frac{(\Phi - 63)^2}{6}$$

and, letting G = min(D; 365 - D)

$$p_2(T) = \log (K_p + 1)^2 \; [0.50 - 0.125 \cos \frac{\pi}{12} (T - 3) \cdot (1 - \cos \frac{2\pi D}{365})$$

$$- 0.5 \exp (-0.1 (T - 19)^2 \cos \frac{2\pi D}{365}$$

$$- 0.45 \exp - (6.7 \times 10^{-5} G^2) \exp - (0.25 (T - 10)^2)]$$

and K_p is planetary magnetic index. There is also a small peak in sporadic-E occurrence at the geomagnetic pole, which can be represented by

$$p_3(E) = 0.3 \exp - \frac{(\Phi - 90)^2}{20} .$$

In these expressions, the units for Φ are degrees and those for T are hours. The Gaussian functions are chosen for their convenient asymptotic properties, and have no other special significance. The probability that $fE_s \geq 3$ MHz is represented by the sum of the three components $p_1(E) + p_2(E) + p_3(E)$.

The magnetic activity dependence of the low latitude ring, contained in $p_2(T)$, is an attempt to fit approximately the published data by an arbitrary mathematical function for purposes of convenient numerical computation.

A computer program has been written to compute P(E) for arbitrary location and time and magnetic activity. Figure 8 (a-f) shows the distribution in CGS of the resultant probability of E-region irregularity for summer, winter and equinox seasons and for two levels of geomagnetic activity (K_p = 2, 4). In order to illustrate the range—azimuth dependence of p(E) from a specific site, Figure 9 has been produced for a location at $\Phi = 61°$. Contours are shown for summer at intervals of 0.2 (that is, 20 percent probability) for Universal midnight and $K_p = 2$. The rough outline of the auroral oval is evident, as is the minimum in E_s occurrence at 65° magnetic latitude and the peak near the geomagnetic pole.

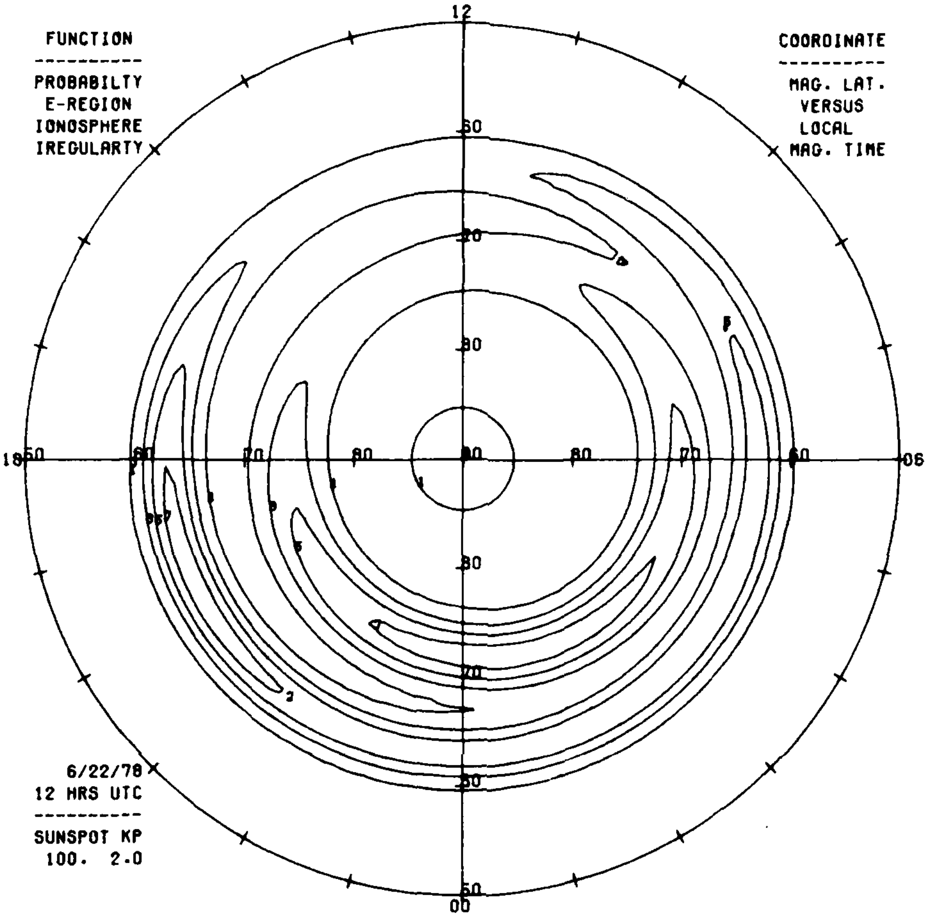

(a)

Figure 8. Contours of Probability of E-region Irregularity in CGS at 12 UT for Summer, Equinox and Winter and for K_p = 2 and 4. Contours are in intervals of 0. 2

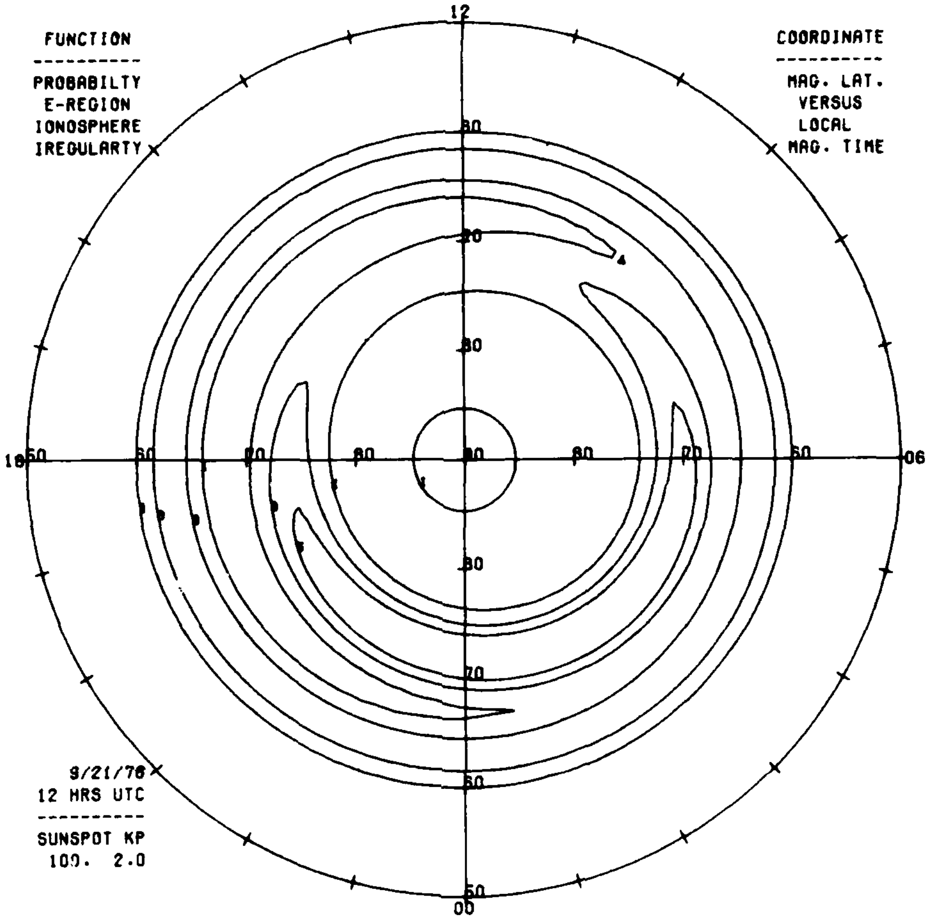

(b)

Figure 8. (Cont)

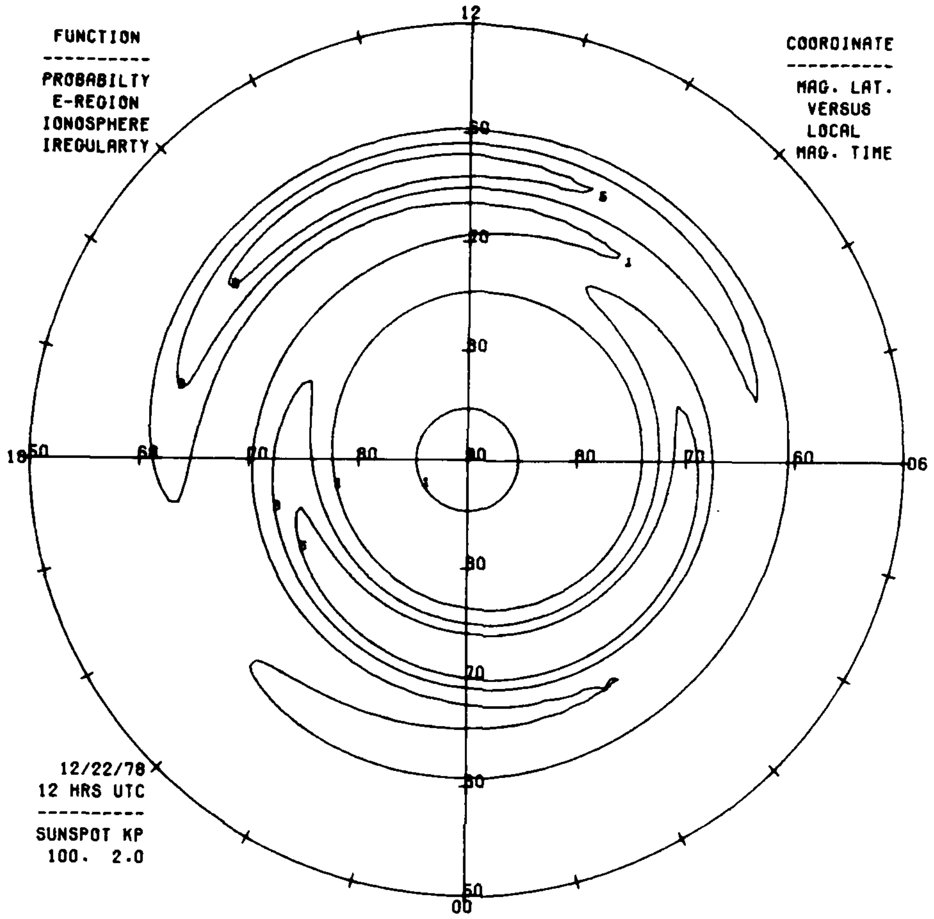

(c)

Figure 8. (Cont)

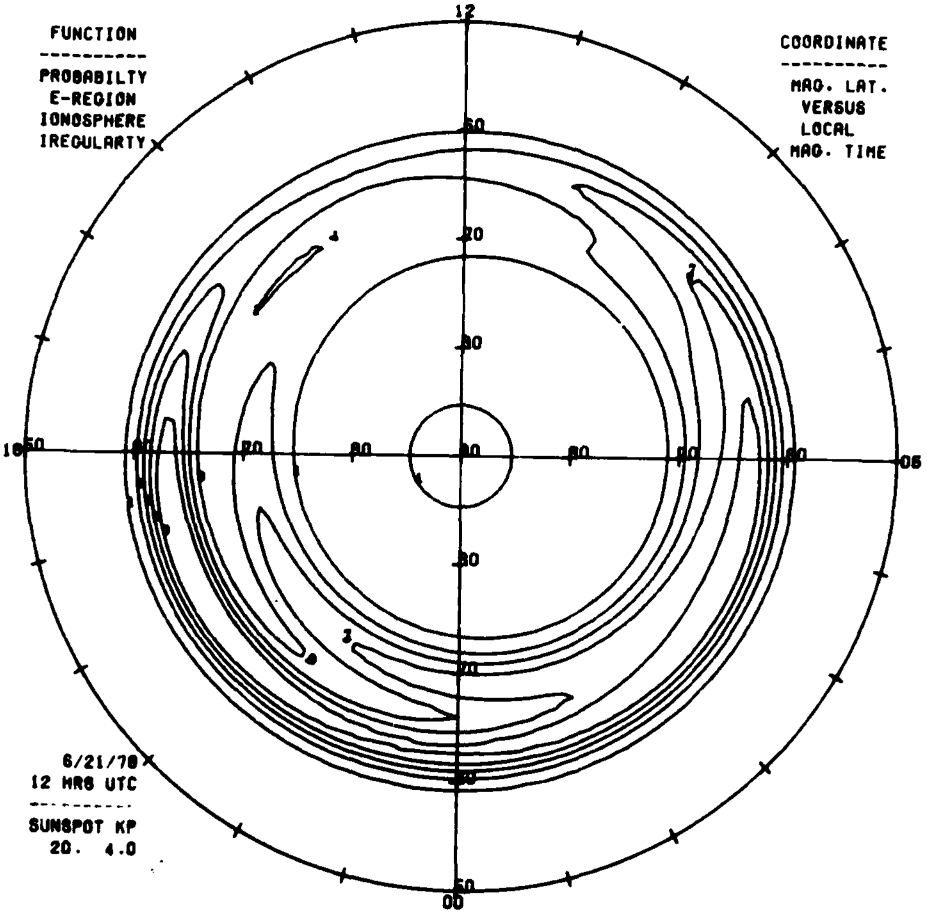

(d).
Figure 8. (Cont)

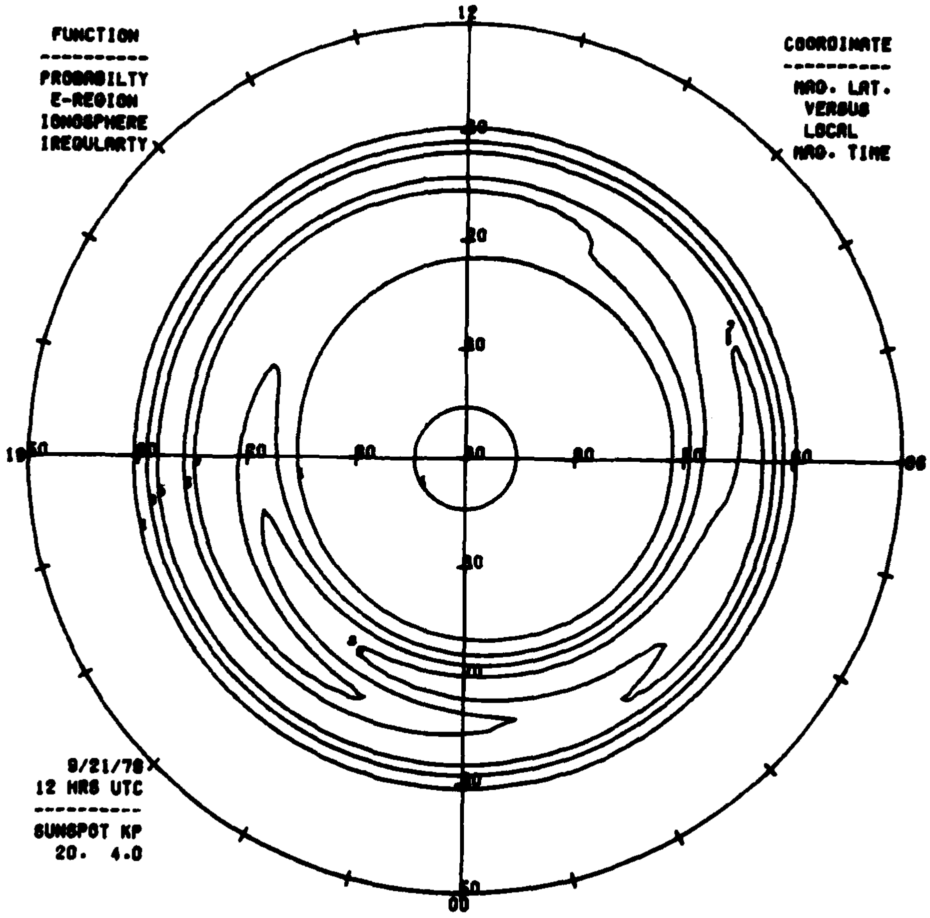

(e)
Figure 8. (Cont)

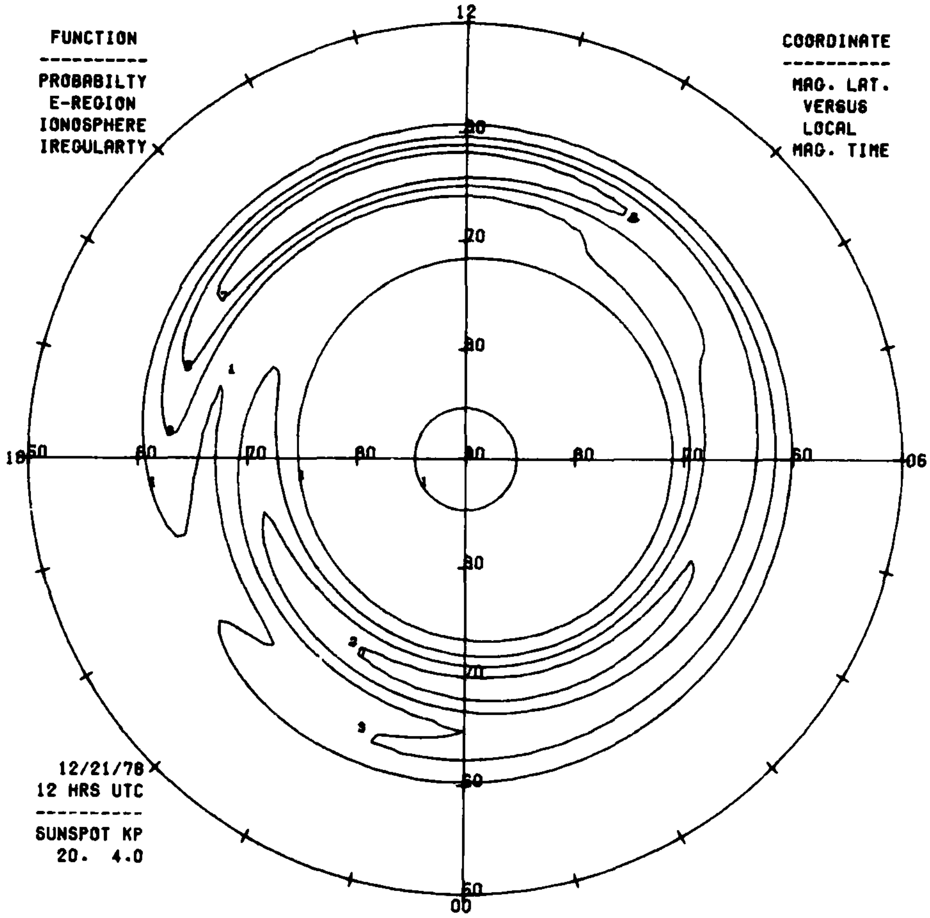

(f)

Figure 8. (Cont)

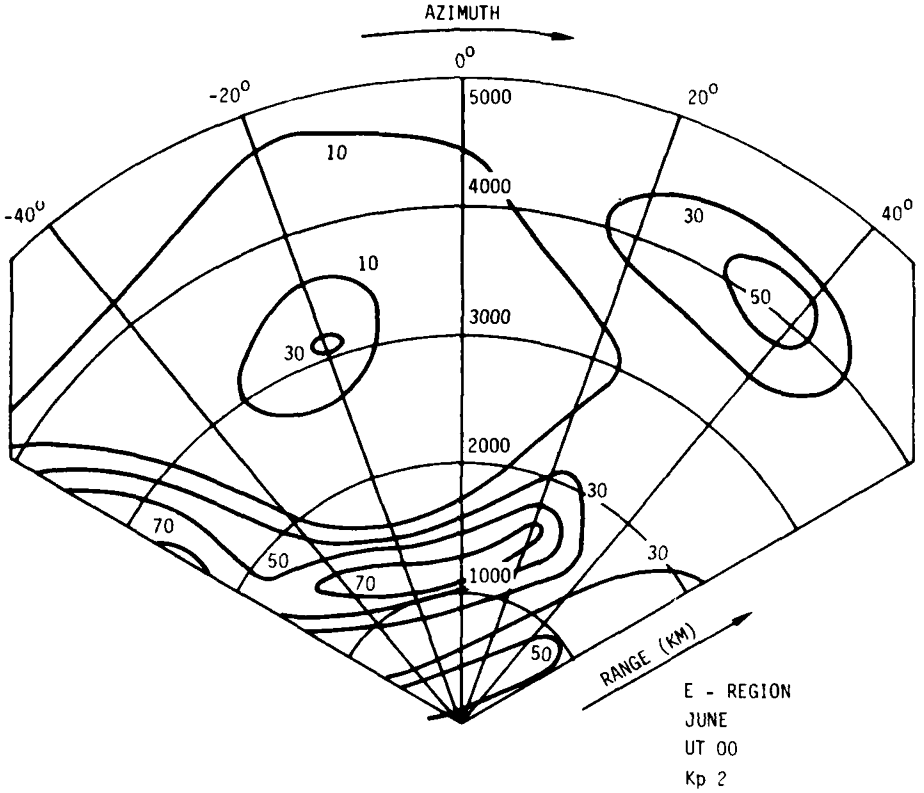

Figure 9. Probability of E-region Irregularity as a Function of Range and Azimuth for Site at 61° CGL; June, $K_p = 2$, UT = 00. Contours labelled in percentage

4.2 F-region Probability of Occurrence

Section 3.2 contained a discussion of the morphology of F-region small scale irregularities in the polar region and their general relationship to HF backscatter (slant-F). A model has been constructed based primarily on the references cited in that section, and this model has been compared to available backscatter data in the auroral and sub-auroral regions.

The F-region irregularity model is considered in two separate parts—the nighttime auroral maximum and the dayside magnetospheric cleft region. The nighttime component expresses the probability of F-irregularity as

$$p_1(F) = p_1(\Phi) \cdot p_1(T)$$

where

$p_1(\Phi)$ is a geomagnetic latitude term

$p_1(T)$ is a geomagnetic time term

and

$$p_1(\Phi) = \exp - a[\Phi - (70.5 - 1.5\,K_p)]^2$$

$$p_1(T) = \exp - b\left[\frac{(T - 2)}{K_p + 1}\right]^2$$

where

$a = +\,0.01178$

$b = +\,0.4834$

K_p = planetary magnetic index

and

Φ is measured in radians.

The dayside cleft region is modelled similarly, as the product of a geomagnetic latitude function and a geomagnetic time function

$$p_2(F) = p_2(\Phi) \cdot p_2(T)$$

where

$$p_2(\Phi) = \exp - [0.1337(\Phi - A)^2]$$

$$p_2(T) = \exp - [0.1003(T - 12)^2]$$

and

$$A = 78 + \cos\frac{\pi}{12}(UT - 18) + \cos\frac{2\pi}{365}(D - 182.5) - 1.5\cos\frac{\pi}{6}(T - 6)\,.$$

Here

UT = Universal Time

and

D = Julian day number.

This model contains latitudinal, seasonal, magnetic, and Universal Time dependencies. It is based on the work of Whalen and Pike[63] who measured the position of the equatorward boundary of the irregularity zone with an airborne ionosonde, and modified by the work of Burch[64] and Oguti and Marubashi.[65] These latter authors showed, respectively, the dependence on the angle between the earth's magnetic axis and the ecliptic plane and geomagnetic latitude and time dependences of the dayside cleft region.

Because of the pronounced seasonal variations in the lengths of the solar-illuminated day at high latitudes, and because many authors (for example, some cited in Section 3. 2) note that solar illumination inhibits formation of F-region irregularities, it was necessary to add a third component of probability of F-irregularity formation, dependent on solar zenith angle (χ).

Thus

$$p_3(F) = A \exp - \frac{(90 - \Phi)^2}{900} \; ; \; \chi > 101°$$

where

$$A = 0.2 \cos \frac{2\pi D}{365} + 0.7$$

$$p_3(F) = 0; \quad \chi < 90°$$

and

$$p_3(F) = 0.909 \, (\chi - 90) \cdot p_3(F) \Big|_{\chi = 101°}$$

for $90° < \chi < 101°$.

---

[63] ~~Whalen~~, J.A., and Pike, C. (1973) F-Layer and 6300-A measurements in the day sector of the auroral oval, J. Geophys. Res. 78:3848.

[64] Burch, J.L. (1972) Precipitation of low-energy electrons at high latitudes; Effects of interplanetary magnetic field and dipole tilt angle, J. Geophys. Res. 77:6696.

[65] Oguti, T., and Marubashi, K. (1966) Enhanced ionization in the ionospheric F_2 region around geomagnetic noon in high latitudes, Repts. Ionos. Spa. Res. (Japan), 20:96.

In these equations there exist three domains of χ: When the sun does not illuminate the lower F-region ($\chi > 101°$) we have a geomagnetic latitude dependence and a seasonal dependence of irregularity probability. When the sun illuminates the ground ($\chi < 90°$) we have total inhibition of irregularity formation. Between these two domains there is a linear matching function ensuring a non-abrupt transition.

The final expression for the probability of F-region irregularity formation is

$$p(F) = p_1(F) + p_2(F) + p_3(F)$$

subject to the condition that p(F) cannot exceed unity. A computer program has been written to compute p(F) for arbitrary location and geophysical variables. Figure 10 (a-f) shows the distribution in CGS of the resultant probability of F-region irregularity for summer, winter, and equinox seasons and for two levels of geomagnetic activity ($K_p = 2, 4$). By taking cuts through one of these contour plots, Figures 11 and 12 have been produced, showing the probability of irregularity as a function of CGL for 00, 03, 06, and 12 MLT, in summer for moderate magnetic activity.

In order to illustrate the range-azimuth dependence of p(F) from a specific site, Figure 13 has been produced for a site at $\Phi = 61°$. Contours are shown for summer, at intervals of 0.2 (that is, 20 percent probability) for Universal midnight. The general outline of the auroral oval is apparent in this figure, with the nighttime maximum occurring close to the observing location and the daytime ("cleft" region) maximum occurring at a range of 4000 km.

4.3 Scatter Volume and Volume Reflectivity

The estimation of the backscattered power from the aurora is a complicated procedure in the case of an HF radar. It is necessary first to compute the volume of auroral scatterers illuminated by the radar and the magnetic aspect angle; a knowledge of the volume reflectivity of the auroral scatterers, as a function of aspect angle and frequency, is then required to complete the computation. The calculation of illuminated volume in the presence of substantial ionospheric refraction is very different from the corresponding calculation at VHF and UHF where straight-line radio propagation can be assumed with accuracy. Appendix C contains a discussion of this subject, and an expression is derived for the scatter volume in terms of radar parameters (antenna beamwidth, equivalent pulse length) and properties of the HF ray trajectories, which themselves depend on ionospheric structure and radar frequency.

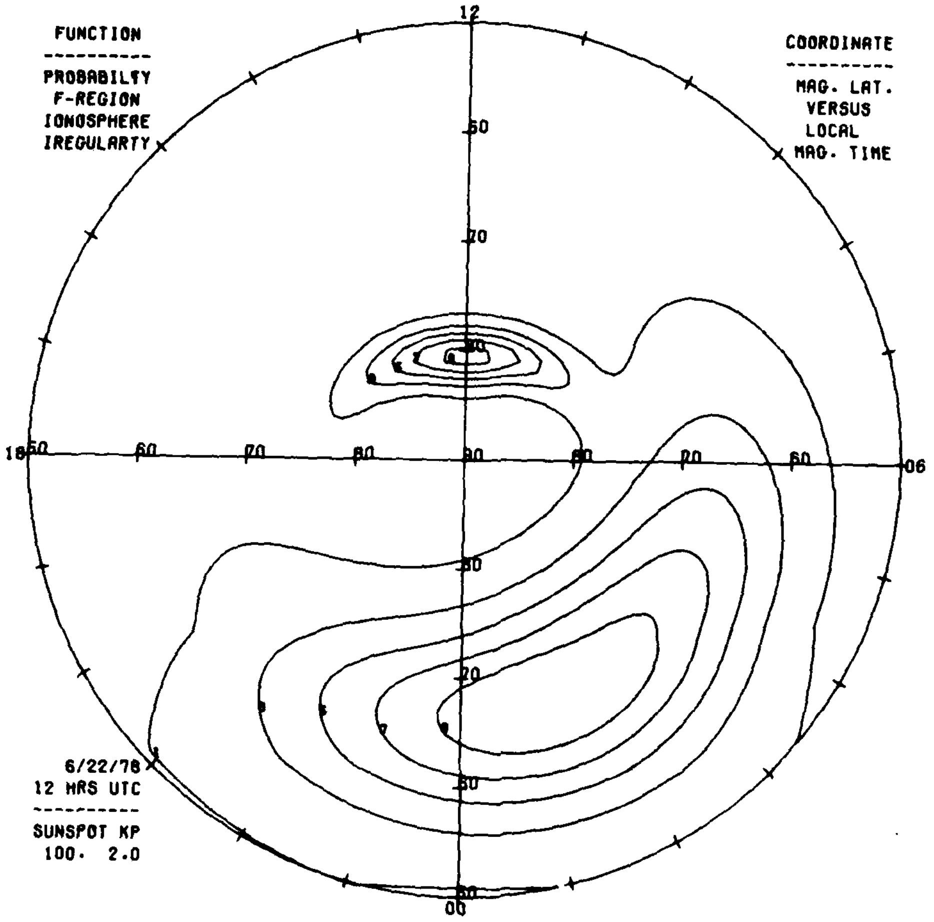

(a)

Figure 10. Same as Figure 8, Except for F-Region

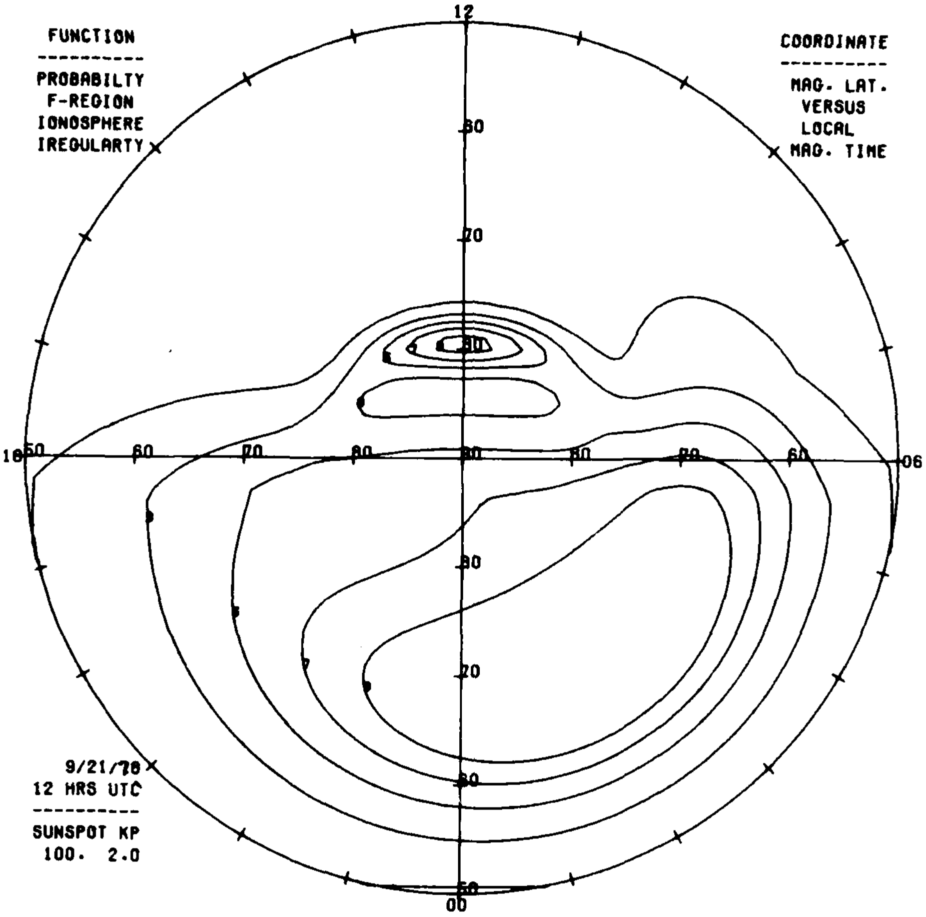

(b)

Figure 10. (Cont)

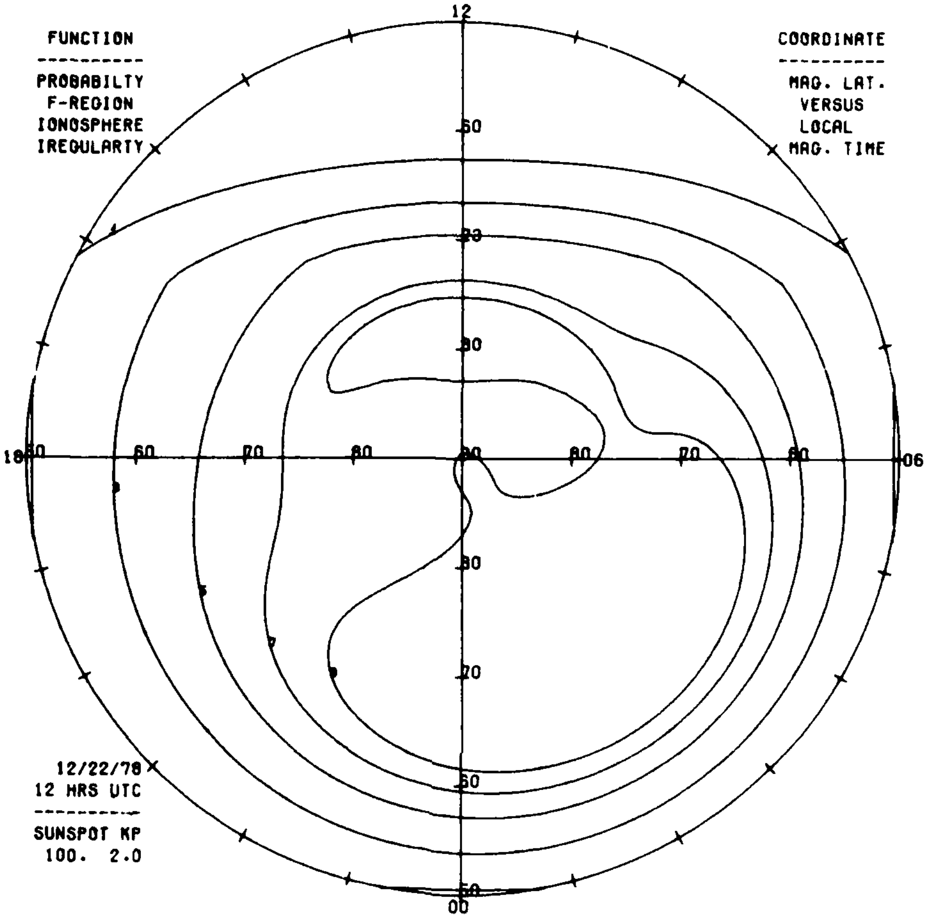

(c)

Figure 10. (Cont)

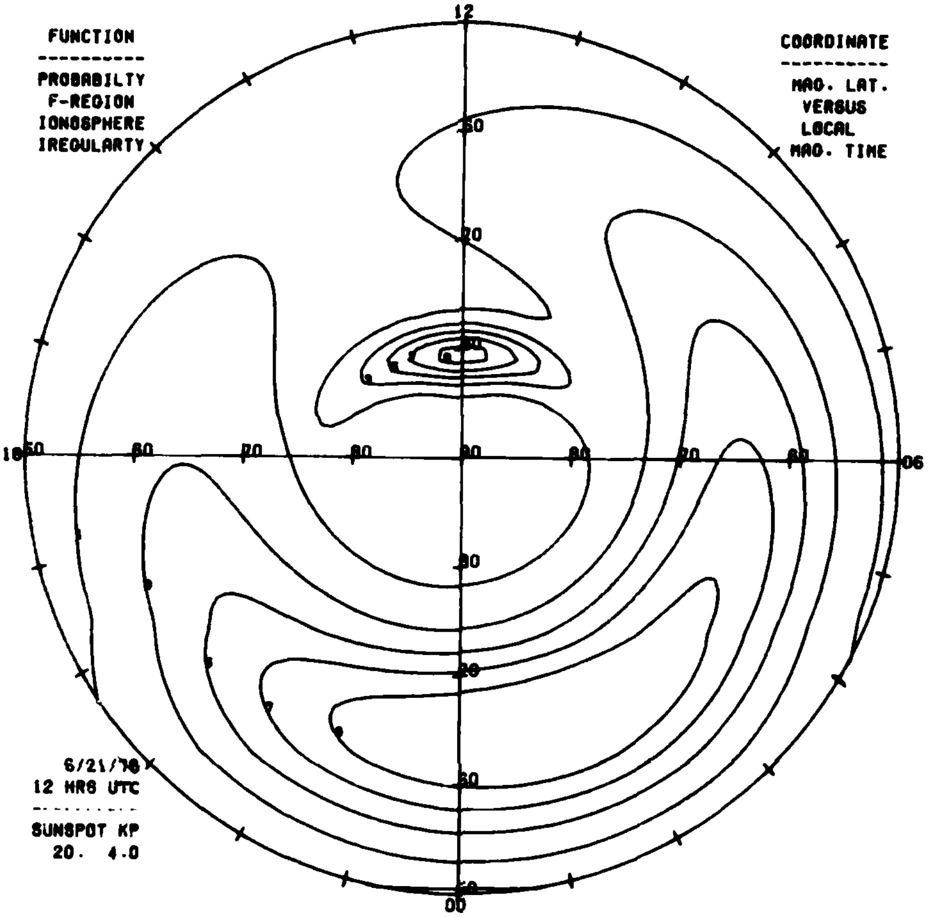

(d)

Figure 10. (Cont)

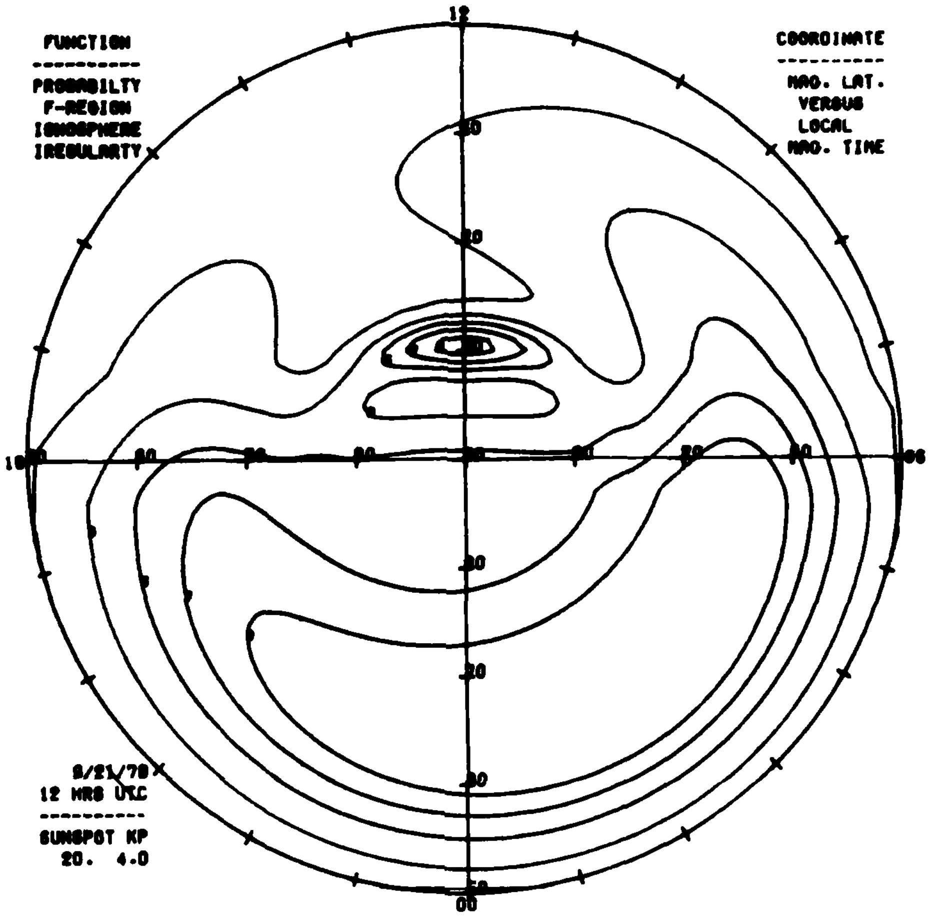

(e)

Figure 10. (Cont)

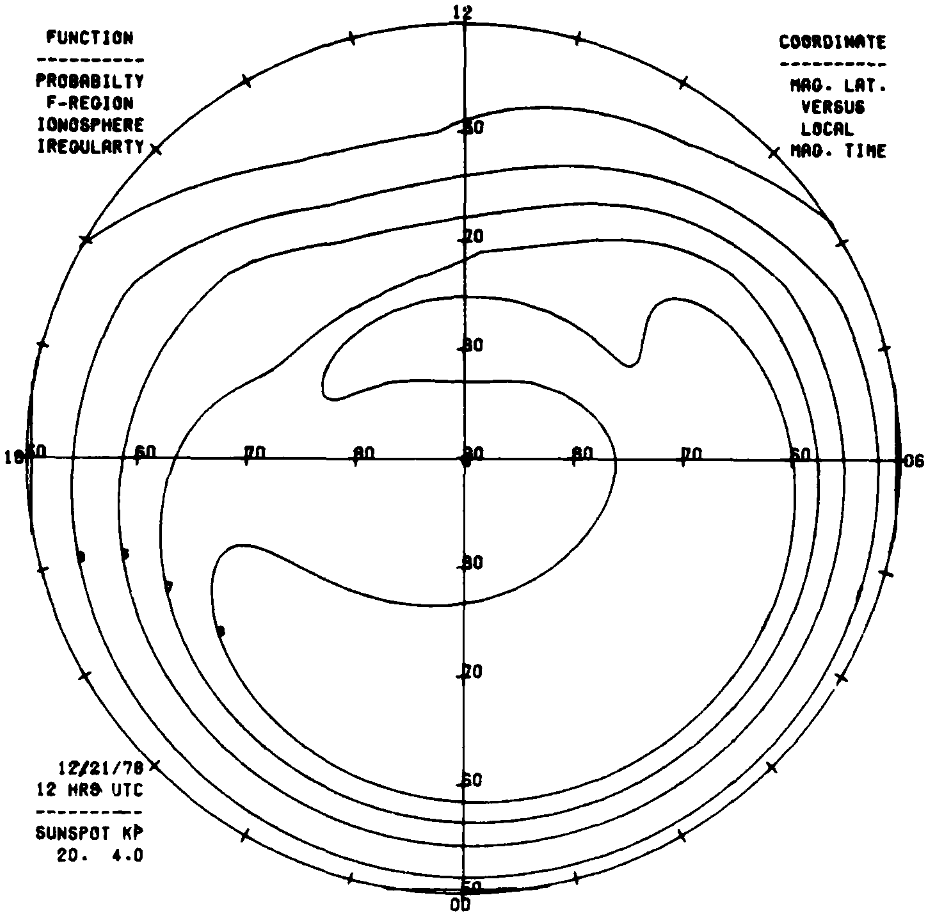

(f)

Figure 10. (Cont)

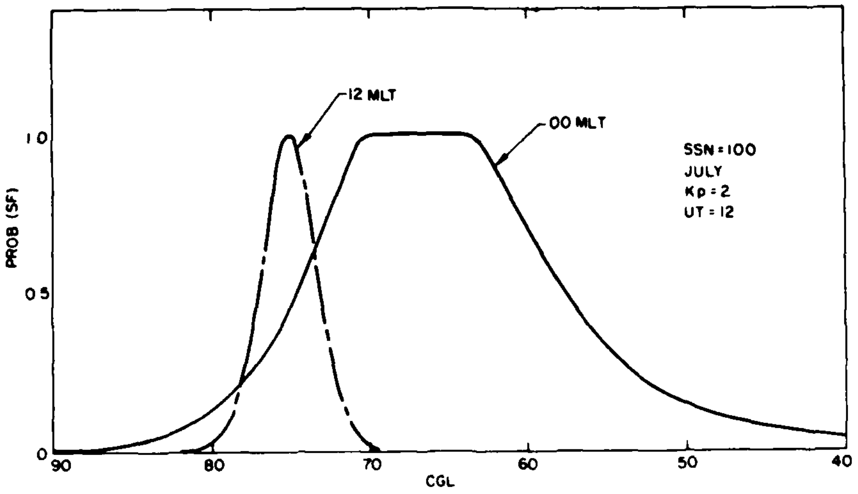

Figure 11. Probability of F-Region Irregularity as Function of CGL for July at Magnetic Midnight and Midday (K_p = 2; UT = 12)

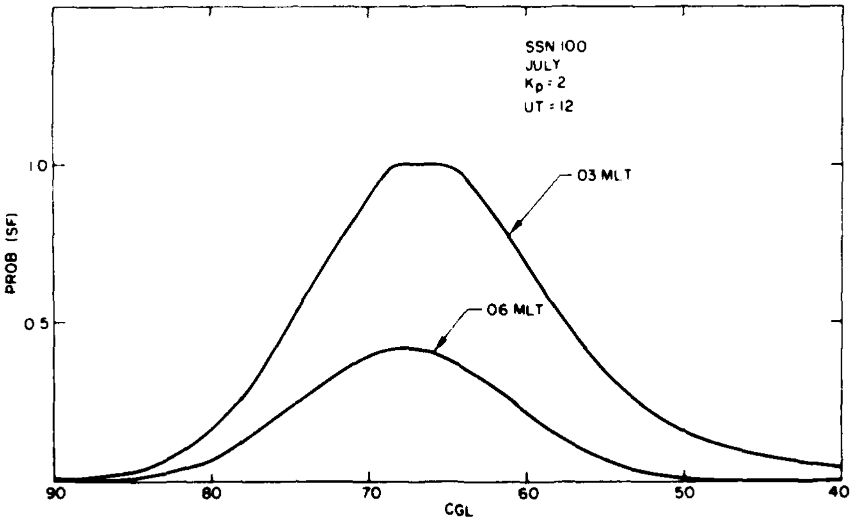

Figure 12. Same as Figure 11, Except for 03 and 06 MLT

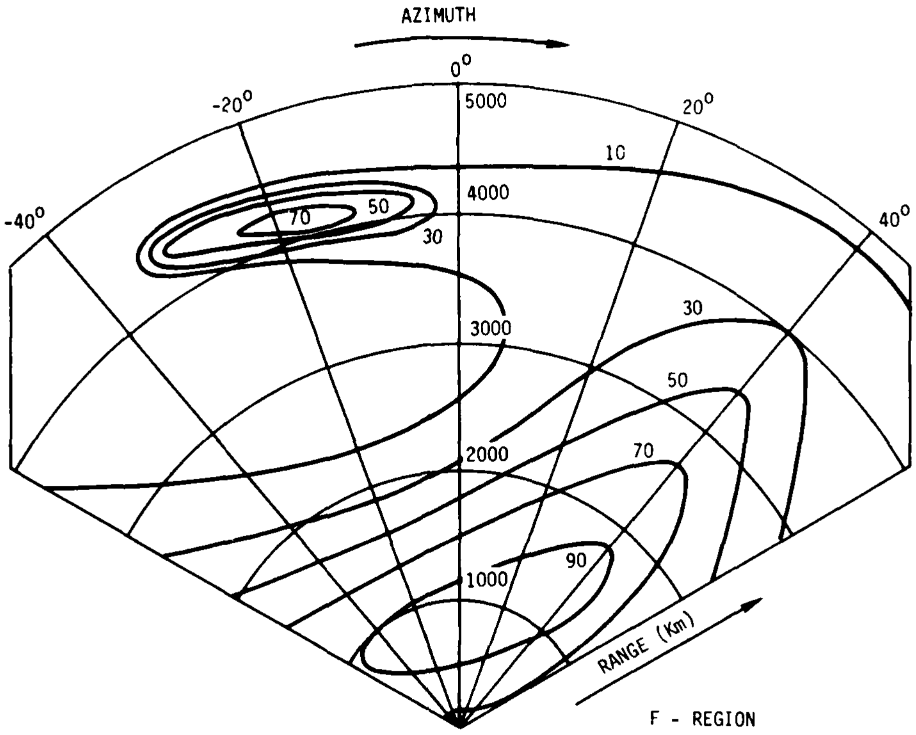

F - REGION
JUNE
UT 00
Kp 2

Figure 13. Same as Figure 9, Except for F-region

The scatter volume for an HF radar, under certain conditions, may be computed relatively simply in a manner analagous to the procedure for VHF and UHF radars. At night and/or at relatively high frequencies in the HF band, the refraction in the ionosphere may be small. Certainly, under these conditions there is very little ionization in the lower ionosphere, so that it is legitimate to compute E-region clutter amplitude on the basis of straight-line propagation. In this case the scatter volume is determined solely by radar pulse length and antenna azimuthal beamwidth (see Figure 14).

The determination of volumetric cross section, that is, the effective point target cross section per unit volume of scatterers, is complicated by the same factors which make the computation of scatter volume difficult. Auroral backscatter measurements at HF have never been translated into reliable volumetric cross-section measurements because of the difficulty in computing the scatter volume. One approach to overcoming this problem is to extrapolate HF cross sections from VHF and UHF measurements, but the frequency scaling law is not known with reasonable precision, partly due to the uncertainty whether the relevant plasma irregularities in each case result from a common physical process. The approach adopted in this report has been to extrapolate data from a HF radar experiment to any location and time by use of the occurrence probability statistics developed in this section.

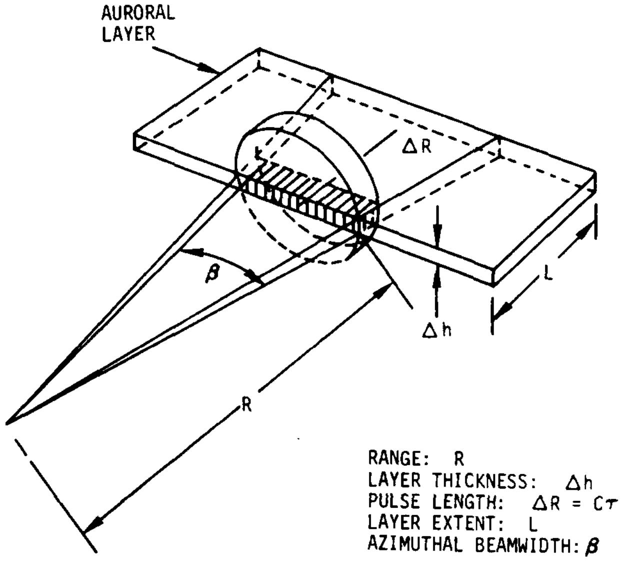

Figure 14. Illustrating Intersection of a Radar Pulse With a Thin Auroral Layer. The scattering volume is determined by azimuthal beamwidth, pulse length, and layer thickness

Data from the Polar Fox II experiment have been analyzed at RADC[66] to provide a "pseudo volumetric cross section." Data for the nighttime hours of October 1971 were reduced to equivalent point target cross sections by solving the radar equation using Polar Fox II radar parameters. A representative value for illuminated volume was used, based on the geometry of ionospheric ray paths in an average nighttime ionosphere (Figure 15, Sales),[67] to reduce this to a volumetric cross

---

[66] Ring, W., and Richards, E. (1978) Fall URSI Symposium, Boulder, Colorado.

[67] Sales, G.S. (1977) URSI Spring Meeting, Palo Alto, California.

section. Ionospheric absorption was taken into account in deducing these cross sections but no attempt was made to include the auroral component of absorption. The measurements of received clutter power which were used were averaged over the entire ± 16 Hz range of the Polar Fox II Doppler processor. Thus, if it were desired to normalize the resultant cross sections in the Doppler domain, it would be necessary to divide them by 32η, where η is a "filling factor" representing the distribution of energy within the range of the Doppler processor (in the case of uniform Doppler distribution, for example, $\eta = 1$). It should be noted also that the range of the Polar Fox Doppler processor was inadequate to permit unambiguous spectral power measurement. Thus the measured Doppler dependence of received power is distorted by the Doppler fold-over which results from spectral power outside the processor range.

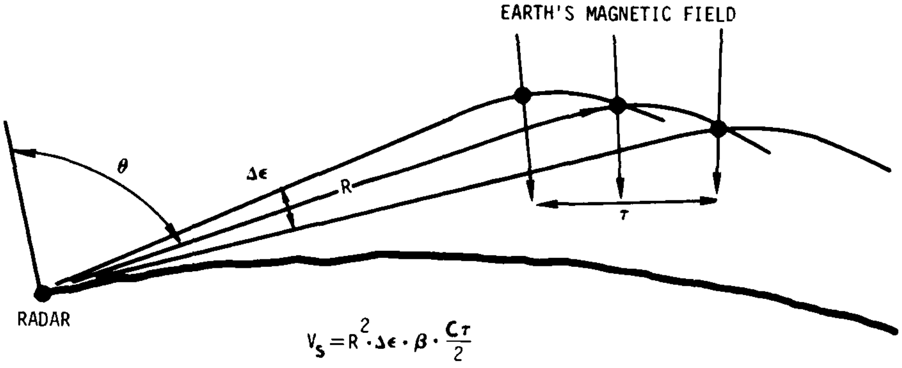

Figure 15. Scatter Volume in the Presence of Ionospheric Refraction. The effective vertical angle at the radar is determined by the pulse length

When the factors noted in the preceding paragraph are considered, it is apparent that the "pseudo volumetric cross section" measurements must be treated with caution. Alternatively, the greatest confidence may be placed in them in applications which approximately duplicate the Polar Fox II measurements, especially in respect to location with respect to the auroral oval and Doppler processor range. Since the present application fits this requirement, it is considered appropriate to extrapolate the Polar Fox II results, provided that illuminated volume is computed in the same approximate way, and auroral absorption is not included in the loss term of the radar equation.

The "pseudo volumetric cross sections" from the RADC Study may be represented by separate normal distributions for E- and F-layers for each of the four frequencies studied, in the range 7-19 MHz (Figures 16 to 19). The medians for these distributions, at 10 MHz, can be estimated as

$$\sigma_v' \sim -99\ \mathrm{dB}(\mathrm{m}^2/\mathrm{m}^3),\quad \text{E-region;}$$

$$\sigma_v' \sim -77.5\ \mathrm{dB}(\mathrm{m}^2/\mathrm{m}^3),\ \text{F-region.}$$

The frequency dependence of median σ_v', in the range 7-13 MHz, can be represented by

$$\frac{d\sigma_v'}{df} = \begin{array}{ll} -3.0\ \mathrm{dB/MHz}, & \text{E-region} \\ -5.2\ \mathrm{dB/MHz}, & \text{F-region.} \end{array}$$

Above about 13 MHz, the frequency dependence is negligible.

In order to estimate the dependence of volumetric cross section on geomagnetic activity, data from the Prince Albert Radar taken at 400 MHz were used (PARL Report, pp 7-8 and 7-9).[52] From these data a dependence on K_p in the range $K_p \leq 5$ can be inferred by fitting a straight line to the σ_{max} measurements:

$$\sigma_{max} = -113 + 2.4\ K_p\quad \mathrm{dBm\ at\ 400\ MHz}.$$

Using this same K_p dependence and assuming that the Polar Fox II median measurements are representative of median geomagnetic activity, the above median "pseudo cross sections" can be rewritten as

$$\sigma_v' = -94 + 2.4\ K_p\ \mathrm{dB}(\mathrm{m}^2/\mathrm{m}^3),\quad \text{E-region;}$$

$$= -83 + 2.4\ K_p\ \mathrm{dB}(\mathrm{m}^2/\mathrm{m}^3),\quad \text{F-region.}$$

It may be noted that Greenwald et al[68] found that the backscattered auroral power at College was approximately proportional to the square of the perturbation of the horizontal component of the magnetic field vector, in qualitative support of the above derived geomagnetic activity dependence.

---

[68] Greenwald, R.A., Eckland, W.L., and Balsley, B.B. (1973) Auroral currents, irregularities, and luminosity, J. Geophys. Res. 78:8193.

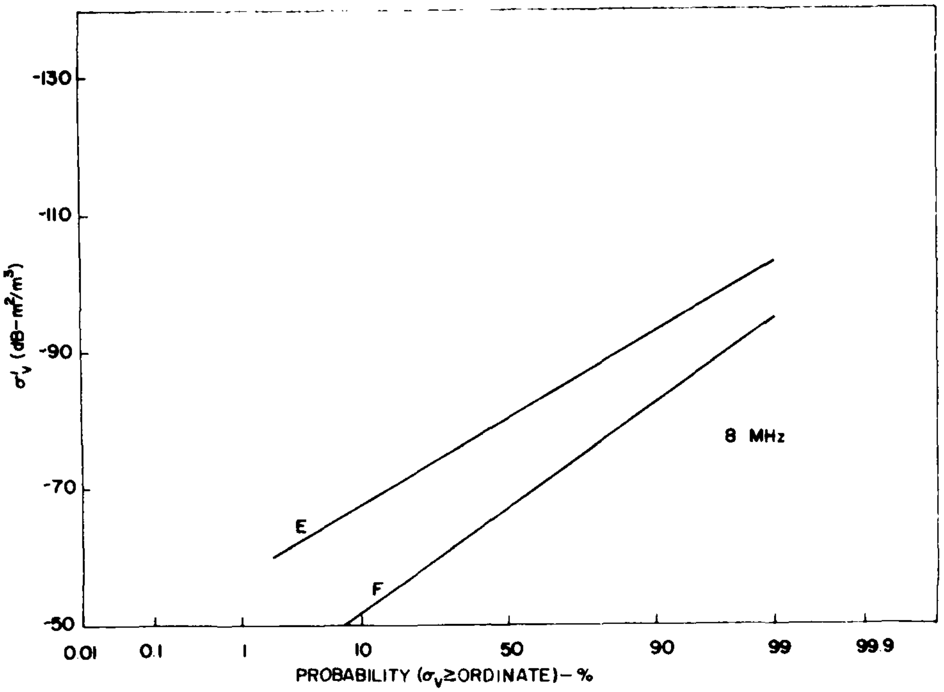

Figure 16. Probability Distribution of "Pseudo" Volumetric Backscatter Cross Section, Measured at 8 MHz by the Polar Fox II Radar for Nighttime Hours in October 1972 (Ring and Richards, 1978)

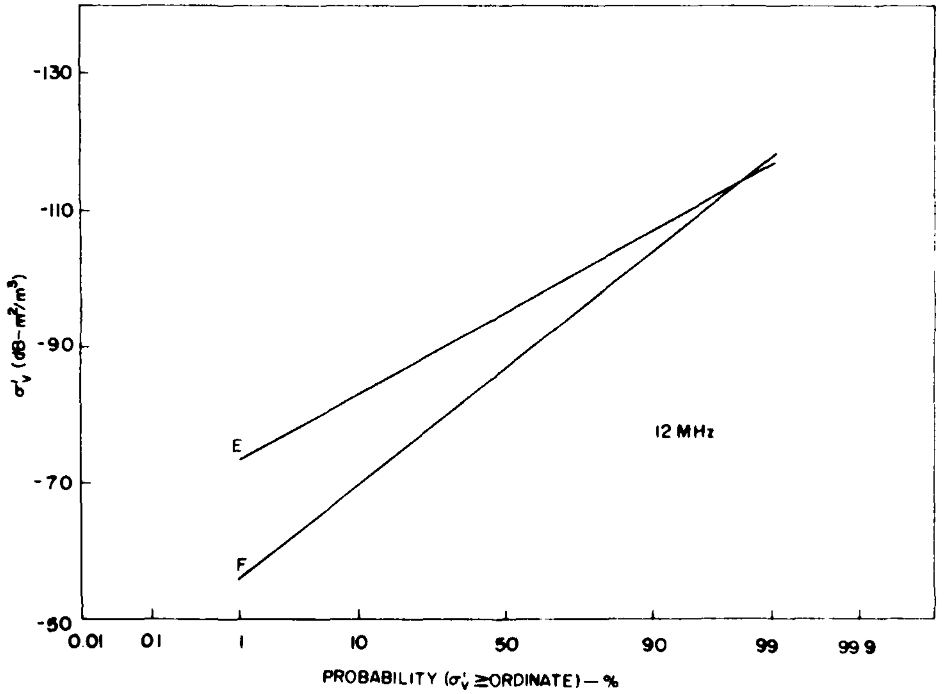

Figure 17. Same as Figure 16, Except at 12 MHz

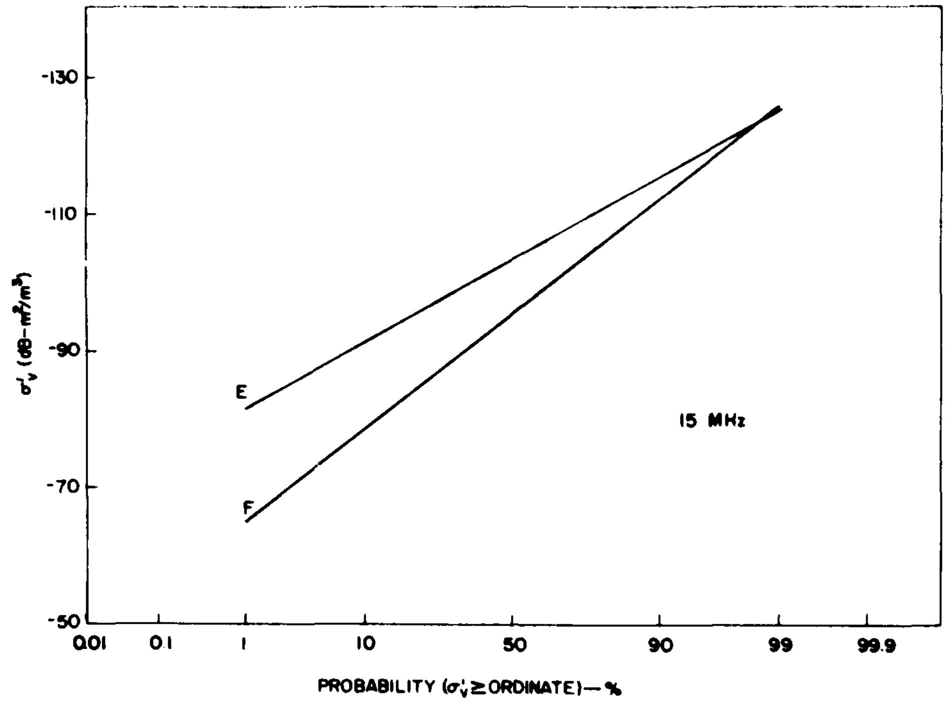

Figure 18. Same as Figure 16, Except at 15 MHz

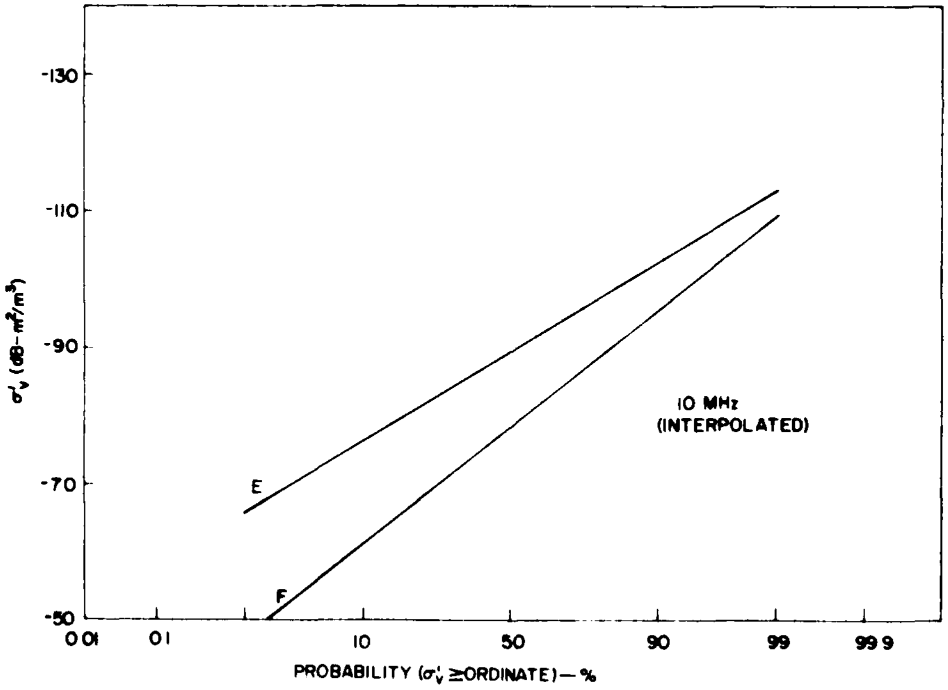

Figure 19. Same as Figure 16, Except Interpolated to 10 MHz

The deviations of the normal distributions representing "pseudo volumetric" reflectivities may be taken as

10 dB (E-layer),
13 dB (F-layer),

more or less independent of frequency in the range 8-13 MHz.

The values deduced above can be used to deduce backscatter clutter amplitudes from the Polar Fox site or from a site at a similar geomagnetic latitude. In order to extrapolate these results to other locations and times, the probability of irregularity occurrence, deduced in Section 4.1 and 4.2 can be used. The underlying assumption is that the volumetric cross section is proportional to the critical frequency of sporadic-E, in the case of E-layer clutter and to the probability of spread-F for F-region clutter. The Prince Albert Radar Study[52] confirms the first of these assumptions. The dependence of σ_{max} on sporadic-E blanketing frequency (f_BE_s) at Fort Churchill is apparent in that σ_{max} increases by ~22 dB per MHz increase in f_BE_s. In order to "calibrate" the probability distribution of sporadic-E critical frequency and relate the probability that $f_oE_s \geq 3$ MHz, used in Section 4.1, measurements of f_oE_s were collected for October 1971 from Fort Churchill, Goose Bay, Ottawa, and St. Johns. The approximate geomagnetic latitudes of these locations are 70°, 65°, 60° and 59° respectively. Figure 20 shows the diurnal variation of f_oE_s for these locations. Note that the median values for this month reflect major features of the space-time distributions of probability ($f_oE_s \geq 3$ MHz) in Section 4.1, particularly the nighttime minimum at $\Phi \sim 65°$ (Goose Bay).

The majority of E-region clutter was observed by Polar Fox II, at night, at a geomagnetic latitude of about 70°. The median nighttime f_oE_s at Fort Churchill ($\Phi \sim 70°$) in October is ~5 MHz. Assuming a log-normal distribution for f_oE_s[69] with a 5 MHz median value, the 3 MHz probability of occurrence would be ~0.83. This is very close to the value predicted by the model described in Section 4.1 for the probability that $f_oE_s \geqq 3$ MHz. Thus, a correspondence can be made between the probability-of-occurrence modelled values and pseudo volumetric cross section values. Taking into account the statistical distribution of the Polar Fox II cross-section data and their frequency dependence, the probability contours of Section 4.1 correspond to the probability that

$$\sigma'_v \geq -89 \text{ dB } (m^2/m^3) \text{ at } 10 \text{ MHz.}$$

---

[69] Cherneyshev, O.V. (1968) f_oE_s Distribution curves, Geomag. and Aeron. 8:902.

The correspondence thus obtained between the probability of sporadic-E occurrence and volumetric cross section permits the calculation of E-region clutter amplitudes to be performed. This will be pursued further in Sections 4.6 and 6.4.

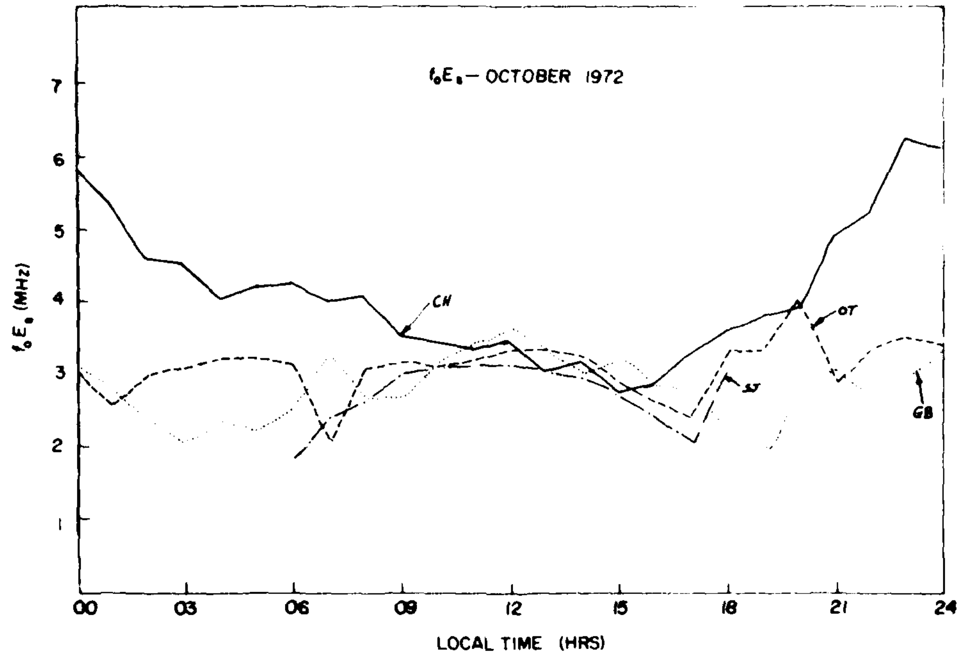

Figure 20. Diurnal Variation of f_0E_S for October 1972 for Fort Churchill (CH), Goose Bay (GB), Ottawa (OT), and St. Johns (SJ)

The quantitative relationship between the probability of spread-F (as derived in Section 4.2) and median F-region volumetric cross section is more difficult to establish because spread-F is not as precisely defined as f_oE_s. By considering an average ionosonde as a radar and solving the radar equation, it is possible to establish the minumum detectable F-region clutter signal and thus the threshold of spread-F measurement. It was decided not to rely on this approach because of many practical uncertainties and the spread-F probability contours derived in Section 4.2 were related to σ_v' median values by simple comparison of the predicted probability values and observed cross-section values for the Polar Fox II coverage area in October. This resulted in the approximation of the 90 percent probability contours in Section 4.2 by contours of median σ_v', which is -77.5 dB (m^2 m^{-3} at

10 MHz for average K_p. Thus the contour plots in Section 4.2 can be used to compute F-region clutter signal amplitude if it is assumed that they represent the probability that $\sigma_v' > -94$ dB (m^2/m^3) at 10 MHz (see Appendix D).

As an example of the foregoing arguments, consider the results of Sections 4.1 and 4.2 at $\Phi = 70°$ (CGL) in June at 00 UT, for $K_p = 2$. From the contour plots

$$p(E) = 0.5 \ ,$$

$$p(F) = 0.8 \ .$$

Thus, at 10 MHz,

$$\text{prob}(\sigma_v'(E) > -89 \text{ dB}(m^2/m^3)) = 0.5 \ ,$$

and

$$\text{prob}(\sigma_v'(F) > -94 \text{ dB}(m^2/m^3)) = 0.8 \ .$$

Therefore, using the statistical distributions for σ_v' (E) and σ_v'(F), their median values are

$$-89 \text{ dB}(m^2/m^3), \qquad \text{E-region},$$

and

$$-85 \text{ dB}(m^2/m^3), \qquad \text{F-region} \ .$$

The values for median σ_v deduced herein may be compared with UHF results, in the case of E-region clutter at least, by using a crude frequency scaling law published by Chestnut et al.[70] in which σ_v increases by ~ 15 dB/400 MHz in the UHF-HF range. Both the Prince Albert Radar and the Perimeter Acquisition Radar[72] (PAR) both measure $\sigma_v \sim -90$ dB(m^2/m^3) at 90° aspect angle at ~400 MHz. Thus, at 10 MHz, $\sigma_v \sim -75$ dB(m^2/m^3). The median "pseudo volumetric cross section" for the E-layer is ~ -89 dB(m^2/m^3). When allowance is made for the ratio of the actual Polar Fox II illuminated volume to that assumed by Ring and Richards[66] and when ionospheric focussing is taken into account, a factor of ~ 15 dB must be added to the "pseudo" cross section. Thus the estimate of $-89 + 15 = -74$ dB (m^2/m^3) is in good agreement with the extrapolated UHF results.

---

[70] Chestnut, W.G., Hodges, J.C., and Leadabrand, R.L. (1968) Auroral Back Scatter Wavelength Dependence Studies, RADC-TR-68-286.

4.4 Aspect Sensitivity of Auroral Clutter

The subject of the magnetic aspect sensitivity of auroral scatter has been extensively treated in the literature but a great deal of confusion still exists regarding the quantitative estimates of the degree of aspect sensitivity. It appears that much of this confusion may be traced to the fact that the geomagnetic field is distorted by the strong ionospheric currents which accompany the aurora (the very currents which generate the plasma instabilities which in turn are responsible for the radio aurora). Despite the fact that highly accurate models are available to describe the earth's magnetic field of internal origin, it is difficult, if not impossible, at present to correct these models for time varying ionospheric current effects. These currents may easily change the apparent direction of the magnetic field in their vicinity by several degrees, and since the apparent radar cross section of the aurora varies by ~ 10 dB per degree of aspect angle variation, this can be a major factor in cross section estimation.

Leadabrand et al[71] and Chestnut et al[70] studied the aspect sensitivity of UHF auroral clutter near normal incidence ($\psi \sim 90°$) and reported a variation of ~ 10 dB per degree off-orthogonality. Unger et al[52] using the Prince Albert Radar at UHF found a much smaller value of ~ 3-6 dB/deg in the range $95° < \psi < 105°$. The most thorough study of UHF aspect sensitivity appears to be that of Mitchell and Brown[72] who used the Perimeter Acquisition Radar at Grand Forks, North Dakota in the 450 MHz band. These authors noted a great variability in measured aspect sensitivity, despite careful attempts to remove sources of observational error and bias, which they interpreted as the result of geomagnetic field distortion, in the neighborhood of the auroral scatterers, by the intense auroral electrojet currents. They reported values of aspect sensitivity in the range 0 ~ 12 dB/deg for diffuse clutter returns and as high as 20 dB/deg for discrete returns. It was noted as a significant feature that discrete clutter returns usually displayed a higher degree of aspect sensitivity than did diffuse returns.

The observations in the previous paragraph refer to E-region clutter at VHF and UHF. There is reason to believe that E-region irregularities may display different aspect sensitivity in the HF band due to the much larger scale size of plasma irregularities contributing to the scatter; it is by no means clear that the plasma instability processes operating in the centimeter and decameter ranges are identical. Furthermore it may also reasonably be anticipated that F-region clutter may exhibit different aspect sensitivity to E-region clutter, again because different instability

---

[71] Leadabrand, R. L., Larson, A. G., and Hodges, J. C. (1967) Preliminary results on the wavelength dependence and aspect sensitivity of radar auroral echoes between 50 and 3000 MHz, J. Geophys. Res. 72:3844.

[72] Mitchell, M J., and Brown, J. L. (1976) PAR Auroral Study, Vol. 5, Final Rept. Contract DASG-74-C-0026, ABMD Systems Command.

mechanisms are almost surely operating in the two altitude regions. Unfortunately there exist few reliable direct measurements at HF, owing to the combination of instrumental difficulties and the uncertainties in taking account of ionospheric refraction. Bates and Albee[73] reported a value of ≥ 6 dB/deg while McDiarmid[74] reported a much lower value of 1.3 - 1.5 dB/deg at a low VHF frequency. As noted in Section 3.2 the observations in England of Baggaley[35] can be interpreted as indicative of an aspect sensitivity of ~10 dB/deg for F-region backscatter at HF.

In view of the paucity of experimental evidence and the apparent great variability of aspect sensitivity (as evidenced by the work of Mitchell and Brown)[72] it seems that the best which can be done at present is to assume a representative value of ~6 dB/deg for HF aspect sensitivity.

4.5 Auroral Clutter Amplitude

4.5.1 REFRACTED CASE

The volume of auroral ionospheric irregularities illuminated by the radar is determined by the azimuthal antenna beamwidth, the radar pulse length, and the aspect sensitivity of the scatter from the irregularities (see Appendix C)

$$V_s = R^2 \cdot \Delta\varphi \cdot \Delta\epsilon \cdot \left(\frac{dP}{d\psi}\right) \cdot \Delta\psi \cdot \frac{1}{F} \tag{1}$$

where

V_s = scattering volume,

R = range to scattering volume,

$\Delta\varphi$ = azimuthal beamwidth of antenna,

$\Delta\epsilon$ = range of elevation angles illuminating scatter volume,

P = group path,

ψ = magnetic aspect angle,

F = focussing factor.

Several parameters which enter Eq. (1) – namely, $\Delta\epsilon$, $\frac{dP}{d\psi}$, and F must be determined by mathematical ray-tracing through a model ionosphere, in the presence of a magnetic field, at the frequency under consideration. In other words,

---

[73] Bates, H. R., and Albee, P. R. (1969) Aspect sensitivity of HF auroral echoes, J. Geophys. Res. 74:1164.

[74] McDiarmid, D. R. (1972) On the aspect sensitivity of radio aurora, Can. J. Phys. 50:2557.

these parameters are complicated functions of frequency and the detailed ionospheric structure between the radar and the clutter volume. As a result of performing such propagation simulation computations, representative values for these parameters can be established as follows:

(1) $\Delta \epsilon$ is determined primarily by the radar pulse length and also by the range,

that is, $\Delta \epsilon = f(\tau , R)$

where τ is the radar pulse length. Since $\Delta \epsilon$ is the range of elevation angles over which orthogonality is achieved with the magnetic field at range R, this parameter is an approximate measure of the vertical extent of the scatter volume (H)

$$H \sim R \cdot \Delta\epsilon \, .$$

Note that $\Delta \epsilon$ is also a function of the magnetic field geometry and thus varies with radar location;

(2) $\frac{dP}{d\Psi}$ is an approximate measure of the horizontal dimension of the scatter volume (L)

$$L \sim \frac{dP}{d\Psi} \cdot \Delta\psi ,$$

where the aspect sensitivity of the scatter function determines the range extent over which scatterers will contribute to the scattered power received at the radar. The range of magnetic aspect angles, $\Delta\psi$, is chosen somewhat arbitrarily as ± 1°. Since a representative figure for aspect sensitivity, in the HF range, is 6 dB per degree, this range effectively defines the horizontal dimension of the scatter volume by its 6 dB points.

(3) F is a measure of the focussing which results from the spatial variation of ionospheric refractive index and the curvature of the ionosphere. It is essentially the ratio of energy density per unit area orthogonal to the ray direction in the ionosphere to the same energy density in free space. Typical values for F near the apogee of ray trajectory are 10-15 dB.

The volume-scattering cross section (σ_v) is defined as the ratio of the equivalent point-target cross section (σ) to the illuminated volume,

$$\sigma_v = \frac{\sigma}{V_s} . \tag{2}$$

Using the standard radar equation, σ is expressed by

$$\sigma = \frac{\left(\frac{S}{N}\right) \cdot (4\pi)^2 \cdot R^4 \cdot L \cdot kT_sB}{P_T \quad G_T \quad A_R} , \tag{3}$$

where

$\frac{S}{N}$ is received signal to noise ratio,

L = total system loss,

k = Bolzmann's constant (1.38 × 10^{-23} joule/°K),

T_s = system noise temperature,

B = receiver bandwidth,

P_T = transmitted power,

G_T = transmit antenna effective gain,

A_R = receive antenna effective area.

The receive antenna effective aperture can be expressed, if desired, in terms of its directive gain, D_R, by the approximate expression

$$\frac{\lambda^2 D_R}{4\pi} = A_R = \frac{41000\,\lambda^2}{4\pi\Delta\phi \cdot \Delta\theta} , \tag{4}$$

where

λ = is the radar wavelength,

$\Delta\phi$ = is the azimuthal 3 dB beamwidth,

$\Delta\theta$ = is the elevation 3 dB beamwidth,

($\Delta\phi$ and $\Delta\theta$ are both expressed in degrees). The use of Eq. (4) is appropriate at low frequencies where it can reasonably be assumed that the radar is external-noise limited, so that antenna efficiency need not be considered.

Equations (1), (2), (3), and (4) may be used to define the volume-scatter cross section as measured by a HF radar as

$$\sigma = \frac{\frac{S}{N} \cdot 4\pi^2 R^2 \cdot L \cdot kT_s B \cdot F}{P_T \cdot G_T \cdot A_R \cdot \Delta\varphi \, \Delta\epsilon \, \frac{dP}{d\psi} \, \Delta\psi} , \tag{5}$$

$$= \frac{\frac{S}{N} \cdot 4\pi^2 R^2 \cdot L \cdot kT_s B \cdot F \, \Delta\theta}{41000 \, \lambda^2 \, P_T \, G_T \, \Delta\epsilon \, \Delta\psi \, \frac{dP}{d\psi}} \tag{6}$$

Alternatively, if the volume scattering cross section is known (or can, for example, be extrapolated from another frequency regime, the received clutter signal can be estimated from Eq. (6) by

$$\frac{S}{N} = \frac{K \sigma_v \lambda^2 P_T G_T \Delta\epsilon \, \Delta\psi \, \frac{dP}{d\psi}}{R^2 \, L \, kT_s \, B \, F \, \Delta\theta} , \tag{7}$$

where

$$K = 41000 \, \frac{\pi}{180} \cdot \frac{1}{16\pi^3} = 1.44 .$$

4.5.2 LINE-OF-SIGHT LIMITING CASE

The computation of received clutter strength is, in general, a complicated process, due principally to the computation of effective scatter volume in the presence of ionospheric refraction. A special case of considerable importance is found in the limit when the refraction approaches zero, namely, at night and at high frequencies; this limit may be referred to as the "line-of-sight" limit, by analogy with the UHF radar case. In this limit the main considerations in the determination of the scatter volume concern the geometry of the propagation path and the geomagnetic field. Figure 21 illustrates the contours of the geomagnetic aspect angle, ψ, for this limit, assuming auroral scatterers at an altitude of 110 km.

The calculation of effective clutter cross section is best performed by convolving the antenna pattern and the radar pulse shape (transformed to a range function) with the volume scatter cross section expressed as a function of geomagnetic aspect angle (in range-azimuth). Special attention is still required in the calculation of the range of elevation angles to be included in the scatter volume. For radar antennas having a wide elevation beam pattern, the "elevation component" of the scatter volume is no longer determined, as it is in the refracted case, by magnetic aspect sensitivity. In many cases it will be sufficiently accurate to overlay an equivalent range-azimuth cell (determined by pulse length and azimuthal beamwidth) on the contours of Figure 21, noting that the range dimension of the cell must be foreshortened by a factor 0.983 cos ϵ, where ϵ is the elevation angle. The range of elevation angles is determined by the projection of the pulse length, in range units, on the thin auroral layer. Figure 22 shows this range-elevation function. The average value of ψ is estimated from the graphical overlay and the effective volume scatter cross section computed therefrom, using a figure of -6 dB per degree off-orthogonality.

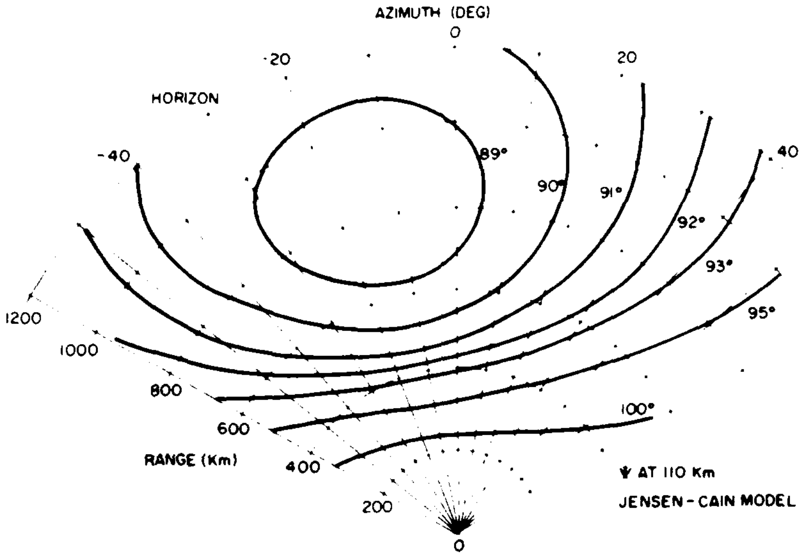

Figure 21. Range-azimuth Variation of Geomagnetic Aspect Angle at 110 km Altitude for Line-of-Sight Propagation From Site at 61° CGL, Using Jensen-Cain Model of the Geomagnetic Field

The effective scatter volume is

$$V_s = R^2 \cdot \phi \cdot \Delta\epsilon \cdot \tau \cdot \frac{c}{2}, \qquad (8)$$

where

$\Delta\epsilon$ is the elevation angle range,
ϕ is azimuthal beamwidth,
τ is pulse length,
c is velocity of light.

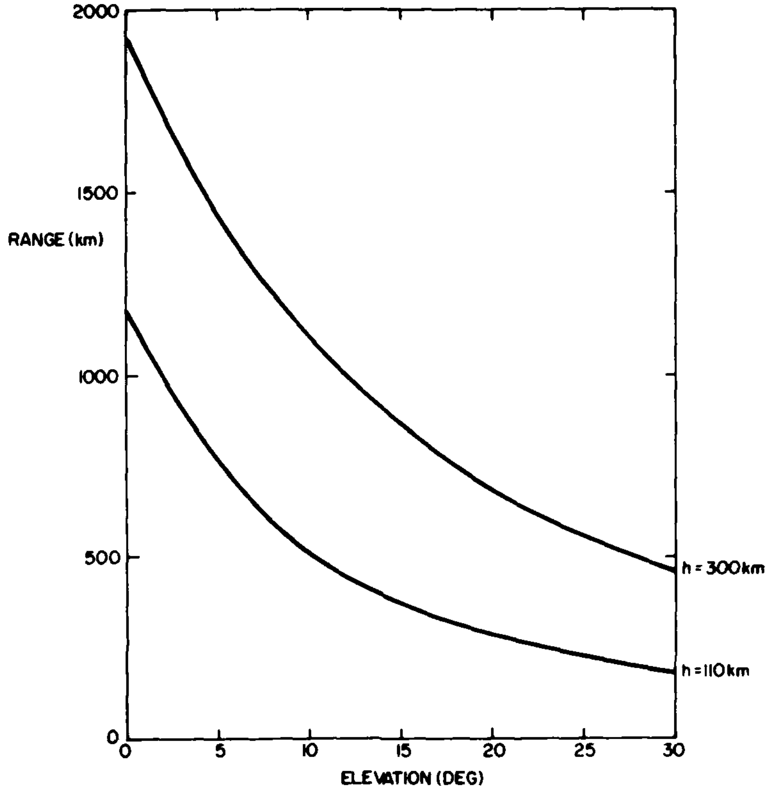

Figure 22. Range-elevation Angle Dependence for Clutter at Altitudes of 110 km and 300 km (line-of-sight propagation)

Note that the radial component of V_s may be limited, in the case of very long pulse length and/or steep incidence on the ionosphere, not by pulse length but by the thickness of the scattering layer in the E region, which is approximately 10 km. Thus if $\tau \cdot \frac{c}{2}$ exceeds 10 sec θ where

$$\theta = \sin^{-1} (0.983 \cos \epsilon) \qquad (9)$$

and ϵ = elevation angle, then the smaller of these two values is used in calculating V_s.

As an example, consider the calculation of E-region clutter amplitude received from a range of 600 km at azimuth 0° at frequency 5 MHz at midnight in winter. Assume azimuthal beamwidth of 5° and equivalent pulse length of 200 μsec.

$$V_s = (600)^2 \times 10^6 \times (5 \times 2) \left(\frac{\pi}{180}\right)^2 \times 10^{-4} \times 3 \times 10^8$$

$$= 3.3 \times 10^{13} \text{ m}^3$$

where the range of elevation angles, $\Delta\epsilon$, *corresponding to the 200 μsec pulse* length is estimated from Figure 22 as 2°.

The median volume scattering cross section at orthogonality at 5 MHz is ~60 dB (m^2/m^3). From Figure 21 the average aspect angle in the illuminated region is approximately 89.5°, so that the actual volume scattering coefficient is -63 dB (m^2/m^3). Thus the equivalent point target cross section of the clutter is 1.65×10^7 m^2.

Solving the radar equation then yields the receiver clutter power

$$P_R = \frac{10^3 \times (30)^2 \times 1.65 \times 10^7}{(4\pi)^3 \times (600)^4 \times 10^{12} \times L^2}$$

where transmitted power = 1 kW and unit antenna gains are assumed, that is,

$$P_R = 132.04 - 2L(\text{dB}) \text{ dBW} .$$

Under the conditions assumed, L ~ 16 dB, so that the received clutter power is

$$P_R = -164.6 \text{ dBW} .$$

Actually, this value of received power should be reduced by a further 3 dB since, in practice it is not usual to receive both signal polarization components. Since the clutter signal is essentially randomly polarized, if only one polarization component is received, the received clutter power in the above example is -167.4 dBW.

4.6 Estimation of Minimum Range for Slant-F

At night the ionosphere may be approximated by a horizontally stratified parabolic layer with vertical refractive index function

$$n^2(Z) = 1 - \frac{1}{\rho^2}\left[1 - \left(\frac{Z_{max} - Z}{Y_m}\right)^2\right] \qquad (10)$$

where

$\rho = \frac{f}{f_o}$,

f = operating frequency,

f_o = maximum plasma frequency,

Z_{max} = height of layer maximum,

Z altitude measured from Z_{max}

Y_m layer semi-thickness.

After refraction in this layer, the ray reaches orthogonality with the magnetic field, according to Snell's Law, where

$$n(Z) = \frac{\sin \phi_o}{\sin I} \tag{11}$$

where

ϕ_o = angle of incidence on layer,

I = magnetic inclination.

The minimum slant range at which orthogonality is achieved corresponds to rays which reach the peak of the layer and are almost penetrating, that is, $Z = 0$ in Eq. (10).

Assuming a given range, R, the angle of incidence on the curved layer is given by

$$\cos \phi_o = \frac{R^2 + 2R_e h_B + h_B^2}{2R(R_e + h_B)} \tag{12}$$

where

R_e = earth radius (6380 km),

h_B = height of underside of layer,

that is

$h_B = (Z_{max} - Y_m)$.

Solving Eqs. (10), (11), and (12) yields the slant range to the layer bottom for which orthogonality is attained; it is then necessary to compute the component of virtual slant range for the refracted part of the raypath, within the layer. Let this component be p'(Z).

Then

$$p'(Z) = \int_{h_B}^{Z} \frac{dZ}{q}$$

where

$$q^2 = n^2 - \sin^2 \phi_o$$

that is,

$$p'(Z) = \int_{h_B}^{Z} \left\{ 1 - \frac{1}{\rho^2} \left[1 - \left(\frac{Z}{Y_m} \right)^2 \right] - \sin^2 \phi_o \right\}^{-1/2} dZ \ . \qquad (13)$$

Upon integrating Eq. (13),

$$p'(Z) = Y_m \ \rho \ \ln \left\{ \frac{\frac{Z}{Y_m} - \left[\left(\frac{Z}{Y_m} \right)^2 + \rho^2 \cos^2 \phi_o - 1 \right]^{1/2}}{1 - \rho \cos \phi_o} \right\} . \qquad (14)$$

The virtual slant range to the orthogonality point is then given by R + p', from Eqs. (12) and (14). The minimum slant range is the value of R + p' for Z = 0, that is, corresponding to rays reaching the peak of the layer. This is plotted as a function of ρ in Figure 22a for an assumed layer bottom height of 300 km, semi-thickness of 100 km, and a magnetic inclination of 70°.

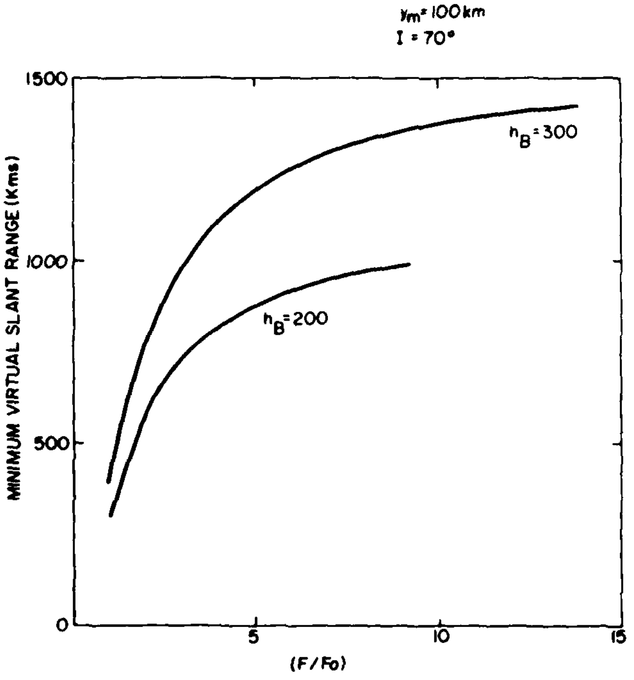

Figure 22a. Minimum Virtual Slant Range for F-region Clutter as a Function of Frequency, Normalized to Critical Frequency of a Spherically Stratified Layer. Y_m = *parabolic layer semi-thickness*, h_B = height of layer bottom, I = geomagnetic inclination

5. DOPPLER SHIFT MODEL

As noted in Section 3.3, the Doppler shift model is based on the theoretical work of Maeda,[39] referred to therein, with some relatively minor modifications which were found necessary in order to being Maeda's velocity predictions into better agreement with available observations. Maeda's calculated *values are* assumed to be appropriate for a planetary magnetic *index*—K_p = 2, that is, an average value. Values of the northward and eastward components of plasma velocity (V_N and V_E) in the CGS were tabulated at intervals of geomagnetic latitude and at 2-hr intervals of geomagnetic time. A numerical interpolation procedure was then used to compute these velocity components at arbitrary latitude and time. A separate model was employed for E-region and F-region velocities respectively. It was assumed that the entire velocity pattern expanded latitudinally by 2° per unit of K_p, reflecting the expansion of the auroral oval with increasing magnetic activity.

5.1 E-Region Velocity Model

For geomagnetic latitudes, $\Phi \geq 85°$

$$V_N = 273 \cos \frac{\pi}{12} (T - 8) ,$$

$$V_E = 273 \cos \frac{\pi}{12} (T - 14) ,$$

where velocity units are m/sec and T is geomagnetic time in hours, and $K_p = 2$.

The values of V_N and V_E for $\Phi \leq 80°$ are shown in Table 1 at intervals of 5° in latitude and 2 hr in time. Figure 23 shows the magnitude of the E-region velocity component $(V_N^2 + V_E^2)^{1/2}$ in geomagnetic coordinates, based on the model described.

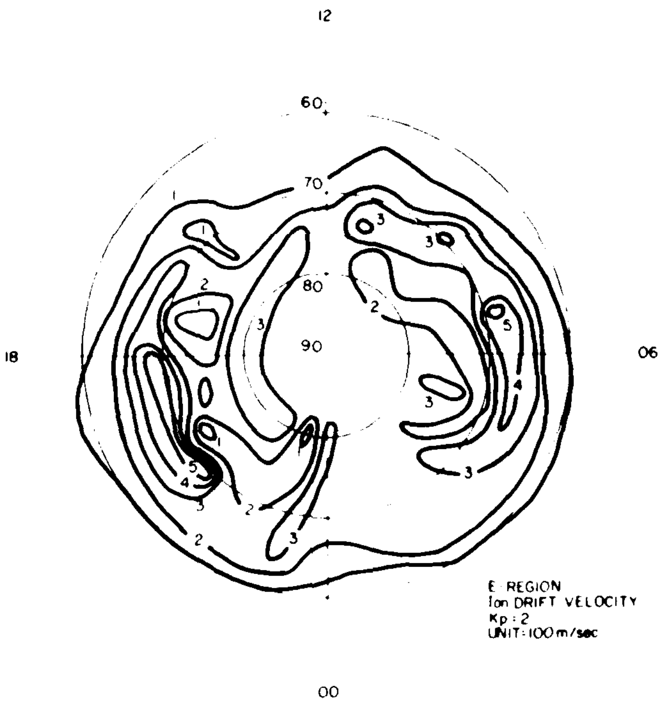

Figure 23. E-region Plasma Drift Velocity in CGS, Computed From Model

Table 1. E-Region Plasma Velocities in CGS

T	$\Phi = 80°$		$\Phi = 75°$		$\Phi = 70°$		$\Phi = 65°$		$\Phi = 60°$	
	V_N	V_E	V_N	V_E	V_N	V_E	V_N	V_E	V_N	V_E
0	-117	-305	-229	-179	-171	-141	- 70	- 83	0	50
2	115	-226	-149	-229	-260	- 80	-211	142	-38	32
4	197	-160	- 22	-254	-340	173	-192	167	-41	29
6	244	- 70	106	72	-352	365	-135	122	-41	29
8	182	0	57	248	-199	264	- 75	51	-41	29
10	173	56	- 94	352	- 63	173	- 66	31	-50	0
12	224	156	27	216	- 43	59	- 34	- 43	-32	-38
14	194	240	182	0	42	- 26	40	- 61	43	-25
16	- 60	341	220	- 89	287	-166	58	- 70	32	-38
18	-135	318	218	0	573	-209	98	-108	38	-32
20	-351	88	-128	0	427	-288	240	- 87	41	29
22	-250	-210	-179	- 32	95	-224	205	-119	49	9

5.2 F-Region Velocity Model

The model for F-region plasma velocity is similar to that for the E-region, except that the latitudinal asymmetry associated with the auroral oval is taken into account explicitly.

Let a geomagnetic latitude boundary be defined as a function of geomagnetic time by

$$\Phi_F = 72 - K_p - 5 \cos \frac{\pi}{12} T .$$

(1) When $\Phi = \Phi_F$

$$V_N = 400 \cos \frac{\pi}{6} (T - 18); \qquad 6 < T < 18$$

$$= 400 \cos \frac{\pi}{6} (T - 18); \qquad T \geq 18;\ T \leq 6 .$$

$$V_E = 0$$

(2) When $\Phi = \Phi_F - 3$

$$V_N = 0$$

$$V_E = 500 + 500 \cos \frac{\pi}{6} (T - 6); \qquad 0 < T < 12$$

$$= -500 - 500 \cos \frac{\pi}{6} (T - 18); \qquad 12 < T < 24 .$$

(3) When $\Phi = \Phi_F - 7$

$$\begin{aligned} V_N &= 0; && T \neq 12 \text{ and } \neq 00 \\ V_E &= 200 + 70 \cos \frac{\pi}{6} (T - 6); && 0 < T < 12 \\ &= -200 - 70 \cos \frac{\pi}{6} (T - 18); && 12 < T < 24 \end{aligned}$$

For $T = 12$, $V_N = 130$, $V_E = 0$

For $T = 00$, $V_N = -130$, $V_E = 0$.

(4) When $\Phi = \Phi_F - 12$

$$\begin{aligned} V_N &= 0; && T \neq 12 \text{ and } \neq 00 \\ V_E &= 60 \cos \frac{\pi}{6} (T - 6); && 0 < T < 12 \\ &= -60 \cos \frac{\pi}{6} (T - 18) && 12 < T < 24 \end{aligned}$$

For $T = 12$, $V_N = 60$, $V_E = 0$

For $T = 00$, $V_N = -60$, $V_E = 0$.

(5) For $\Phi > 85°$

$$\begin{aligned} V_N &= -400 \cos \frac{\pi T}{12} \\ V_E &= 400 \cos \frac{\pi}{12} (T - 18) . \end{aligned}$$

(6) For $\Phi = 80°$, V_N and V_E are given by the values in Table 2.

As was the case for E-region velocity, a computer program was written to estimate the velocity for F-region plasma at arbitrary latitude and time, using the analytic relationships noted above and performing numerical interpolation where the velocity components are specified numerically. The only magnetic activity dependence contained in both the E- and F-region models is the latitudinal expansion effect. Although various reports have appeared in the literature regarding a dependence of velocity on magnetic activity, this must still be regarded as an unresolved issue. The careful study by Unger et al[52], using the backscatter radar technique, did not reveal any pronounced systematic dependence of Doppler shift on geomagnetic activity. Although it is clear that large and often erratic variations in plasma velocity do occur, the model described here is regarded as a reasonable characterization of average velocities.

Table 2. F-Region Plasma Velocities at $\Phi = 80°$

T	V_N	V_E
0	-400	0
2	-267	-297
4	- 35	-398
6	0	-400
8	104	-386
10	169	-362
12	400	0
14	169	362
16	104	386
18	0	400
20	- 35	398
22	-267	297

5.3 Doppler Shift Computations

The velocity model described in Sections 4.1 and 4.2 gives the north and east components of E- and F-region plasma motion in the CGS. In order to compute the resultant Doppler effect on the radar signal, it is necessary to perform appropriate coordinate transformations so as first to calculate the radial component of motion relative to the radar. Figure 24 illustrates the situation (in the approximation of plane geometry). M and G are respectively the geomagnetic and geographic poles and P is the location of the clutter-producing plasma. S is the location of the radar site. V_N and V_E are the velocity components provided by the model, whose resultant, V, is the actual plasma velocity vector. The components of V in the geodetic system are V'_N and V_E and the radial velocity component relative to the radar is V_S. It is required to determine V_S in terms of V_N, V_E, and both the geographic and geomagnetic locations of both P and S.

As noted in the preceding paragraph, the plane geometric treatment of this problem is inaccurate and is mentioned only for purposes of illustration. In fact, a spherical trigonometric solution is necessary (see Appendix B). A computer program was written to perform the necessary coordinate transformations and coupled to the program generating the velocity components. The resultant radial component of velocity relative to the site at (44.5° N; 6[illegible] W) was computed as a function of range and azimuth and geomagnetic activity, for both E- and F-regions.

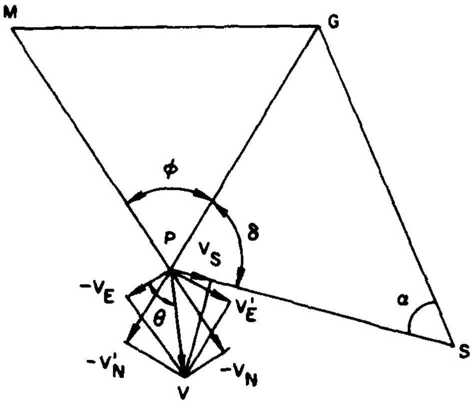

Figure 24. Computation of Radial Component of Plasma Velocity for Site at S, When Velocity Components (V_E, V_N) are Specified in Geomagnetic Coordinates. M is geomagnetic pole, G is geographic pole. Plane geometry is assumed

The radial component of velocity was transformed to a Doppler shift, normalized to the radar frequency (units of Hz/MHz), and using the formula

$$\frac{\Delta f}{f_o} = \frac{-2V_S}{C}$$

where

f_o = radar frequency,

V_S = radial velocity component,

C = velocity of light.

Note that, by convention, a negative Doppler shift signifies an approaching velocity.

Figures 25 and 26 show typical results of these computations for E- and F-region irregularities respectively (for a local meridian time at the site of 03 MLT). It is apparent that much complex structure exists in these Doppler maps, and the rough outline of the auroral oval can be seen clearly in the F-region map. Also noteworthy is the range of Doppler frequencies predicted by the model. It is by no means unusual to see Doppler offsets of 5 Hz/MHz, and values as high as 6-7 Hz/MHz are occasionally present in localized "hot-spots." Although computations were performed for two levels of geomagnetic activity (K_p = 2, 4) only the results for average activity (K_p = 2) are presented here. Because of the manner in which geomagnetic activity enters the model, the effect of increasing K_p is primarily to expand the auroral oval by 1.5° per unit K_p. A qualitative estimate of the effect of this on the Doppler maps can be made by noting the position of the auroral oval and its related Doppler features and applying an appropriate "expansion factor".

Translation of these maps to actual radar frequencies is a simple linear scaling procedure, based on the defining equation.

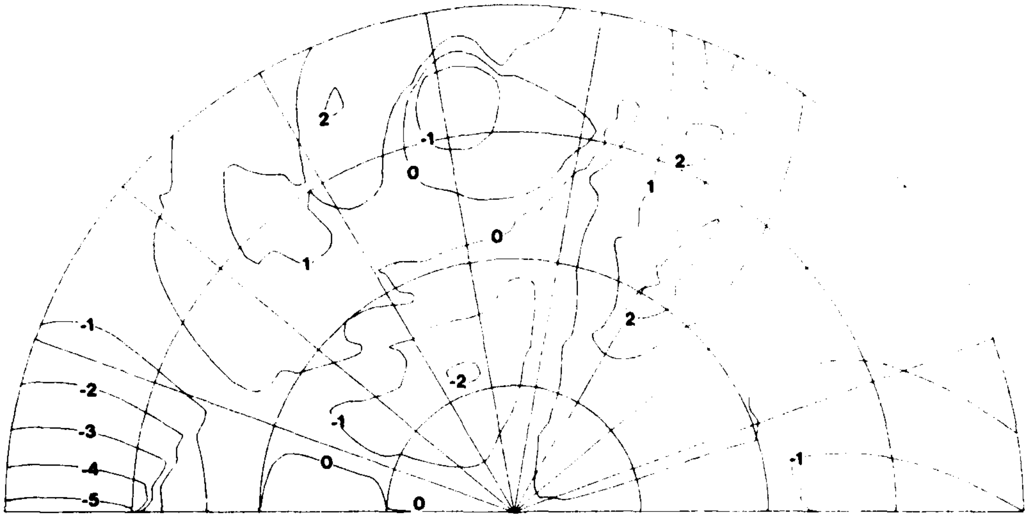

Figure 25. Contours of E-region Doppler Shift Computed for Site at (44.5° N, 67.5° W) at 0730 UT. Contour units are Hz/MHz (that is, normalized to radar frequency). Azimuth is shown in 10° intervals with the horizontal line indicating geographic East - West. Range is shown in 5° (that is, 556 km) intervals

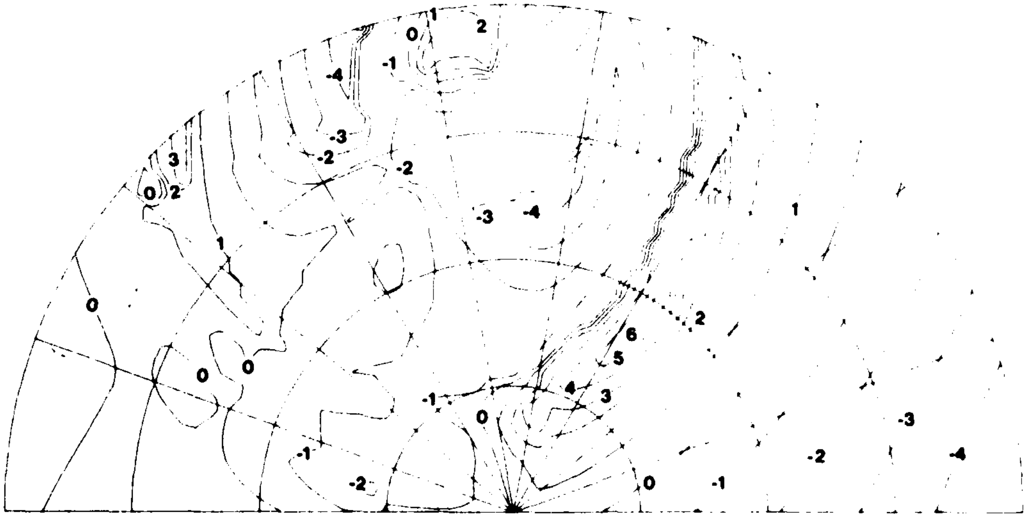

Figure 26. Same as Figure 25, Except for F-region Clutter

As an example of the use of the Doppler model, Figure 27 shows the variation with Universal Time of Doppler shift at 10 MHz, for E-region clutter at a range of 600 km from a site located in Northern Scotland. The dashed curve shows the time dependence for a northward-looking radar, while the solid curve shows the similar dependence for a look-azimuth of -60°. Note the characteristic reversals of Doppler direction around noon and midnight respectively. This has been observed in many experimental studies. The results of Leadabrand et al[75] at Fraserburgh, Scotland and of Unwin[22] are in reasonable quantitative agreement with the predictions developed here. Figure 28 shows similar calculations, based on the model, for the F-region clutter. Note the generally larger values of Doppler shift, the greater azimuthal difference, and again the diurnal pattern exhibiting reversals near noon and midnight.

A further example of the use of the Doppler models is illustrated in Figures 29 and 30, for E-region and F-region clutter respectively. These figures show the azimuthal variation of Doppler shift at 00 UT and 03 UT at 10 MHz for a range of 600 km. Note that E-region velocity at midnight reverses close to the direction of magnetic north as found in several experimental studies.

5.4 Doppler Spread

The spectrum of the signal backscattered by auroral irregularities indicates a kind of turbulent motion of the scatterers with a random spread of Doppler frequencies which can often be characterized by a simple statistical distribution function. Statistical data concerning the spectral distribution of HF signals backscattered by the aurora are relatively rare. This is accentuated by the fact that the present application requires that the spectrum be measured over a very large dynamic range (up to 60 dB or more). Very few experiments have been conducted with equipment capable of achieving such large dynamic range. The Polar Fox II experiment, which did possess a large dynamic range, included measurement of the spectral width at a number of amplitude levels below the peak return near zero Doppler shift. Unfortunately, this data has never been analyzed in a form suitable for the present purpose. A study of Doppler spread data, using original Polar Fox II data tapes has been initiated at RADC, but no results are available for inclusion in this report.

---

[75] Leadabrand, R. L., Schlobohm, J. C., and Baron, M. J. (1965) Simultaneous very high frequency and ultra high frequency observations of the aurora at Fraserburgh, Scotland, J. Geophys. Res. **70**:4235.

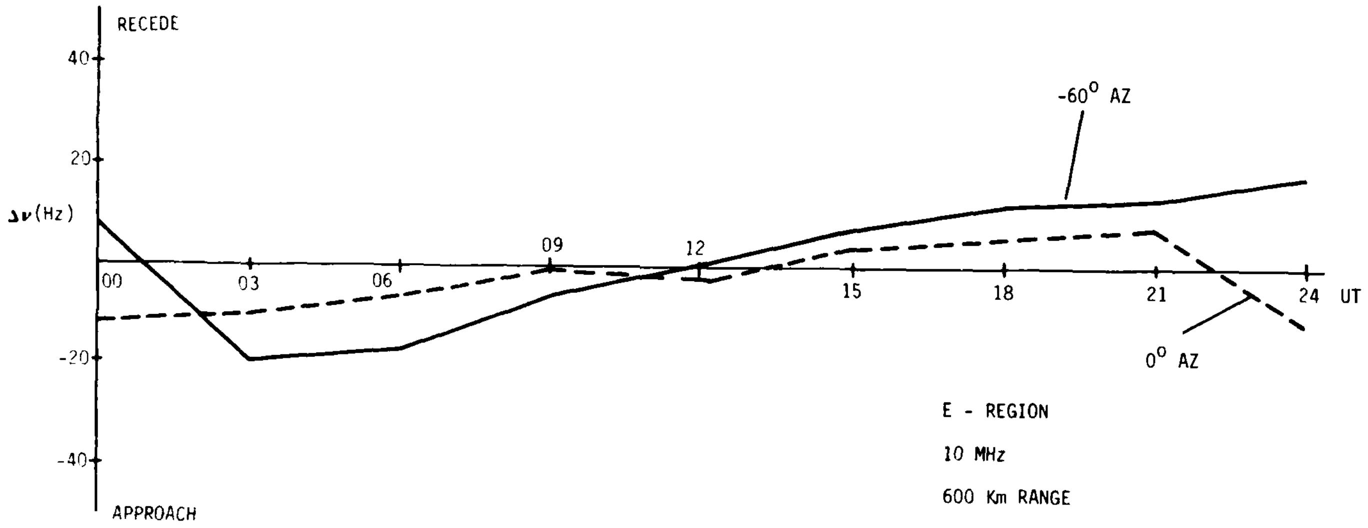

Figure 27. Universal Time Dependence of E-region Doppler Shift at 10 MHz, for Azimuths 0 and -60 degrees, From Site at 61° CGL, at Constant Range of 600 km

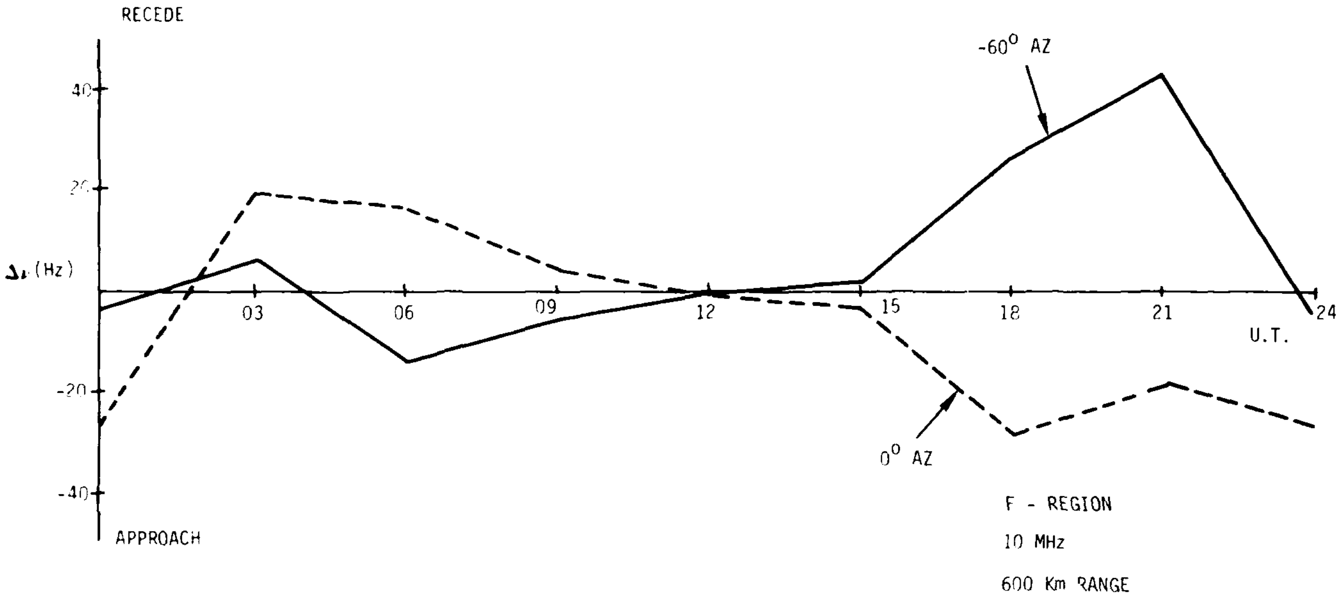

Figure 28. Same as Figure 27, Except for F-region

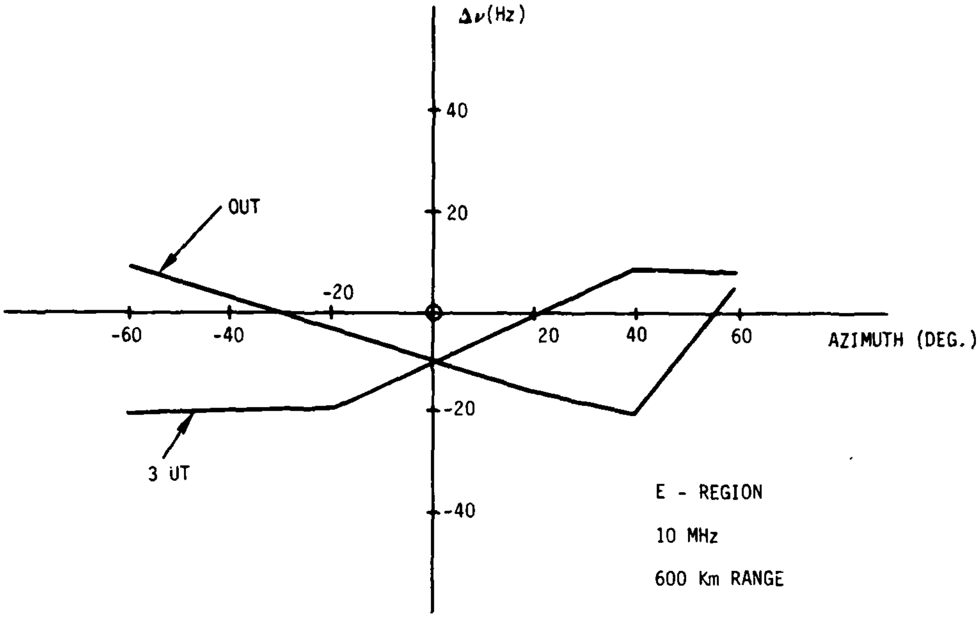

Figure 29. Azimuthal Dependence of F-region Doppler Shift at 10 MHz, for Universal Times 00 and 03, From Site at 61° CGL Constant 600 km Range

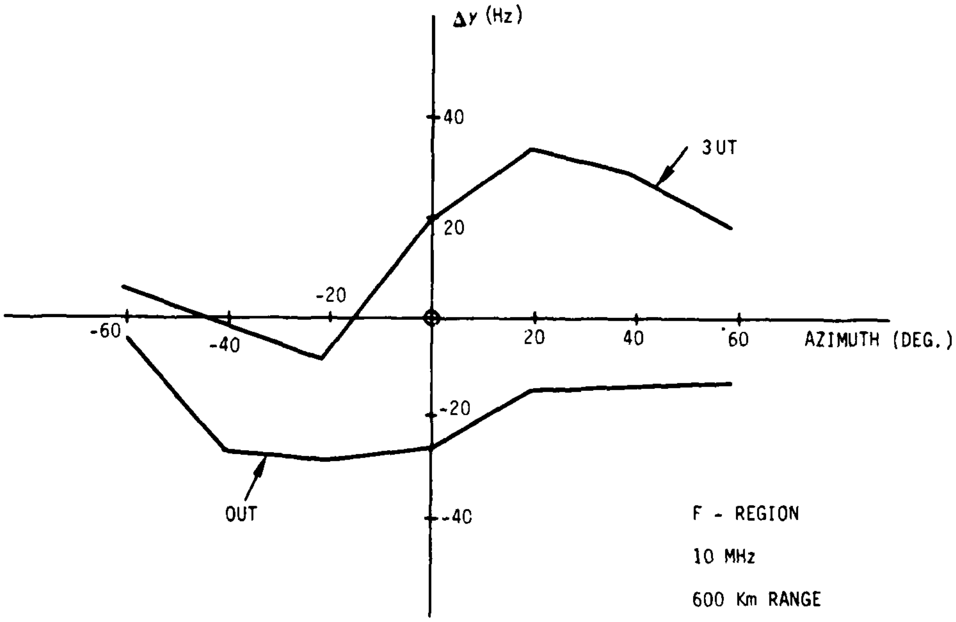

Figure 30. Same as Figure 29, Except for F-region

The Polar Cap III experiment also possessed sufficient dynamic range to permit measurement of spectral spread down to levels of the order of -60 dB below ground clutter. Again, however, the documented results of this experiment do not permit a useful model to be constructed which meets the present requirements. Both Polar Fox II and Polar Cap III measured the spectral properties of HF signals forward scattered over the skywave path. It is considered risky to apply these results to auroral backscatter, due to the important differences in geometry and to the greatly different signal levels involved.

In the absence of relevant HF data on spectral spread of auroral backscatter, it has been decided to adopt a preliminary model based on UHF radar data, specifically data from the Chatanika radar operated by SRI.[76] This model can be replaced by another, based on Polar Fox II data, when the appropriate analysis has been completed at RADC. Using spectral spread data from the above reference, the width of the Doppler spectrum of diffuse auroral backscatter may be conveniently approximated by a Gaussian function having the form

$$\Delta V = 750 \exp - (V^2/a^2)$$

where

ΔV = velocity spread at half-power points of the velocity spectrum (m/sec),

V = velocity at which the backscattered power is maximum (m/sec),

a = 300 m/sec.

This functional form reflects the observations that the width of the Doppler spectrum decreases as the spectral peak moves away from zero Doppler shift.

6. PREDICTABILITY OF AURORAL CLUTTER

Since auroral radar clutter is intimately related to electric fields and currents in the magnetosphere—ionosphere system, the question of its predictability hinges largely on the predictability of these phenomena. It is well known that the electric fields and convection of plasma in the magnetosphere are in turn dependent upon conditions in the interplanetary medium and ultimately on the degree and nature of activity on the sun, so that the question of predictability is ultimately concerned with the extent to which solar disturbances can be predicted. Although considerable progress has been made in understanding solar-terrestrial relationships in

---

[76] Moorcroft, D. R., and Tsunoda, R. T. (1978) Rapid scan doppler velocity maps of the UHF diffuse and radar aurora, J. Geophys. Res. 83:1482.

recent years, the extent of knowledge on this subject falls far short of a capability for long term prediction of auroral clutter activity, with only a few well-defined exceptions. At present, and in the forseeable future, the best that can be hoped for is prediction on a scale of ~ 1 hr, based on appropriate monitoring of conditions in the near-earth environment. A notable exception to this conclusion is the fact that large scale geomagnetic storms exhibit certain repeatable properties which can be used for prediction purposes.

Global geomagnetic storms are associated with a characteristic class of disturbance in the solar corona and chromosphere. They often, but not always follow another kind of solar-geophysical event known as a Polar Cap Absorption (PCA) event. PCA's are the result of energetic particles (mostly protons) of solar origin which enter the earth's atmosphere in the polar cap regions and produce enhanced D-region ionization—hence their name. They are usually followed, after an interval of one to several days, by a world-wide geomagnetic storm associated with (among other things) enhanced auroral clutter. These storms may last from one to ten days, the latter being an extreme case. An interesting feature of this sequence of events is that the solar active regions which are initially responsible for the terrestrial events are often long-lived. If they persist for a time longer than the solar rotational period (27 days) they have a high probability of generating another geomagnetic storm on successive solar rotations. In fact it is quite common for these solar active regions to persist for several solar rotations, giving rise to recurrent geomagnetic storms at 27-day intervals, although generally of decreasing intensity as the solar active region weakens and disperses.

6.1 Statistical Considerations

Apart from the recurrent world-wide geomagnetic storms, which are in any case relatively infrequent events, the major problem of predictability of auroral clutter is associated with the predictability of auroral substorms—a much more frequent event, confined to the vicinity of the auroral oval. The most readily available indicator of substorms is the disturbance of the geomagnetic field recorded by the ground based magnetometers. Various indices of geomagnetic disturbances have been developed; the Auroral Electrojet (AE) index is derived from selected high latitude observatories while the planetary geomagnetic index (K_p) is intended to be representative of a more global level of magnetic activity. The statistics of K_p have been studied, in recent years, by Elkins[16] and Cage and Zawalick.[77] Pazich[78]

---

[77] Cage, A. L., and Zawalick, E. J. (1972) A Discussion of the Geomagnetic Indices K_p and A_p, 1932 to 1971, AFCRL-72-0693, AD 756828.

[78] Pazich, P. M. (1976) Conditional Probabilities of the Geomagnetic Index A_p, AFGL-TR-76-0034, AD A023675.

has studied the statistics of A_p (an average daily geomagnetic index related to K_p). Elkins[79] has studied statistics of AE. The results of all these studies can be applied to the statistical determination of the likelihood of auroral geomagnetic disturbance and thereby, through the use of the model developed in Section 4 for example, to the statistical prediction of auroral clutter.

Elkins[16] showed that the probability distribution of K_p over a 38-year period was approximately Gaussian, with a median value of 1.5, and upper and lower deciles of 3.7 and 0 respectively (in the range $K_p \leq 6$). There are, however, pronounced solar cycle and seasonal dependences in magnetic activity as shown by Cage and Zawalick,[77] by Pazich,[78] and by Elkins[79]. The maximum in the solar cycle trend of geomagnetic activity follows the peak sunspot number by about 1-2 years while the seasonal effect is characterized by maxima in the equinoxes. The variation of average yearly K_p over a typical solar cycle ranges from ~1.6 at ~1-2 years following solar minimum to ~2.8 following solar maximum. The average seasonal variation of K_p over a 40-year period shows maxima of about 2.5 in March and September with minima at ~2.0 in winter and 2.1 in summer.

Elkins[16,79] has used the statistics of K_p to estimate the number of periods in a 10-year interval for which K_p remains above a particular value. His results are summarized in Table 3, where the number of periods of duration (T) hours for which $K_p \geq (K_p)_o$ is tabulated. This data can be used to establish the frequency with which a radar might be expected to experience severe clutter, in terms appropriate to operational analysis.

Table 3. Duration of Magnetically Disturbed Periods

T(hrs)/$(K_p)_o$	2	3	4	5	6
3	11,000	5600	2200	800	300
6	1800	620	210	63	18
9	300	90	26	5.2	1.3
12	70	16	4.5	0.7	0.1

6.2 Interplanetary Parameters

The configuration of the magnetosphere is known to depend strongly on the direction of the magnetic field in the interplanetary medium. It has been found, for example, that the equatorial boundary of the auroral oval moves equatorward by an average of 0.5-0.6 degrees per gamma increase in the southward component

---

[79] Elkins, T.J. (1973) An Empirical Model of the Polar Ionosphere, AFCRL-TR-73-0331, AD 766240.

of the interplanetary magnetic field—IMF.[80, 81] Many authors have noted the association between the southward turning of the IMF and the occurrence of auroral substorms. Arnoldy[82] showed, for example, that a southward-turning IMF often precedes substorms by about one hour. Estimates of the interval between an IMF event and its related auroral oval manifestations vary, but are usually less than one hour. Pike et al[83] for example, reported that the Explorer 35 Satellite, at geocentric distances of 35-60 earth radii, detected southward IMF turning followed be equatorward shift of the equatorward oval boundary after a time interval of 10-30 minutes. It therefore seems that with an interplanetary satellite at reasonable distance, provided that it is suitably located relative to the sun, a reasonably confident prediction of auroral activity could be made with 10-60 min typical advance warning.

Recently, Akasofu[84] has claimed to have found a quantitative relationship between the auroral electrojet magnetic index and parameters of the interplanetary medium, as expressed by

$$AE \sim BV^2 \sin^4 \theta/2$$

where

AE = auroral electrojet index,
B = IMF intensity,
V = solar wind velocity,
θ = direction of IMF relative to the ecliptic plane.

If confirmed by subsequent investigation, this relationship would be useful in predicting not only the occurrence but also the intensity of auroral clutter.

---

80. Kamide, Y., Burch, J.L., Winningham, J.D., and Akasofu, S-I (1976) Dependence of the latitude of the cleft on the interplanetary magnetic field and substorm activity, J. Geophys. Res. 81:698.

81. Kamide, Y., and Winningham, J.D. (1977) A statistical study of the instantaneous nightside aurural oval: The equatorward boundary of electron precipitation as observed by the Isis 1 and 2 satellites, J. Geophys. Res. 82:5573.

82. Arnoldy, R.L. (1971) Signature in the interplanetary medium for substorms, J. Geophys. Res. 76:5189.

83. Pike, C.P., Meng, C-I., Akasofu, S-I., and Whalen, J.A. (1974) Observed correlations between interplanetary magnetic field variations and the dynamics of the auroral oval and the high-latitude ionosphere, J. Geophys. Res. 79:5129.

84. Akasofu, S-I. (1979) Planet; Space Sci. 27:425.

6.3 Satellite Imagery

The advent of large scale auroral imaging from a satellite platform has not only increased understanding of the dynamics of the aurora, but also provides a basis for short-term auroral activity prediction. The U.S. Air Force operates the Defense Meteorological Satellite Program (DMSP) in which two satellites, in approximately circular 1000 km orbits, record images of large portions of the north and south polar regions on a routine basis. These satellites have an orbital period of ~90 min and are 90° apart in longitude, that is, 6 hr apart in local time, one being in the noon-midnight meridian and the other in the dawn-dusk time zone. Figure 31 shows a typical DMSP image, recorded over northern Europe at ~0120 UT on 12 February 1975. The outlines of the U.K. and of the European continent are clearly visible in the city lights. A moderately active aurora is visible to the north of the U.K. The use of this kind of real-time data lies in the known fact that auroral substorms tend to commence in the midnight sector of the auroral oval and subsequently propagate around the oval in a time interval ~ 1 hour. Thus a satellite measurement in the midnight sector of the auroral oval, at the time of substorm onset, can provide some warning of subsequent auroral activity at other longitudes within the next 30 min to 1 hour. Akasofu[85] has published a detailed description of the development of auroral and polar magnetic substorms. While much apparently remains to be learned about these complex phenomena, the present level of understanding is sufficient to permit a short term predictive capability to be developed, based on suitable satellite observations in real time.

6.4 Ground-Based Magnetometers

Suitably located magnetometers can be used to indicate the location and intensity of the auroral electrojet and thence the location and intensity of auroral clutter. The use of such magnetometer data in a predictive mode is subject to similar limitations as those relating to satellite observations. In fact, since a ground-based magnetometer measurement is a relatively localized one compared, for example, to DMSP imagery, its usefulness may be quite limited unless a meridional chain of magnetometers was employed. Meridional chains of magnetometers have been established in Alaska and North America for research purposes.

---

85. Akasofu, S-I. (1968) Polar and Geomagnetic Substorms, Springer-Verlag, New York.

Figure 31. DMSP Photograph of Northern Europe Showing Moderately Active Aurora

6.5 Backscatter Sounder in the Polar Cap

One of the most promising techniques for continuous monitoring of auroral clutter is the location of a HF backscatter sounder close to the geomagnetic pole. Because of the long range at which both E- and F-region backscatter can be observed at HF, due to ionospheric refraction, the entire auroral oval can be monitored from a single location (Bates et al).[86] Similar remarks apply to the question of predictability, based on this kind of data, as for other techniques. The problems of data reduction and interpretation with this technique are likely to be more severe than with satellite or magnetometer data.

---

86. Bates, H.F., Akasofu, S-I., and Kimball, D.S. (1973) First results from the north polar auroral radar, J. Geophys. Res. 78:3857.

References

1. Hakura, Y. (1965) Tables and maps of geomagnetic coordinates corrected by the higher order spherical harmonic terms, *Rept. Ionosph. Space Res. (Japan)*, **19**:121.
2. Gustafsson, G. (1970) A revised corrected geomagnetic coordinate system, *Arkiv f. Geofysik*, **5**(No. 40):595.
3. Eather, R.H. (1973) The auroral oval - A reevaluation, *Rev. Geophys. Space Phys.* **11**:155.
4. Spiro, R.W., Heelis, R.A., and Hanson, W.B. (1978) Ion convection and the formation of the mid-latitude ionization trough, *J. Geophys. Res.* **83**:4255.
5. Rush, C.M., Miller, D., and Gibbs, J. (1974) The relative daily variability of foF_2 and h_mF_2 and their implications for HF radio propagation, *Radio Sci.* **9**:749.
6. Miller, D., and Gibbs, J. (1974) *Ionospheric Analysis and Ionospheric Modelling*, AFCRL-TR-74-0364, AD A002311.
7. Barghausen, A.F., Finney, J.W., Proctor, L.I., and Schultz, L.D. (1969) *Predicting Long-Term Operational Parameters of High-Frequency Sky-Wave Telecommunication Systems*, ESSA Tech. Report, ERL 110-ITS-78.
8. Haselgrove, J. (1955) *Proc. Cambridge Conf. on Physics of the Ionosphere, Physical Soc.*, (London), p 355.
9. Jones, R.M. (1966) *A Three-Dimensional Ray Tracing Computer Program*, ESSA Tech. Rept. IER 17-ITSA 17.
10. Wong, M.S., Vanguri, K.S., and Friedman, M.P. (1973) *Geomagnetic Field Models for Ray Tracing*, AFCRL-TR-73-0294, AD 776241.
11. Miller, D., and Gibbs, J. (1977) *Ionospheric Analysis and Ionospheric Modelling*, RADC-TR-77,53, AD A038298.
12. Bradley, P.L., and George, P.A. (1974) A new method of predicting the ionospheric absorption of high frequency waves at oblique incidence, *Telecomm. J.* **41**:307.

13. Hartz, T. R., Montbriand, L. E., and Vogan, E. L. (1963) A study of auroral absorption at 30 Mc/s, *Can. J. Phys.* 41:581.
14. Hargreaves, J.K., and Cowley, F.C. (1967) Studies of auroral radio absorption events at three magnetic latitudes - II. Differences between conjugate regions, *Planet. Space Sci.* 15:1571.
15. Foppiano, A. (1975) CCIR, IWP 611, Docs. 3 and 10.
16. Elkins, T. J. (1972) *A Model of Auroral Substorm Absorption*, AFCRL-TR-72-0413, AD 749859.
17. IAGA Commission 2, Working Group 4 (1969) International geomagnetic reference field, 1965.0, *J. Geophys. Res.* 74:4407.
18. Mead, G. D. (1970) International geomagnetic reference field 1965.0 in dipole coordinates, *J. Geophys. Res.* 75:4372.
19. Jensen, D.C., and Cain, J.C. (1962) An interim geomagnetic field (abstract), *J. Geophys. Res.* 67:3568.
20. Cain, J.C., and Sweeney, R.E. (1970) Magnetic field mapping of the inner magnetosphere, *J. Geophys. Res.* 75:4360.
21. Besprozvannaya, A.S., and Shchuka, T.I. (1971) *Geomag. and Aeron.* 6:878; and (1972) Space-time distribution of E_s *formations associated with* visible auroral forms, *Geomag. and Aeron.* 12:401.
22. Unwin, R.S. (1959) Studies of the upper atmosphere from Invercargill, New Zealand, *Ann. de Geophys.* 15:377.
23. Presnel, R.I., Leadabrand, R.L., Dyce, R.B., Schlobohm, J.C., and Berg, M.R. (1959) *Upper Atmosphere Clutter Research*, RADC-TR-59-34, AD A070112.
24. Hellgren, G., and Meos, J. (1952) Localization of auroral with 10 m high power radar technique, using a rotating antenna, *Tellus* 4:249.
25. Brooks, D. (1965) Observations of radio auroral echoes and simultaneous magnetic disturbance, *J. Atmos. Terr. Phys.* 27:1151.
26. Czechowsky, P., Dieminger, W., and Kochan, H. (1974) Backscatter results from Lindau - I. observations of radio-aurora, *J. Atmos. Terr. Phys.* 36:955.
27. Sprenger, K., and Glode, P. (1964) Some properties of radio aurora in medium latitudes, *J. Atmos. Terr. Phys.* 26:193.
28. Aarons, J. (1973) High latitude for F-layer irregularities, *J. Geophys. Res.* 78:7441.
29. Bates, H.F. (1971) *J. Atmos. Terr. Phys.* 33:111.
30. Shimazaki, T. (1959) The occurrence of spread-F and the geomagnetic field, *J. Rad. Res. Labs.* (Japan) 7:437.
31. Penndorf, R. B. (1960) *Research Concerning Forecasting Anomalous Propagation at High Latitudes*, AFCRL-TN-60-1162.
32. Tao, K. (1965) World-wide maps of the occurrence percentage of spread-F in years of high and low sunspot numbers, *J. Radio Res. Labs.* (Japan) 12:317.
33. Singleton, D.G. (1960) The geomorphology of spread-F, *J. Geophys. Res.* 65:3615.

34. Davis, R. M. (1973) *Dependence of High Latitude Spread-F Occurrence on Solar and Magnetic Activity*, U.S. Dept. of Commerce, OT Rept. 73-23.

35. Baggaley, W. J. (1970) Backscatter observations of F-region field-aligned irregularities during the I.Q.S.Y., *J. Geophys. Res.* **75**:152.

36. Peterson, A. M., Villard, O. G., Leadabrand, R. L., and Gallagher, P. B. (1955) Regularly-observable aspect - sensitive radio reflections from ionization aligned with the earth's magnetic field and located within the ionospheric layers at middle latitudes, *J. Geophys. Res.* **60**:497.

37. Weaver, P. F. (1965) Backscatter echoes from field-aligned irregularities in the F-region, *J. Geophys. Res.* **70**:5425.

38. Millman, G. H. (1975) *An Evaluation of HF Ionospheric Backscatter Echoes*, G. E. Company Rept. R75EMH19.

39. Maeda, H. (1977) Neutral winds and ion drifts in the polar ionosphere caused by convection electric fields - 2, *J. Atmos. Terr. Phys.* **39**:849.

40. Heppner, J. P. (1977) Empirical models of high latitude electric fields, *J. Geophys. Res.* **82**:1115.

41. Heelis, R. A., Hanson, W. B., and Burch, J. L. (1976) Ion convection velocity reversals in the dayside cleft, *J. Geophys. Res.* **81**:3803.

42. Tsunoda, R. T., Perrault, P. D., and Hodges, J. C. (1976) Azimuthal distribution of HF slant E echoes and its relationship to the polar cap electric field, *J. Geophys. Res.* **81**:3834.

43. Taieb, R. (1966) A study of sporadic E at high latitudes, *J. Geophys. Res.* **71**:5757.

44. Doupnik, J. R., Banks, P. M., Baron, M. J., Rino, C. J., and Petriceks, J. (1972) *J. Geophys. Res.* **77**:4268.

45. Banks, P. M., and Doupnik, J. R. (1975) A review of auroral zone electrodynamics deduced from incoherent scatter radar observations, *J. Atmos. Terr. Phys.* **37**:951.

46. Unwin, R. S. (1966) The morphology of VHF radio aurora at sunspot maximum - II. The behaviour of different echo types, *J. Atmos. Terr. Phys.* **28**:1183.

47. Unwin, R. S., and Baggaley, W. J. (1972) *Ann. Geophys.* **28**:111.

48. Greenwald, R. A., Eckland, W. L., and Balsley, B. B. (1975) Radar observations of auroral electrojet currents, *J. Geophys. Res.* **80**:3635.

49. Flood, W. A. (1960) VHF auroral backscatter measurements, *J. Geophys. Res.* **65**:2261.

50. Gartlein, C. W., Sprague, G., and Waag, R. C. (1960) 41 Mc/s IGY auroral radar at Ithaca, New York, *J. Geophys. Res.* **65**:2255.

51. Watkins, C. D. (1961) Auroral radio-echoes and magnetic disturbance, *J. Atmos. Terr. Phys.* **20**:131.

52. Unger, J. H. W., Hardin, R. H., and Horan, H. H. (1973) *Joint Radar Propagation Study*, Bell Telephone Labs, October 1.

53. Edwards, L. C., Katz, A. H., Patton, D. E., and Campbell, L. W. (1973) *Polar Fox II - Experimental Phase, Vol. II, Executive Summary*, RADC-TR-73-203.

54. Katz, A.H. (1971) HF Auroral Backscatter Study, AVCO Rept. AVSD-0378-71-RR.

55. Hower, G.L., Ranz, D.M., and Allison, C.L. (1966) Comparison of HF radar echoes and high latitude spread-F measurements, J. Geophys. Res. 71:3215.

56. Swenson, E.M. (1972) Aspect-sensitive reflections from ionization irregularities in the F-region, J. Atmos. Terr. Phys. 34:1469.

57. Malik, C., and Aarons, J. (1964) A study of auroral echoes at 19.4 megacycles per second, J. Geophys. Res. 69:2731.

58. Oksman, J., Moller, H.G., and Greenwald, R. (1979) Comparisons between strong HF backscatter and VHF radar aurora, Radio Sci. 14:1121.

59. Abel, W.J., and Newell, R.E. (1969) Measurements of the afternoon radio aurora at 1295 MHz, J. Geophys. Res. 74:231.

60. Greenwald, R.A., and Eckland, W.L. (1975) A new look at radar auroral motions, J. Geophys. Res. 80:3642.

61. Greenwald, R.A., Weiss, W., Neilsen, E., and Thomson, N.R. (1978) STARE: A new radar auroral backscatter experiment in northern Scandinavia, Radio Sci. 13:1201.

62. Barber, D., Sutcliffe, H.K., and Watkins, C.D. (1962) Some radar observations of meteors and aura at 300 and 500 Mc/s using a large radio telescope - II. Observations of the aurora borealis, J. Atmos. Terr. Phys. 24:599.

63. Whalen, J.A., and Pike, C. (1973) F-Layer and 6300-A measurements in the day sector of the auroral oval, J. Geophys. Res. 78:3848.

64. Burch, J.L. (1972) Precipitation of low-energy electrons at high latitudes: Effects of interplanetary magnetic field and dipole tilt angle, J. Geophys. Res. 77:6696.

65. Oguti, T., and Marubashi, K. (1966) Enhanced ionization in the ionospheric F2 region around geomagnetic noon in high latitudes, Repts. Ionos. Spa. Res. (Japan), 20:96.

66. Ring, W., and Richards, E. (1978) Fall URSI Symposium, Boulder, Colorado

67. Sales, G.S. (1977) URSI Spring Meeting, Palo Alto, California.

68. Greenwald, R.A., Eckland, W.L., and Balsley, B.B. (1973) Auroral currents, irregularities, and luminosity, J. Geophys. Res. 78:8193.

69. Cherneyshev, O.V. (1968) f_oE_s Distribution curves, Geomag. and Aeron. 8:902.

70. Chestnut, W.G., Hodges, J.C., and Leadabrand, R.L. (1968) Auroral Back Scatter Wavelength Dependence Studies, RADC-TR-68-286.

71. Leadabrand, R.L., Larson, A.G., and Hodges, J.C. (1967) Preliminary results on the wavelength dependence and aspect sensitivity of radar auroral echoes between 50 and 3000 MHz, J. Geophys. Res. 72:3877.

72. Mitchell, M.J., and Brown, J.L. (1976) PAR Auroral Study, Vol. 5, Final Rept. Contract DASG-74-C-0026, ABMD Systems Command.

73. Bates, H.R., and Albee, P.R. (1969) Aspect sensitivity of HF auroral echoes, J. Geophys. Res. 74:1164.

74. McDiarmid, D.R. (1972) On the aspect sensitivity of radio aurora, Can. J. Phys. 50:2557.

75. Leadabrand, R. L., Schlobohm, J. C., and Baron, M. J. (1965) Simultaneous very high frequency and ultra high frequency observations of the aurora at Fraserburgh, Scotland, J. Geophys. Res. 70:4235.

76. Moorcroft, D. R., and Tsunoda, R. T. (1978) Rapid scan doppler velocity maps of the UHF diffuse radar aurora, J. Geophys. Res. 83:1482.

77. Cage, A. L., and Zawalick, E. J. (1972) A Discussion of the Geomagnetic Indices K_p and A_p, 1932 to 1971, AFCRL-72-0693, AD 756828.

78. Pazich, P. M. (1976) Conditional Probabilities of the Geomagnetic Index A_p, AGFL-TR-76-0034, AD A023675.

79. Elkins, T. J. (1973) An Empirical Model of the Polar Ionosphere, AFCRL-TR-73-0331, AD 766240.

80. Kamide, Y., Burch, J. L., Winningham, J. D., and Akasofu, S-I (1976) Dependence of the latitude of the cleft on the interplanetary magnetic field and substorm activity, J. Geophys. Res. 81:698.

81. Kamide, Y., and Winningham, J. D. (1977) A statistical study of the instantaneous nightside auroral oval: The equatorward boundary of electron precipitation as observed by the Isis 1 and 2 satellites, J. Geophys. Res. 82:5573.

82. Arnoldy, R. L. (1971) Signature in the interplanetary medium for substorms, J. Geophys. Res. 76:5189.

83. Pike, C. P., Meng, C-I., Akasofu, S-I., and Whalen, J. A. (1974) Observed correlations between interplanetary magnetic field variations and the dynamics of the auroral oval and the high-latitude ionosphere, J. Geophys. Res. 79:5129.

84. Akasofu, S-I. *(1979) Planet; Space Sci. 27:425.*

85. Akasofu, S-I. (1968) Polar and Geomagnetic Substorms, Springer-Verlag, New York.

86. Bates, H. F., Akasofu, S-I., and Kimball, D. S. (1973) First results from the north polar auroral radar, J. Geophys. Res. 78:3857.

87. Maehlum, B. N. (1968) Universal-time control of the low-energy electron fluxes in the polar regions, J. Geophys. Res. 73:3459.

88. Vondrak, R. R., Smith, G., Hatfield, V. E., Tsunoda, R. T., Frank, V. R., and Perrault, P. D. (1978) Chatanika Model of the High-Latitude Ionosphere, for Application to HF Propagation Prediction, RADC-TR-78-7, AD A053154.

Appendix A

F-Region Irregularities

The "permanent maximum" in spread-F noted by Penndorf[31] and Tao[32] appears to be an artifact caused by observational bias. The region of intense F-region irregularities in the dayside auroral oval is known to be caused by direct injection into the earth's atmosphere of thermalized interplanetary plasma, with peak flux in the 10 ~ 100 eV region. Whalen and Pike[63] have shown that this region of irregularities extends for at least several hours on either side of magnetic midday. Direct satellite measurements of the particle fluxes which produce the irregularities have been reported by Maehlum[87] and Burch.[64] Both authors show that there are marked variations in the flux with the tilt angle between the geomagnetic axis and the ecliptic plane. Specifically, Maehlum shows a pronounced variation with Universal Time of the high latitude daytime boundary of precipitation between ~74° and ~84° in summer, while Burch shows a smaller but significant variation (about 4° over the course of a year) for the low latitude boundary. The highest dayside location of the poleward boundary, observed by Maehlum, occurs at 18 UT, while the lowest occurs at 8 UT. Thus there is a variation with Universal Time of the latitudinal extent of the precipitation region of ~8° - 10°, with the maximum width at 18 UT. Maximum spread-F should thus be observed at the location where 18 UT corresponds to magnetic local noon, namely the Foxe Basin in Northern Canada. At this location the irregularity region is most extensive.

---

[87] Maehlum, B. N. (1968) Universal-time control of the low-energy electron fluxes in the polar regions, J. Geophys. Res. 73:3459.

Appendix B

Doppler Geometry

The calculation of the plasma velocity component radial to the radar involves the solution of two spherical triangles (see Figure B1). In these triangles

M = geomagnetic pole
G = geographic pole
P = point from which radar energy is being backscattered
S = radar site location
A = magnetic declination
B = magnetic longitude of P
ϕ_P = colatitude of P
ϕ_S = colatitude of S
R = clutter range
α = clutter azimuth
a = magnetic colatitude of G
B = magnetic colatitude of P.

The velocity components (V_N and V_E) are specified by the model of Sections 5.1 and 5.2, relative to M.

Solving triangle MPG yields A,

$$\tan A = \frac{\sin B \sin A \sin \phi_P}{\cos a - \cos b \cos \phi_P}$$

where a, b, c are measured in angular units on the earth's surface.

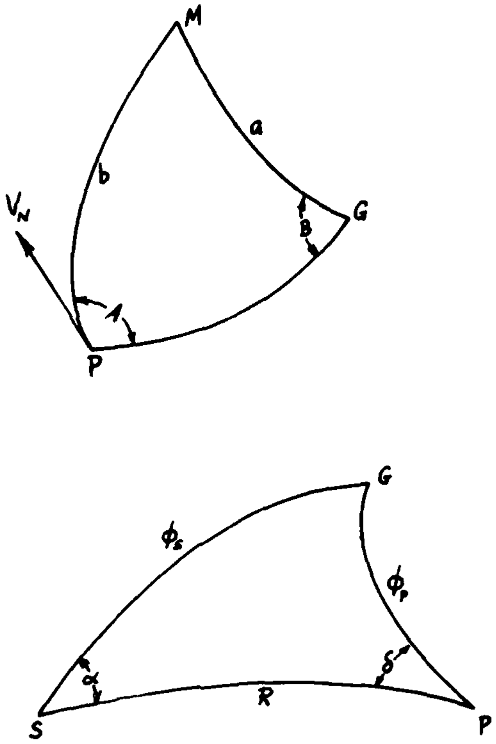

Figure B1. Geometry for Doppler Shift Calculations in Spherical Coordinate System. P = point of clutter origination; S = radar site; G = geographic pole; M = geomagnetic pole

Knowledge of A permits the velocity vector to be transformed into the geodetic system.

Solving triangle SGP yields δ, the angle required to compute the velocity component radial to the radar from the geodetic components,

$$\tan \delta = \frac{\sin \alpha \sin \phi_S \sin R}{(\cos \phi_S - \cos \phi_P \cos R)}$$

where R is measured in angular units.

The velocity vector may be represented in the geomagnetic system by

$$V = \left(\sqrt{V_N^2 + V_E^2}\right)\angle\theta$$

where

$$\theta = \tan^{-1}\left(\frac{V_N}{V_E}\right).$$

Then the radial velocity component relative to the radar (S) is

$$V_R = V \cos \beta$$

where

$$\beta = \theta + A + \delta \, .$$

Appendix C

Backscatter Volume

Computation of backscatter volume in the presence of ionospheric refraction (see Figure C1).

The figure depicts two rays leaving the radar (R) at an angular separation ($\Delta\epsilon$) in the vertical plane, and undergoing ionospheric refraction. The magnetic field vector $\vec{H}$ is illustrated at three adjacent points on each ray; the central of each set of three points, A and B respectively are the locations of geomagnetic orthogonality ($\psi = 90°$) corresponding to the leading and trailing edges of the transmitted pulse. Thus the mean of the group path lengths (along the ray trajectories) RA and RB correspond to the radar range and AB defines one dimension of the scattered volume, determined by the radar resolution.

The scatter volume dimension normal to AB, in the vertical plane is determined by magnetic aspect sensitivity. Let C, D, and E, F respectively be pairs of points on either side of the orthogonality points at which the backscatter cross section is reduced by a specific amount (say 6 dB) from its maximum value at orthogonality. CD and EF are then given by $2\frac{dP}{d\psi} \cdot \Delta\psi$ where P is group path length and $\Delta\psi$ is the departure of the geomagnetic aspect angle from orthogonality which is necessary to reduce the backscatter cross section by the required amount. $\Delta\psi \sim \pm 1°$, for 6 dB reduction.

The third component of scatter volume is the azimuthal component, $R\Delta\phi$ where

R = radar range,

$\Delta\phi$ = azimuthal antenna beamwidth.

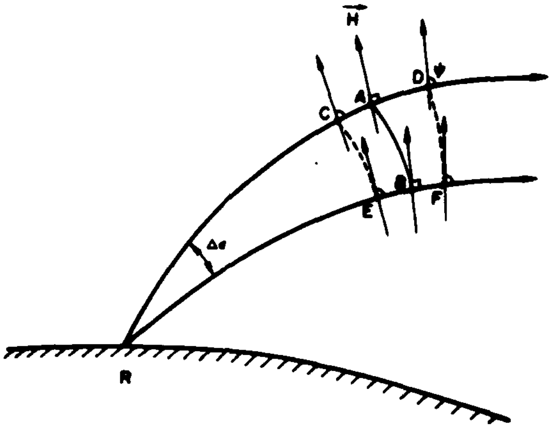

Figure C1. Definition of Scatter Volume for Refracted Ionospheric Propagation

Thus the scatter volume is given by

$$V_S = 2R^2 \Delta\phi \cdot \Delta\epsilon \cdot \frac{dP}{d\psi} \cdot \Delta\psi \cdot \frac{1}{F} .$$

The factor F in this expression is included to take account of ionospheric focussing.

The parameters $\Delta\epsilon$, $\frac{dP}{d\psi}$ and F must be determined by numerical (or in some special cases, analytical) ray tracing in modelled ionospheres.

Figure C2 shows the upper part of a computed ray trajectory in the plane of propagation and also the geomagnetic aspect angle variation along the trajectory. By appropriate scaling from this figure, the value of $\frac{dP}{d\psi}$ at $\psi = 90°$ can be estimated as 4.0 km/degree. Figure C3 shows the variation with group path and altitude of the geomagnetic orthogonality point (solid line) and the value of $\frac{d\psi}{dP}$ (dashed line) at different elevation angles of take-off at the transmitter. This gives an indication of the amount of variability to be expected for a typical case (in this instance, 6 MHz propagation from a site at 61° CGL at 0° azimuth at 00 UT in January at sunspot number 100).

Figure C4 shows the group path to the geomagnetic orthogonality point (for the same set of conditions as the previous two figures) as a function of elevation angle at the radar. Shown also is the range of elevation angles ($\Delta\epsilon = 0.9°$) corresponding to a 250 μsec pulse at a radar range of 1000 km.

The focussing factor, F, is highly variable and difficult to compute. For some representative cases, values of $F \sim 10$ were found. The significance of the focussing factor may be seen by noting that the vertical dimension of the scattering volume estimated from Figure C3 is much less than $R\Delta\epsilon$, which is the equivalent vertical dimension for straight line radio propagation.

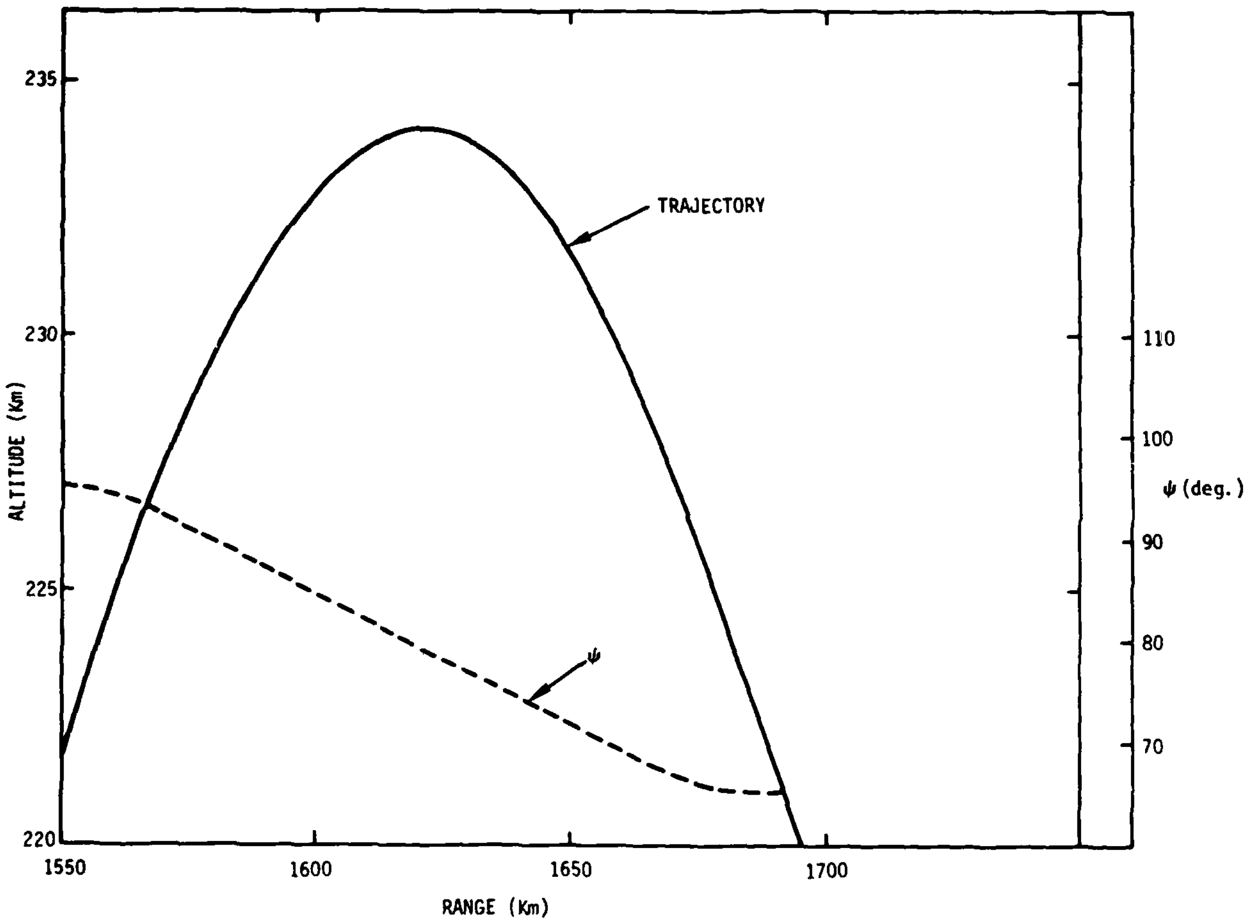

Figure C2. Ray Trajectory in the F-region, Showing the Variation of Geomagnetic Aspect Angle With Range

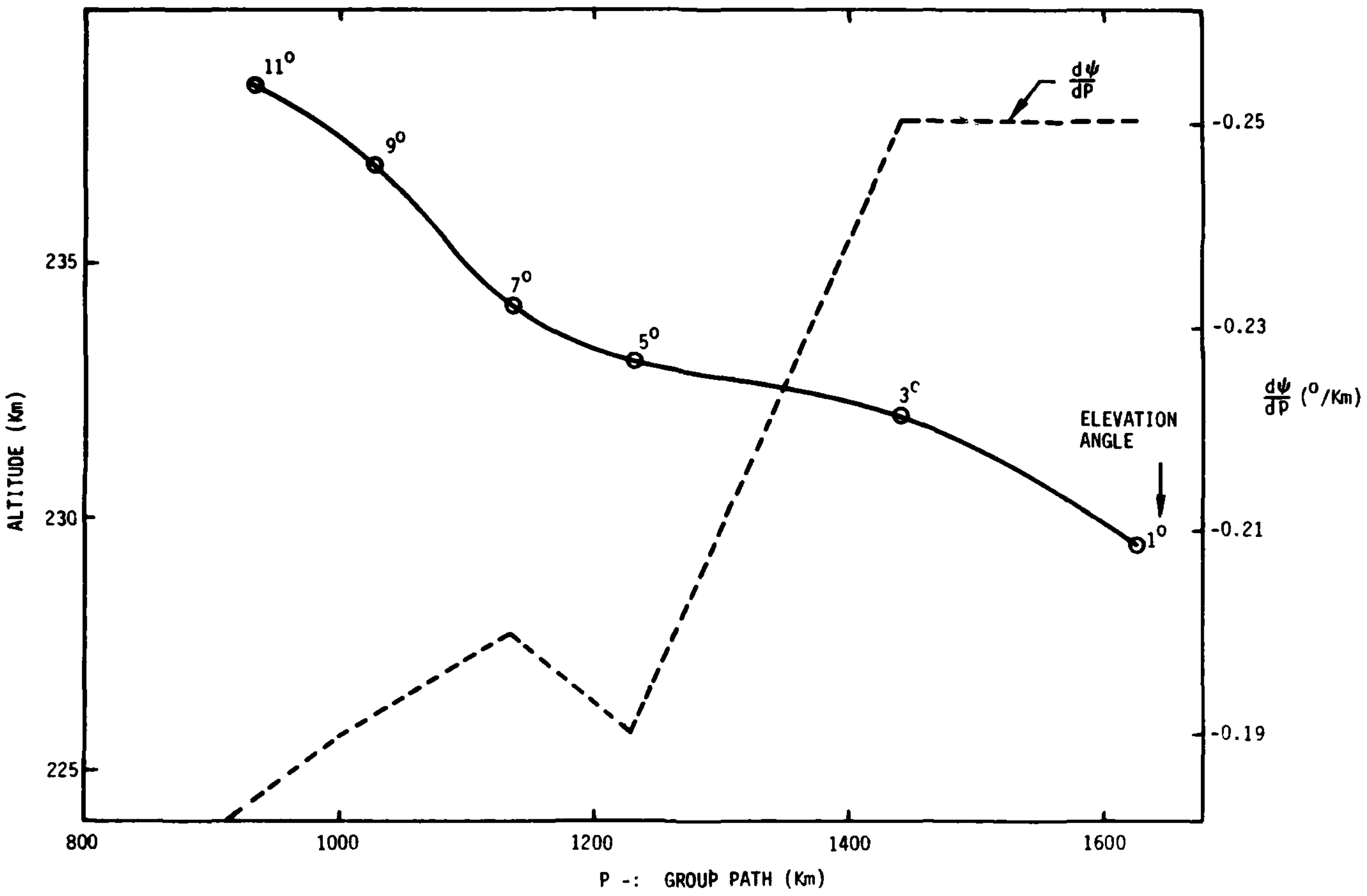

Figure C3. Variation Along Ray Trajectory of Altitude and Rate of Change of Geomagnetic Aspect Angle With Group Path and Take-off Elevation Angle at the Radar

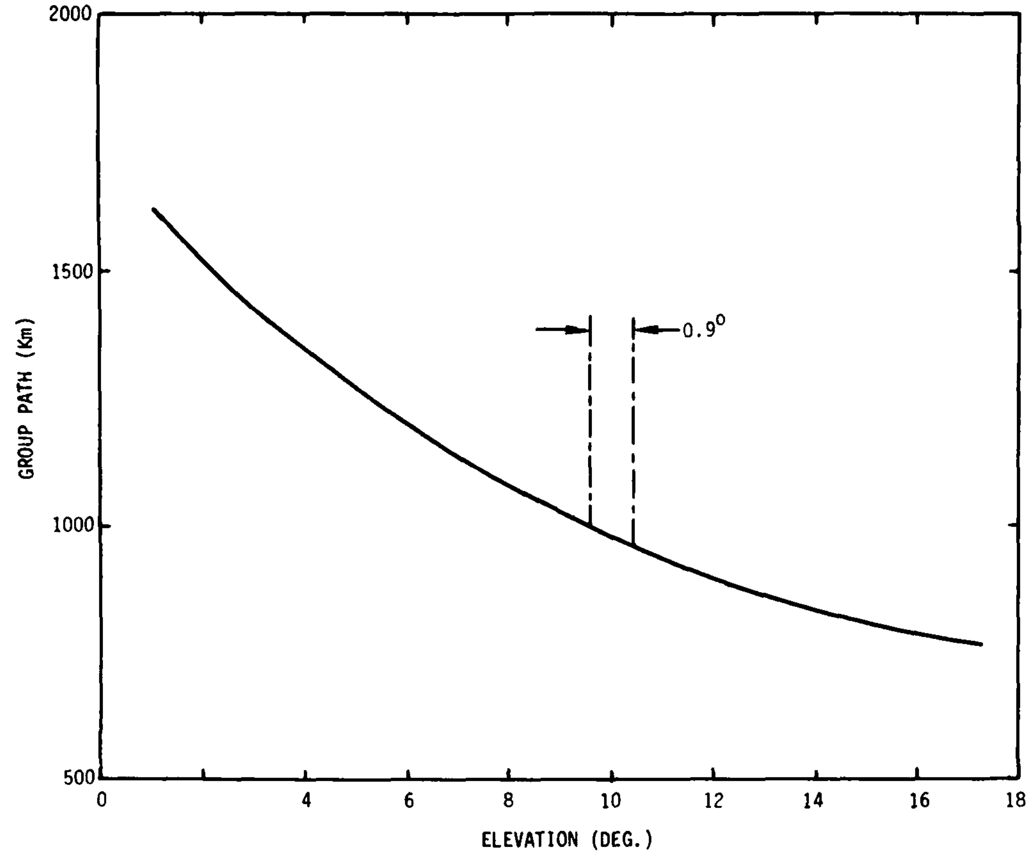

Figure C4. Variation Along Ray Trajectory of Group Path With Elevation Angle of Take-off, Showing the Range of Elevation Angles, at 1000 km Radar Range, Defined by the Radar Pulse

Appendix D

F-Region Volumetric Cross Section

The probability of occurrence of F-region irregularity, p(F) was modelled in Section 4.2 in terms of the probability of spread-F as observed by vertical incidence ionosondes. This model can be used to estimate F-region volume reflectivity by "calibrating" it with Polar Fox II cross section data. Figures 16-19 show probability distributions of F-region "pseudo volumetric" cross section measured by Polar Fox II during nighttime hours of October 1972, at different frequencies. Using the model of Section 4.2, the probability of F-region irregularity in the Polar Fox coverage area in October is approximately 90 percent. From Figure 19 the value of 10 MHz cross section which is exceeded 90 percent of the time is -94 dB m^2/m^3. Thus in order to maintain the measured difference between E- and F-region median values of cross section, for October nighttime, the 50 percent value of p(F) must be equated to -94 dB m^2/m^3, for average K_p.

The procedure adopted here makes the not unreasonable assumption that the volume cross section is proportional to p(F) and that both quantities have similar probability distributions. The disadvantages in the use of spread-F incidence as a measure of backscatter cross section is that it is too crude a parameter, having too small a dynamic range and too easily saturated. Thus the range of estimated backscatter cross sections may be somewhat truncated.

Appendix E

Simple Doppler Shift Models

Section 5 of this report contains the development of a detailed model for the Doppler Shift experienced by a radar signal backscattered from auroral irregularities. This model is much more complex than previous models used in connection with the radar aurora and may in some applications be too cumbersome to implement or be unnecessarily precise. Simpler models have been used based on the assumption that radar backscatter originates in a line current segment (for example, Unger et al,[52] PARL report). These models are based on the common assumption that the zonal component of velocity greatly exceeds the meridional component. Figure E1 shows in the upper diagram a straight line velocity vector (V), showing the reversal of the radial component (V_r) as the azimuth (α) goes through zero at true north.

$$V_r = V \sin \alpha \ .$$

A more accurate model, but one still having the advantage of simplicity is illustrated in the lower diagram, where the velocity (V) is assumed tangent to a line of constant geomagnetic latitude, which is the approximate behavior of the auroral electrojet.

If

Φ_c = co-latitude of this line,
Φ_s = co-latitude of radar site, 0 ,

then

$$0A = \Phi_s - \Phi_c ,$$

and

$$V_r = V \cdot \frac{\Phi_s}{\Phi_c} \cdot \sin \alpha .$$

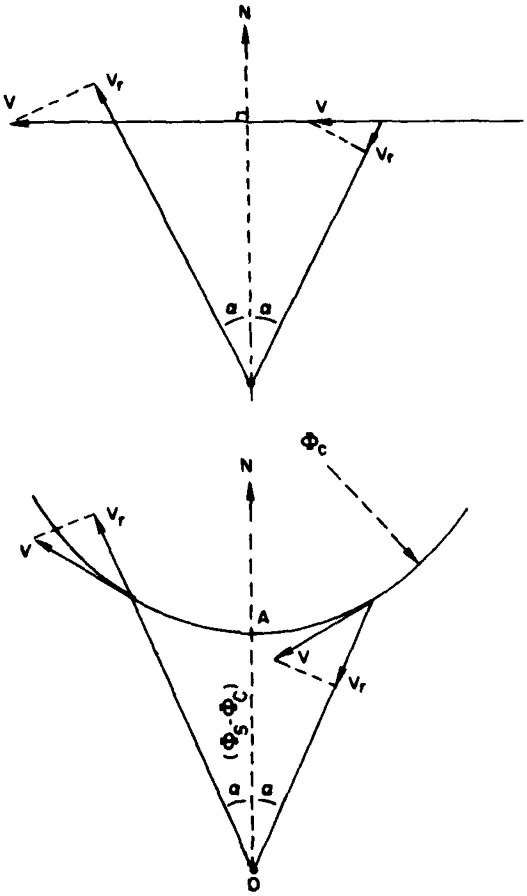

Figure E1. Simplified Models for Doppler Calculations: Straight Line Motion (upper diagram); Curved Velocity Trajectory Along Circle of Constant Geomagnetic Latitude (lower diagram)

Figure E2 shows the azimuthal variation of Doppler Shift derived from such a model with $\Phi_c = 22°$, $\Phi_s = 29.5°$, and V = 400 m/sec, for a frequency of 10 MHz. Note that there is a maximum azimuth

$$\alpha_{max} = \sin^{-1}\left(\frac{\Phi_c}{\Phi_s}\right)$$

at which the line-of-sight becomes tangent to the velocity vector locus. The tendency of the Doppler vs azimuth curve to approach horizontal in this model, at large azimuths, is frequently observed in experimental studies of auroral backscatter.

The straight-line model may be more appropriate for clutter deep within the polar cap, while the circular model is more appropriate for clutter in the vicinity of the auroral oval.

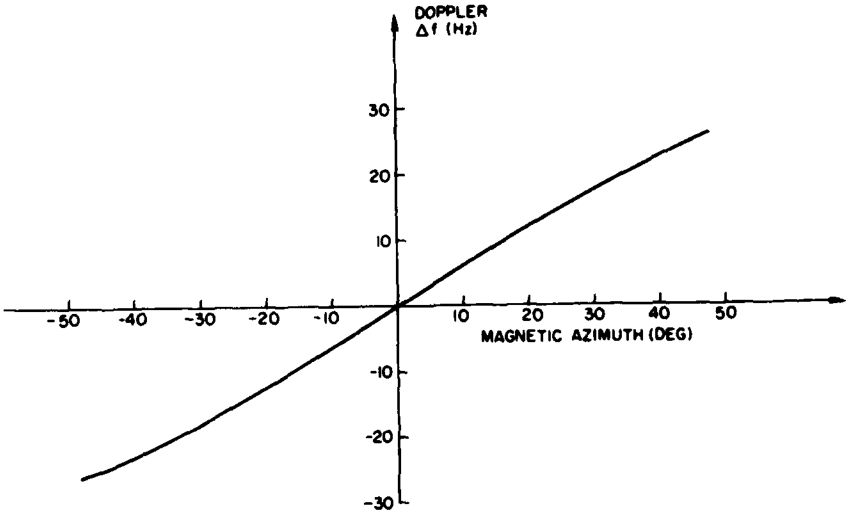

Figure E2. Doppler Shift Calculated on Basis of Curved Trajectory Model in Figure E1, as a Function of Magnetic Azimuth

Appendix F

Auroral E-Layer Effect

Up until this point it has been assumed that the nighttime ionospheric refraction, below the altitude of E-region irregularity maximum, is small. This assumption permits the use of straight-line geometrical propagation to determine the geomagnetic aspect angle at 100 km altitude. It is known, however, that a thick refracting layer of ionization is often present on the night side of the auroral oval. The peak electron density of this layer varies sporadically, and the location of the layer varies with geomagnetic activity. Recent studies, using the Chatanika incoherent scatter radar in Alaska[88] have revealed details of this auroral E-layer which permit construction of a representative model, through which ray tracing can be performed to establish the probable regions of maximum E-region auroral clutter.

The model consists of a torus-shaped region of ionization having a parabolic vertical distribution of ionization centered at 110 km altitude with 10 km semi-thickness. The latitudinal effect is described by another parabola.

The peak density of the layer was chosen to correspond to a critical frequency of 3 MHz, which is supported by Chatanika radar measurements for low-to-moderate magnetic activity levels. Numerical ray tracing was performed at 6 MHz and 12 MHz in the model ionosphere described here, using the Jensen-Cain 6th order expansion of the geomagnetic field to determine geomagnetic aspect angles. The

---

[88] Vondrak, R. R., Smith, G., Hatfield, V. E., Tsunoda, R. T., Frank, V. R., and Perrault, P. D. (1978) Chatanika Model of the High-Latitude Ionosphere, for Application to HF Propagation Prediction, RADC-TR-78-7, AD A053154.

models were constructed for $K_p = 0, 2, 4$. Figure F1 shows contours of 90° aspect angle resulting from this simulation. The dashed lines are for 12 MHz and the solid lines for 6 MHz propagation. These contours may be compared to the 90° contour in Figure 21, which is for unrefracted propagation. The combination of the two sets of contours determines the total effect of E-region clutter.

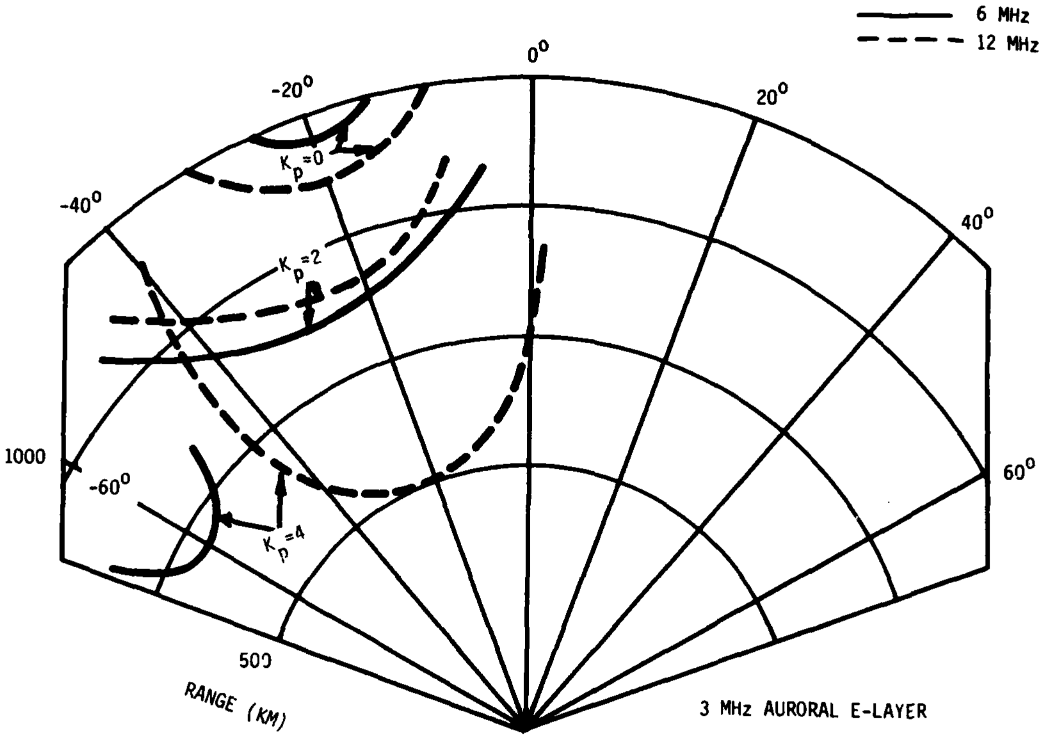

Figure F1. Contours of Calculated Geomagnetic Orthogonality at Altitude 110 km Using an Ionospheric Model Containing an Aurural E-layer. Dashed lines are for 12 MHz and solid lines for 6 MHz. Site is located at 61° CGL

MISSION
of
Rome Air Development Center

RADC plans and executes research, development, test and selected acquisition programs in support of Command, Control Communications and Intelligence (C^3I) activities. Technical and engineering support within areas of technical competence is provided to ESD Program Offices (POs) and other ESD elements. The principal technical mission areas are communications, electromagnetic guidance and control, surveillance of ground and aerospace objects, intelligence data collection and handling, information system technology, ionospheric propagation, solid state sciences, microwave physics and electronic reliability, maintainability and compatibility.

Printed by
United States Air Force
Hanscom AFB, Mass. 01731